Design, synthesis, and characterization of 2,3 derivatives of 4,5,6,7-tetrahydrobenzothiophene modulators of RORγt and evaluation of their inhibitory effect on Th17 response in-vitro and in-vivo

Ahmed Said Abd El Hamid Said Fouda

Division of Surgical & Interventional Sciences
Department of Surgery, McGill University
Montreal, April 2024

McGill

To my Father

Table of contents

Retinoic-acid-receptor-related-orphan-receptor-gamma-t (RORγt) is expressed in T helper 17 (Th17) cells and regulates their activity and cytokine production. Th17 is implicated in many autoimmune diseases and in solid allograft rejection. Previous studies have shown that Th17 contributes to antibody mediated rejection (AMR) through the promotion of tertiary lymphoid tissue and production of donor specific antibodies. Th17 cells secretes IL17A, IL21, IL22 and other cytokines that promote both cellular and humoral immune responses, B-cell proliferation, antibody production and class switching, macrophage recruitment and other inflammatory pathways. Accordingly, we hypothesised that RORγt inhibitors can reverse graft rejection including the form known as AMR before irreversible organ damage has occurred. The objectives of the current study were to discover, develop novel RORγt inverse agonists that can treat AMR in HLA incompatible transplantation and to evaluate their effectiveness in treating graft rejection in a mouse model. We used in-silico methods to identify novel RORγt modulators. We further synthesised, evaluated them using in-vitro methods and in a mouse model of total mismatch skin graft. We identified 4,5,6,7 tetrahydro-benzothiophene derivatives as potent inverse agonists of RORγt. They reduce Th17 signature cytokines expression in vitro. We further identified a small molecule TF-S14, a potent inverse agonist of RORγt, as an effective treatment for acute AMR in an accelerated rejection mouse model of skin allograft and a potential clinical trials candidate. In conclusion, the current study paves the way to the use of RORγt inverse agonists as add-on therapy to maintenance immunosuppression for organ transplantation. Due to the central role of Th17 in organ rejection, in context of clinical trials, the novel RORγt inverse agonist can be indicated for acute, late, or chronic solid graft rejection of cellular or humoral origin.

Le récepteur orphelin gamma t lié au récepteur de l'acide rétinoïque (RORγt) est exprimé dans les cellules T helper 17 (Th17) et régule leur activité et la production de cytokines. Le Th17 est impliqué dans de nombreuses maladies auto-immunes et dans le rejet d'allogreffes solides. Les études ont montré que Th17 contribue au rejet médié par les anticorps (RAM) grâce à la promotion du tissu lymphoïde tertiaire et à la production d'anticorps spécifiques du donneur. Les cellules Th17 sécrètent IL17A, IL21, IL22 et d'autres cytokines qui favorisent les réponses immunitaires cellulaires et humorales, la prolifération des lymphocytes B, la production d'anticorps et le changement de classe, le recrutement de macrophages et d'autres voies inflammatoires. Nous avons émis l'hypothèse que les inhibiteurs de RORγt peuvent inverser le rejet de greffe avant que des lésions organiques irréversibles ne se produisent. L'objectif de la présente étude était de découvrir, de développer de nouveaux agonistes inverses du RORγt capables de traiter la RAM et d'évaluer leur efficacité dans le traitement du rejet de greffe dans un modèle murin. Nous avons utilisé des méthodes in silico pour identifier des nouveaux modulateurs RORγt. Nous les avons ensuite synthétisés et évalués à l'aide de méthodes in vitro et in vivo. Nous avons identifié des dérivés de 4,5,6,7 tétrahydro-benzothiophène comme de modulateurs de RORγt qui réduisent l'expression des cytokines de Th17 in vitro. Ensuite, nous avons identifié TF-S14, un puissant modulateur de RORγt, comme traitement efficace de la RAM aiguë dans un modèle murin à rejet accéléré d'allogreffe cutanée qui possède un profil d'effets secondaires favorable. En conclusion, la présente étude ouvre la voie à l'utilisation des agonistes inverses du RORγt dans la transplantation d'organes. Au cas où ils auraient été testés dans des essais cliniques, les nouveaux modulateurs peuvent être indiqués pour le rejet aigu, tardif ou chronique de greffe solide.

Acknowledgments

- First and foremost, I thank Allah, the most gracious and the most merciful for the strength and all blessings he gave me.

- I wish to express my sincere thanks to my supervisors: Dr Jean Ivanov Tchervenkov, Professor of Surgery, Faculty of Medicine and Health Sciences, McGill University; Dr Steven Paraskevas, Professor of Surgery, Faculty of Medicine and Health Sciences, McGill University, for the great help and guidance they provided me, in all parts of the present study.

- I feel grateful to the colleagues in my laboratory and Research Institute of McGill University Health Centre, for their great support to me during the time I spent in the laboratory.

- I thank McGill University Health Centre and the Royal Victoria Hospital Foundations for their unwavering support to my project since I joined the program and until now.

- Finally, I want to express my sincere gratitude to my beloved Mother, Wife, my Children and all Family members for their kind support and assistance during this study.

In the current study, we addressed two knowledge gaps. First, there is currently no effective therapy to treat graft rejection in highly sensitized patients or more precisely to prevent or treat antibody mediated rejection which can arise following incompatible HLA transplantation. To address this problem, we proposed a treatment based on RORγt inverse agonists that can eventually suppress the activity of Th17 cells which is one if the key players involved in such immune response. Because RORγt inverse agonists are still in experimental phases and none of them is clinically approved yet, we sought to elect the best possible RORγt inverse agonist that was discovered and evaluated in clinical trials; however, during our initial search for a suitable agent, we found that many of the trials on RORγt inverse agonists were either stopped or cancelled due to lack of efficacy or safety concerns. Eventually, we were faced with another knowledge gap in the drug discovery field which we defined as that "despite the big number of discovered RORγt inverse agonists there is no single small molecule that was a promising clinical drug candidate". We decided to address this problem by first identifying the root cause of the problem and we thought it is that "the processes of electing the RORγt lacked a collaborative approach where in many cases a brilliant scientist in a certain field was obliged to take a decision that he was not trained for because there was no multidisciplinary team to assist in decision making". According to problem analysis, we then decided to design our molecule in a conservative approach where compound safety is priority, physicochemical properties second then receptor engagement third and finally

and least important the novelty of the chemical scaffold. With this approach we designed the molecule based on a biologically friendly chemical scaffold. In other words, the human body has been exposed to compounds that have very close chemical similarity which did not cause serious toxicities or side effects. Solving this problem according to this approach, we successfully discovered the novel class of RORγt inverse agonists the derivatives of 4,5,6,7 tetrahydro-benzothiophene. Once we solved our second defined knowledge gap related to the discovery of safe and effective RORγt inverse agonist, then we proceeded with our solution, which is the novel RORγt inverse agonists, to solve the original problem for which we initiated the research project. In this effort we first confirmed the association between Th17 and high sensitized organ recipients and reported that these patients have higher than normal percentage of Th17 cells circulating in their blood. Once we established and confirmed this association, we then developed a mouse model for accelerated skin graft rejection. We found this model very useful for testing novel anti-rejection therapies and in our submitted work to communication biology we emphasized on all aspects and details of this mouse model to enable the scientific community to use the same model without any need for getting into cycles of excessive trail and error. After developing this model, we were able to create an experimental scenario that mimics the real-life clinical situation. In this experimental scenario we had our RORγt inverse agonist invention in hand to evaluate its immunosuppressive effect on Th17 and its potential to prolong graft survival in animal model of solid graft rejection. In our animal experiment

that in currently under publication we show that RORγt inverse agonist can prolong graft survival in complete MHC mismatch transplantation into a sensitized mice to the extent that the graft survival rate approaches that of the same graft that is transplanted in non-sensitized mice. Moreover, these compounds inhibit antibody class switching and halt the buildup of B cell memory. This finding is novel and has not been reported before by any researcher and we expect it will open the venue for other researchers in the field to explore the potential of other RORγt inverse agonists in other organ transplantation models. In fact, and for our own surprise this therapy may revolutionize the science of immunosuppression in transplantation field, and we are looking forward to participating and guide our colleagues and researchers in this specialty, having big aspirations that this work will provide a new hope to patients who are currently suffering and looking for the community to help and support them. In summary, in this study we report two novel findings. First, the 2,3 derivatives of 4,5,6,7 tetrayhydro-benzothiophenes are potent inverse agonists of RORγt that can modulate the activity of Th17 cells. Second, RORγt modulators are effective in prolonging graft survival through a unique mechanism by inhibiting IgM to IgG3 class switching and the production of de novo donor specific antibodies or DSAs of IgG3 class and equally other classes promoted by Th17 signature cytokines such as the late in production IgG2a. In addition, RORγt invere agonists inhibit leukocyte infiltration to the skin graft and block the hyper acute cellular response through Th17 inhibition.

List of abbreviations

25HC	25-hydroxycholesterol
25NC	25-NBD cholesterol
AhR	aryl hydrocarbon receptor
AMR	antibody mediated rejection
APC	antigen presenting cells
APCI	atmospheric pressure chemical ionization
APSI	appearance potential soft ionization
ATG	anti-thymocyte globulin
ATGAM	lymphocyte immune globulin, anti-thymocyte globulin
Bcl-xL	B-cell lymphoma-extra large
C4d	complement 4d
C5	complement 5
CAR	constitutive androstane receptor
CD3	cluster of differentiation 3
CD4	cluster of differentiation 4
CD8	cluster of differentiation 8
CD16	cluster of differentiation 16
CD18	cluster of differentiation 18
CD20	cluster of differentiation 20
CD25	cluster of differentiation 25
CD28	cluster of differentiation 28
CD45	cluster of differentiation 45

CD52	cluster of differentiation 52
CD117	cluster of differentiation 117
CD127	cluster of differentiation 127
CD138	cluster of differentiation 138
CD169	cluster of differentiation 169
CDC	complement-dependent cytotoxicity crossmatch
CDI	1,1′-carbonyldiimidazole
Cl_{in}	intrinsic clearance
CMV	cytomegalovirus
cPRA	calculated panel reactive antibody
DBD	DNA-binding domains
dGTP	deoxyguanosine triphosphate
DIPEA	N,N-diisopropylethylamine
DMARD	disease modifying anti-rheumatic drugs
DSA	donor specific antibody
E_{bconf}	energy of conformer (pocket bound)
E_{conf}	energy of conformer
EDC	1-ethyl-3-(3-dimethylaminopropyl) carbodiimide
ERRα	estrogen-related receptor alpha
FBS	fetal bovine serum
Fc	fragment crystallizable region
FDA	food and drug administration
FEP	free-energy perturbations

FES	free-energy surface
FKBP	FK506 binding protein
FP	fluorescence polarization
FXR	farnesoid X receptor
G	Gibbs energy
G_{EXP}	experimental Gibbs energy
G_{FEP}	FEP calculated Gibbs energy
GMP	guanosine monophosphate
GR	glucocorticoid receptor
GTP	guanosine triphosphate
GVHD	graft versus host disease
HLA	human leukocyte antigen
HNF4α	hepatocyte nuclear factor 4 alpha
HNF4γ	hepatocyte nuclear factor 4 gamma
HTVS	high-throughput virtual screening
IBD	inflammatory bowel disease
IgG	immunoglobulin G
IgG1	immunoglobulin G 1
IgG2a	immunoglobulin G 2a
IgG3	immunoglobulin G 3
IgG4	immunoglobulin G 4
IgM	immunoglobulin M
IL1β	interleukin 1 beta

IL2	interleukin 2
IL2R	inteleukin 2 receptor
IL4	interleukin 4
IL6	interleukin 6
IL6R	interleukin 6 receptor
IL10	interleukin 10
IL12	interleukin 12
IL13	interleukin 13
IL17	interleukin 17
IL17A	interleukin 17A
IL17F	interleukin 17F
IL21	interleukin 21
IL22	interleukin 22
IL23	interleukin 23
ILC	innate lymphoid cells
ILC1	innate lymphoid cell 1
ILC2	innate lymphoid cell 2
ILC3	innate lymphoid cell 3
IVIG	intravenous immunoglobulin
Lin	lineage
LipE	lipophilic efficiency
$LipE_{ilogP}$	lipophilic efficiency based on ilogP
$LipE_{logD}$	lipophilic efficiency based on log D

LXR   liver X receptor

Ly6G   lymphocyte antigen 6 complex locus G

MDR1-MDCKII canine MDR1 knock-out, human MDR1 knock-in MDCKII

MMF   mycophenolate mofetil

MsCl   methane-sulfonyl chloride

mTOR   mammalian target of rapamycin

MUE   mean unsigned error

NEt3   triethylamine

NK   natural killer

PBMCs   peripheral blood mononuclear cells

PPARα   peroxisome proliferator-activated receptor alpha

PPARβ   peroxisome proliferator-activated receptor beta

PPARγ   peroxisome proliferator-activated receptor gamma

PPARδ   peroxisome proliferator-activated receptor delta

PRCA   pure red cell aplasia

PXR   pregnane X receptor

RDF   radial distribution function

RLU   relative light units

rmsf   root-mean-square fluctuation

ROCK2   Rho associated coiled coil containing protein kinase 2

RORα   retinoic acid receptor-related orphan receptor alpha

RORβ   retinoic acid receptor-related orphan receptor beta

RORγ   retinoic acid receptor-related orphan receptor gamma

RORγt	retinoic acid receptor-related orphan receptor gamma t
RORE	ROR response element
SP	standard precision
SRC-1	steroid receptor coactivator 1
Tfh	T follicular helper
Tfh1	T follicular helper 1
Tfh2	T follicular helper 2
Tfh17	T follicular helper 17
TGFβ	transforming growth factor beta
Th1	T helper 1
Th2	T helper 2
Th17	T helper 17
TNF	tumor necrosis factor
TPSA	topological polar surface area
TR	thyroid hormone receptor
TR-FRET	time-resolved fluorescence energy transfer
XP	extra precision

List of figures

List of tables

List of schemes

Introduction

&

aim of the work

Transplantation is a lifesaving procedure for end stage kidney disease patients, that decreases the mortality, the morbidity and health-care costs compared to dialysis. (Garcia et al., 2012; Tonelli et al., 2011) Kidney transplantation candidates are categorized according to their immunoreactivity against donor HLA antigens into three groups highly sensitized, moderately sensitized, and non-sensitized. Sensitization of solid organ recipients is a medical challenge that affects the future expansion of transplantation surgery intervention to a wider in-need population. Highly sensitized kidney patients are good examples of the problem, and they are estimated to be 8.5-30% of kidney transplantation candidates on the waitlists at transplantation centers based on centers candidacy criteria. (Jordan et al., 2015; Parsons et al., 2017; Perosa et al., 2021) Highly sensitized patients are defined by a high calculated panel reactive antibody (cPRA) of >80%, where they have pre-formed antibodies against HLA of >80% of the possible donors and develop antibody mediated rejection (AMR) and their chance of keeping a kidney graft is low. (Gebel et al., 2016) Moderately sensitized (cPRA =20-80%) and non-sensitized (cPRA <20%) patients also develop an AMR at lower rates by producing de novo antibodies against their donor antigens. With the current advances in immunosuppression, acute cellular, AMR or mixed rejection that happens days or weeks after transplantation became fewer common causes of kidney transplant rejection; while the rejection due to chronic AMR became the most common cause of graft rejection which occurs typically 1-10 years post-transplantation. The graft survival rates for cadaveric kidney recipients almost doubled over the last two decades due to the advancements in donor/recipient matching process. However, for living donor kidney recipients, these rates remained constant since the introduction of cyclosporine immunosuppressive regimens

in 1980s with no significant added advantage with matching strategies. For highly sensitized patients, although antigenic matching had positive impact on graft survival in this group, it is difficult to locate a matching donor in this category and their chances to get a kidney transplantation is still limited. (Lamb et al., 2011; Park et al., 2021) In Australia, Canada and UK, the current ten years kidney transplant survival rates are 59, 58 and 56% respectively; while in USA, the rate drops to 43%. This difference is attributed to restrictions on life-time immunosuppressive insurance coverage. These restrictions lead to a non-adherence to the immunosuppressive maintenance therapy and eventually graft rejection due to an uncontrolled immunologic activity against the graft. (Gill & Tonelli, 2012) The current graft survival rates are achieved mainly due to the use of conventional anti-rejection immunosuppressants such as cyclosporine A, tacrolimus, and corticosteroids and induction immunosuppression. These agents are only effective in preventing T-cell mediated kidney rejection in moderately sensitized and non-sensitized patients. They are not effective in the treatment of highly sensitized patients who remain on waitlists as their chances of getting compatible kidneys are limited. In addition, the conventional immunosuppression regimens are not effective in instances where an acute or chronic AMR has developed which are more frequent in cases of HLA incompatible kidney transplantation. (Park et al., 2021) The limitations of the currently approved and widely used immunosuppression regimens dictate the necessity for finding and introducing new therapies to overcome acute cellular and AMR in highly sensitized recipients as well as acute and chronic AMR in incompatible HLA kidney transplantation. For highly sensitized transplantation candidates, in addition to plasmapheresis, rituximab (B-cell depleting antibody) and bortezomib (anti-cancer proteasome inhibitor) are

proposed treatments for AMR based on off-label trials, but their efficacy is still under evaluation. (Lachmann et al., 2017; Park et al., 2021) The rational for the suggested therapies is that highly sensitized candidates have better patient survival when they get HLA incompatible kidney transplantation compared to their survival while remaining on dialysis. (Park et al., 2021) However, in case these recipients could keep their graft under standard immunosuppression regimens, they may require repeated doses of rituximab and plasmapheresis. In addition to such efficacy limitations, currently approved and other off label immunosuppressants have significant side effects that in many cases limit their use in kidney transplantation patients. (Tonelli et al., 2011) Therefore, there is a need to develop new anti-rejection immunosuppressants that are better targeted and less toxic than the currently used ones. Previous research has highlighted the role of Th17 in promoting lymphoid neogenesis inside the graft creating a tertiary lymphoid tissue in which humoral immune response is elicited leading to AMR. (Deteix et al., 2010) In animal studies, Th17 has been shown to promote neutrophilic infiltration into cardiac graft in T-bet deficient mic. The neutralization of IL17A in this model resulted in reduction of infiltrating neutrophils, lymphocytes, eosinophils and macrophages. (Yuan et al., 2008) Other studies pointed at Th17 and other IL17A producing cells among the possible target cells that contribute to both cellular rejection and AMR by promoting B-cell differentiation and antibody class switching. (Zhang & Reed, 2016) The neutralization of IL6 or blockade of IL6R have been shown to improve clinical outcomes of chronic AMR reducing donor specific antibodies (DSAs) levels and C4d scoring. (Jordan et al., 2022) The monoclonal antibodies treatment showed good long term safety profile in adult and pediatric kidney transplantation patients. (Jordan et al., 2022; Pearl et al., 2022) Although the investigators

did not measure the effect of IL6 neutralization on the differentiation of T cells to Th17 phenotype. IL6 is known to promote the differentiation of T cells to Th17 phenotype and Th17 association with DSAs production is a key mechanism that requires further investigation. A key regulator of Th17 activity is the nuclear receptor and transcription factor retinoic-acid-related orphan receptor gamma t (RORγt), which is also considered the master regulator of Th17 and other IL17A producing cells. (Ivanov et al., 2007) Accordingly, we hypothesized that **RORγt inverse agonists can prevent and treat AMR in highly sensitized solid organ transplantation recipients**. This therapeutic effect can occur through decreasing the expression of IL17A, IL21 and IL22 which are the signature cytokines of Th17 and other RORγt positive immune cells. Such a reduction in Th17 signature cytokines will eventually inhibit the formation of tertiary lymphoid tissue, decrease B lymphocytes activity, block its differentiation, and inhibit antibody class switching. This will finally lead to the inhibition of AMR and increase solid graft survival. The first objective of the current study is to discover and develop novel small molecule class of RORγt modulators that possess favorable physicochemical properties, oral bioavailability, and low toxicity profile. The second objective of the current study is to evaluate the effects of the novel RORγt inverse agonists on Th17 differentiation and the production of Th17 signature cytokines against reference RORγt inverse agonists. The third objective of the current study is to evaluate the immune modulatory effects of the novel RORγt inverse agonists on Th17 cells and other immune cells that express RORγt in the context of solid organ graft rejection and specifically during acute cellular rejection and AMR in a sensitized murine model of complete mismatch skin transplantation.

Literature review

Graft rejection mechanisms

Both cellular and humoral responses are observed in allograft rejection. T-cell mediated rejection is often acute. This type of rejection is less frequently seen in transplantation now due to the successful immunosuppression and improved cross matching protocols. The mechanism underlying T-cell mediated rejection is believed to be Th1 mediated activation of CD8+ T cells and natural killer (NK) cells, this type of rejection is very well controlled with immunosuppressive induction therapy, calcineurin and mTOR inhibitors maintenance therapy. (Djamali et al., 2014) B-cell mediated or commonly known as antibody mediated rejection can be hyper acute, acute, or chronic. This kind of rejection is hard to prevent and even when prevention is achieved for a short period it is hard to maintain long term. Chronic antibody mediated rejection progresses slowly and accumulates miniature injuries to the allograft over time. This type of rejection is now considered the major cause of renal graft rejection. (Djamali et al., 2014; Lachmann et al., 2017) In hyper-acute AMR, which is becoming very rare now, a strong humoral reaction (HLA antibody mediated rejection) followed by complement activation and a strong non-specific cellular cytotoxicity is observed. This kind of rejection is clinically predictable in highly sensitized transplantation candidates using detection methods such as complement-dependent cytotoxicity crossmatch (CDC). It can be prevented by B-cell depletion, low or high IVIG desensitization treatment and plasmapheresis in addition to following a strict donor/recipient cross-matching approach. (Zachary & Leffell, 2014) These restrictions and sophisticated prevention protocols lead to a delay in transplantation of highly sensitized patients resulting in a longer waiting time for this patient population. (Gebel et al., 2016) In cases of acute and chronic antibody mediated rejection, the patients develop de novo antibodies against the HLAs and other donor

antigens. (Lachmann et al., 2017) The occurrence of such types of rejections cannot be clinically determined per individual either because the recipients were not sensitized to the donor antigens in the first place and the reaction occurs spontaneously following transplantation or they have a very low DSAs titer that is below the CDC detection limits. The low DSAs titers can be detected by other methods such as flow cytometry crossmatch that is not routinely performed.   Despite their utility in stratifying transplantation candidates, cPRA measurements using a mixed lymphocytes reaction provide information about lymphocytes cross-matching rather than complete donor/recipient antigen phenotype cross-matching. In addition, cPRA provides data about the existing preformed anti-HLAs antibodies rather than the expected to develop de novo antibodies which will be completely unknown until they are produced. (Konvalinka & Tinckam, 2015)

Molecular mechanisms underlying antibody mediated rejection.

Antibody mediated rejection starts with the production of antibodies against donor specific antigens known as donor specific antibodies or DSAs. These antibodies bind to their antigens primarily located on the basement membrane of the transplanted organ which is the kidney in the case of renal transplantation. Following that binding, a well-defined cascade of events resembling the body's response to bacterial antigens occurs. (Djamali et al., 2014) The binding of antibodies to HLAs and other non-HLA antigens leads to the activation of complement classical pathway and a membrane attack complex is formed. (Murata & Baldwin, 2009; Zhang & Reed, 2016) The products resulting from complement binding such as C5 work as chemokines, and they attract neutrophils, macrophages, monocytes and other cell types. These cells which are non-specific attack the cells pound to the antibodies regardless of the antigen type. CD8+ T cells, NK cells and T helper cells

are also believed to be effectors in the chronic rejection following complement binding. (Ricklin et al., 2010) Following the activation, the insoluble complement activation product C4d is deposited on the kidney basement membrane which allows for its use as a diagnostic marker for antibody mediated rejection. (Murata & Baldwin, 2009) Interestingly, targeting complement alone with anti-C5 antibody eculizumab showed limited success that didn't extend beyond one year in positive cross match (moderately sensitized or non-sensitized). (Cornell et al., 2015) This specific observation highlighted the significance of complement independent antibody mediated rejection as previously suggested in several studies and clinically recognized as C4d negative AMR. (Haas, 2013) The mechanism underlying this pathway is described as antibody dependent cytotoxicity, where the effector cells are activated by the Fc portion of the antibody through direct binding. (Resch et al., 2015) Following the activation of complement and the engagement of different cell types at the site of inflammation, the feedback given to B cells is complex in nature and involves a wide range of cytokine, chemokine signaling and a wide range of cell types including different subtypes of T helper cells, monocytes, macrophages, neutrophils and dendritic cells. This feedback leads to the proliferation of effector B cells with the subsequent continuous production of DSAs. (Clatworthy, 2011)

Th17 role in graft rejection

Th17 is a distinct population of T helper cells that is involved in innate and adaptive immunity. They are abundant in gut mucosa and believed to protect the body against the infiltration of natural microbiota and pathogenic bacteria to blood circulation by two mechanisms; first, by enhancing intestinal mucosal integrity and tight junctions' repair; second, by recruiting macrophages, natural killer, and cytotoxic cells to infiltration sites.

(Song et al., 2015) On the other hand, Th17 cells are believed to be involved in autoimmune diseases involving tissue damage as well as in transplant rejection. In these conditions, IL17 is believed to be profibrotic. (Hünemörder et al., 2015) In is frequently observed that Th17 activity is increased in the conditions characterized by the production of high levels of autoantibodies such as systemic lupus, rheumatoid arthritis, and multiple sclerosis. Like AMR, these conditions are initiated by antibodies and depend on complement activation and Fc receptor binding for subsequent inflammation to occur. (Fang et al., 2009) It has been shown that transplantation patients with chronic allograft dysfunction have an increased Th17 phenotype. (Chung et al., 2016) This observation suggests a close relationship between Th17 activation and DSAs production, however this relationship is not well investigated. In addition to their suggested B-cell helper cell model inside and outside the primary and secondary lymphoid tissue germinal centers, Th17 are believed to promote the generation of tertiary lymphoid tissues in the allograft, which harbors B-cell differentiation and antibody class switching outside the germinal center. This interesting model argues for a central role of Th17 in initiating the events leading to graft rejection. The activation leads to IL17A, IL17F, IL21 production. These cytokines trigger the formation of tertiary lymphoid tissue, B-cell activation, and autoantibodies production. In this isolated environment the autoreactive B and T cells escape negative selection. (Cardinal et al., 2017) Applying this model to transplantation, the terms alloreactivity and autoreactivity to HLA and non-HLA antigens are both involved in the inflammatory response to the allograft. (Patakas et al., 2012; Zhang & Reed, 2016)

AMR, IgG classes, preformed and de novo antibodies

As previously mentioned, AMR starts with antibody formation followed by complement activation or direct binding of effector cells. The antibody classes involved in complement binding dependent AMR are IgG1, IgG3 and to a less extent IgG2a while IgG4 is involved in non-complement dependent AMR. (Vidarsson et al., 2014; Zhang, 2018) Antibody class switching requires IL21 secretion from Tfh or other closely identified Thf1, Tfh2, Tfh17 cells. Antibody class switching to a specific antibody subclass requires additional cytokines. IL4 and IL13 promote class switching to IgG1, while IFNγ promotes IgG2a. IL17A promotes class switching to IgG2a and IgG3 subclasses. (Firacative et al., 2018; Olatunde et al., 2021; Tuzlak et al., 2021) class switching to IgG4, on the other hand, is promoted by IL4, IL13 in presence of TGFβ and IL10. (De Sainte Marie et al., 2020) IgG1 and IgG3 are class I DSAs as the target HLA class I. This class is detected early following transplantation and is responsible for acute AMR. IgG2a and IgG4 are class II. These two classes are detected later and involved in subclinical and chronic AMR. IgG2a has a week complement binding and activation potential, while IgG4 is believed to be the major player in chronic AMR through non-complement recruitment mechanisms where the immune cells like CD8+ cells, macrophages bind directly to the antibody Fc portion rather than C4d aggregates on the basement membrane. (Zhang, 2018) Preformed DSAs in sensitized patients can be class I, class II or both and their presence affects transplantation decision making. (Ma et al., 2016) Similarly, de-novo antibodies can be from any class, however their formation is unpredictable. Strategies should be adopted to target the processes leading to their production such as targeting Th17 cells.

Molecular mechanisms of immunosuppression

Immune suppression is an important pharmacotherapeutic intervention that is essential in maintaining life quality, reduction of mortality and morbidity of patients suffering from autoimmune diseases and other medical conditions caused or aggravated by the activation of the immune system such as the case in allograft rejection. Immunosuppressants can be chemically classified as steroidal immunosuppressants, non-steroidal immunosuppressant small molecules, antibodies, and other macromolecules of bio-origin. Steroidal immunosuppressants describe the corticosteroids that target the corticosteroid nuclear receptor such as prednisone and dexamethasone. Non-steroidal immunosuppressant small molecules are a heterogenous collection of small molecules that targets the immune cell at nuclear, cytoplasmic or cell surface receptors such as azathioprine and methotrexate. Antibodies include polyclonal and monoclonal antibodies that target the surface receptors of the immune cells such as anti-thymocyte globulin and anti-CD25 monoclonal antibodies. The fourth group includes other macromolecules of bio-origin that don't fall under the description of the other three categories such as cyclosporine and tacrolimus.

Steroidal immunosuppressants

Steroids describe a large group of molecules of natural and synthetic origin. Natural steroids are classically classified into glucocorticoids that contribute to metabolic homeostasis, mineralocorticoids which contribute to fluid and mineral homeostasis and gonadocorticoids or sex hormones. The immunosuppressive effects of glucocorticoids were discovered in 1940s and provided the bases for modeling synthetic steroids starting by the synthesis of prednisone in 1950 and dexamethasone in 1957, which are widely

used to treat acute and chronic inflammatory conditions, autoimmune disease and as transplantation induction and maintenance therapy. (Arth et al., 1958; Nobile, 1994) Steroids reduce the volume and activity of immune system and inhibit leukocytes proliferation. Most popular Corticosteroid regimen consists of a high intraoperative dose of 5 to 10 mg/kg of methylprednisolone, which is followed by maintenance 1 mg/kg per day of prednisone, which is tapered to 0.05-0.1 mg/kg per day of prednisone by the first year. (Steiner & Awdishu, 2011) Due to the undesirable side effects of maintenance corticosteroids therapy such as effects on growth in pediatric patients, increased risk of infections, bone disorders, metabolic complications, adrenal insufficiency, cardiovascular risks, neuropsychiatric, gastrointestinal, and muscular side effects, several studies suggested withdrawing the corticosteroids treatment completely starting three months following successful transplantation. (Dashti-Khavidaki et al., 2021; Woodle et al., 2021) Steroids are used as a part of triple maintenance therapy regimen along with a calcineurin inhibitor and an antimetabolite such as mycophenolate mofetil. (Olaso et al., 2021)

Antibodies and immunoglobulins

Immunosuppressive antibodies and immunoglobulins are widely used to treat autoimmune diseases and to prevent graft rejection. The most well-known immunosuppressive human monoclonal antibody is anti-TNF alpha adalimumab which is the first in class to get FDA approval to treat rheumatoid arthritis and is also used for psoriasis, ulcerative colitis, and sarcoidosis. Ustekinumab anti IL12 and IL23 is another human monoclonal antibody originally approved for psoriasis is showing comparable endoscopic remission results in treatment of Crohn's disease and was effective and safe in treatment of ulcerative colitis in refractory patients and in patients with prior drug

failures. Dupilumab anti-IL4 & IL13 is another human monoclonal antibody that is showing excellent safety and comparable efficacy to topical corticosteroid in treatment of eczema, atopic dermatitis asthma and eosinophilic esophagitis. In organ transplantation, antibody treatment is used as induction immunosuppression therapy.

Anti-thymocyte globulin (ATG)

Horse lymphocyte immune globulin, anti-thymocyte globulin (ATGAM) and thymoglobulin rabbit anti-thymocyte globulin (ATG) target T-cell surface proteins such as CD2, CD3, CD4, CD8, CD16, CD18, CD25 and CD45. (Jha et al., 2021; Kim et al., 2012) Binding to surface receptors activates immune signals that leads to complement-mediated lysis of lymphocytes. (Mohty, 2007) ATGAM was the first anti-thymocyte approved and indicated for treating and preventing acute rejection after kidney transplantation. (Gaber et al., 1998; Hardinger et al., 2004) ATG was initially approved for treating acute rejection, and was only recently as induction immunosuppression, although it has been used for induction therapy since 1998. (Alloway et al., 2019; Brennan et al., 1999; Gaber et al., 1998; Grafals et al., 2014; Shim et al., 2023) Thymoglobulin and ATGAM treatments are associated with adverse effects like serum sickness, hematological toxicities (thrombocytopenia, leucopenia), cytomegalovirus infections, anaphylactic reactions, and lymphoma. However, their benefits in improving graft survival outweigh their risks and more notably risk of lymphoma in kidney transplantation receipts. (Gaber et al., 2010; Hardinger et al., 2008; Heifets et al., 2004; Kashiwagi et al., 1968; Mourad et al., 2004; Opelz et al., 2006)

Interleukin-2 receptor (IL2R) antagonist

Basiliximab is a chimeric monoclonal antibody that binds with the alpha chain (CD25) of IL2 receptor (IL2R) presented on the surface of the activated helper T cells so that it blocks its binding with IL2 and consequently prevents helper T-cell proliferation without causing their lysis as in the case with the use of ATG. (Olyaei et al., 2001) Basiliximab is approved as a prophylaxis against acute rejection following renal graft transplantation. (Kahan et al., 1999; Nashan et al., 1997; Willoughby et al., 2009) It is currently recommended to be used in recipients with low risk of rejection. (Ajlan et al., 2021) A meta-analysis of studies done on basiliximab and ATG as induction have shown that basiliximab has a similar efficacy to ATG, however it is superior to ATG when comparing long term side effects, where basiliximab induction is associated with lower rates of neoplasm compared to ATG. (Wang et al., 2018) Basiliximab is well tolerated and was not associated with serious adverse effects and was not different from placebo including infections and risks of developing lymphomas, however hypersensitivity reactions can occur after administration. (Nashan et al., 1997; Webster et al., 2004)

Anti-CD52 antibodies

Alemtuzumab is a humanized monoclonal antibody that triggers antibody dependent cell lysis by binding to CD52 molecule on the surface of T and B cells, macrophages, and NK cells. Although it is approved for B-cell lymphocytic leukemia, its use for induction therapy in kidney transplantation has been increasing since 1998 as it has been shown to be superior to conventional induction therapy in reducing acute rejection. (Chukwu et al., 2022; Hanaway et al., 2011) For this purpose, it is administrated intravenously as a single dose of 30 mg intraoperatively. Lower dose of 20 mg has been shown to be as effective

as the standard dose in preventing acute rejection with less side effects. (Guthoff et al., 2020) Like other lymphocyte depleting agents, alemtuzumab use increases the risk of infections such as CMV infection, lymphoproliferative malignancies. (Guthoff et al., 2020; Holmøy et al., 2019) It can cause autoimmune diseases such as thyroiditis, hepatitis, hemolytic anemia, anti-glomerular basement membrane disease, and agranulocytosis. (Guarnera et al., 2017; Meyer et al., 2013) It might cause hematological adverse effects such as thrombocytopenia, neutropenia, and lymphopenia. In addition, it may cause cytokine release syndrome and infusion-related reactions. (Holmøy et al., 2019)

<u>Anti-CD20 antibodies</u>

Rituximab is a chimeric anti-CD20 monoclonal antibody. CD20 is expressed on the surface of pre-B cells, premature and mature B cells. The receptor is not expressed on the surface of pro B cells or plasma cells. Rituximab is approved for the treatment of B cell lymphomas. It has been used in combination with IVIG or plasmapheresis to decrease antibody levels as a part of a desensitization protocol for highly sensitized kidney recipients. (Ide et al., 2015; Vo et al., 2014) It had also been used to treat acute and chronic AMR. (Sood & Hariharan, 2018) In a non-randomized clinical study it has been used at 1 g dose on days 7 and 22 along with high-dose IVIG (2 g/kg of body weight on days 0 and 30) pre-transplantation in highly sensitized patients. With this protocol the PRA decreased from 77±19% to 40±30%. (Vo et al., 2008) A meta-analysis of studies reporting clinical use of rituximab suggested that patients responded to rituximab favorably based on one or more of graft survival, function, creatinine levels, DSAs or B cell depletion outcomes. (Hychko et al., 2011)

Macromolecules

Tacrolimus

Tacrolimus suppresses the activation of calcineurin. It binds to an immunophilin, FK506 binding protein (FKBP). This complex inhibits calcineurin phosphatase and eventually inhibits the production and release of IL2 from activated T cells. This ultimately attenuates IL2 dependent activation signals leading to apoptosis of T cells and other immune cells dependent on T cell help. (Bentata, 2020) It is effective in the prevention and treatment of cellular acute rejection. Tacrolimus is used as a maintenance immunosuppression alone or in combination with steroids and antimetabolites. The starting dose of tacrolimus can be as high as 0.1-0.2 mg/kg per day and can be reduced to as low as 0.05mg/kg. (Chinnadurai et al., 2021; Chua et al., 2022) The maintenance dose of tacrolimus is calculated based on its blood levels to maintain trough levels of 5-15 ng/ml. (Hwang et al., 2021) Tacrolimus is not effective in the prevention or treatment of chronic AMR rejection. In addition, it was thought to be a risk factor of developing chronic AMR, however other studies found no association between tacrolimus use and AMR. (Kim et al., 2021; Sablik et al., 2018) Similarly, it has limited efficacy in treatment of acute cellular rejection, or AMR in highly sensitized patients. (Olaso et al., 2021)

Cyclosporine A

Cyclosporine A is a calcineurin inhibitor that has a broad pharmacological effect on the cells of immune system. The inhibition of calcineurin attenuates T cell response to IL2 activation signals and leads to other changes inside the cytoplasm such as the increase in calcium content leading to apoptosis. (Azzi et al., 2013) Cyclosporine A is now widely replaced by tacrolimus due to side effects. It is recommended doses are 2-6 mg/kg IV for

one dose over 2 to 6 hours and this is taken 12 hours pre-transplantation then 5-15 mg/kg per day by orally. (Mahalati et al., 2001) Similar to tacrolimus it has a narrow therapeutic window and monitoring blood levels is recommend maintaining a trough level of 150–300 ng/ml post-transplantation and 50-100 ng/ml at 12 months. (Tedesco & Haragsim, 2012) It is effective in prevention and treatment of acute cellular rejection and ineffective in the prevention or treatment of AMR. It is also ineffective in treatment of either cellular rejection or AMR is highly sensitized patients. (Rodriguez-Ramirez et al., 2022)

mTOR inhibitors

First generation mTOR inhibitors rapamycin or sirolimus and its analogue everolimus are both approved for maintenance therapy in kidney transplantation in combination with cyclosporine and steroids. (Nelson et al., 2022) Like tacrolimus they bind to FKBP, however they inhibit mTOR rather than calcineurin phosphatase. Like tacrolimus they interfere with IL2 dependent T cell activation and proliferation, however this is through the inhibition of activation signaling post to IL2 binding to IL2R rather than production and release of IL2. (Schuler et al., 1997) Sirolimus starting dose is 2 to 6 mg per day that is tapered to maintain trough levels of 5 to 10 ng/ml. (Ghasemi et al., 2020) Everolimus dose is 1.5 to 3 mg divided twice daily to maintain tough levels of more than 3 to 8 ng/ml. Trough levels above 8ng/ml are associated with increased toxicity. (Mabasa & Ensom, 2005; Pascual, 2009) Sirolimus is not recommended as standalone maintenance therapy as it has been associated with higher incidence of adverse events, biopsy proven acute rejection, allograft loss, sepsis and death. (Nelson et al., 2022) Everolimus has been associated with peripheral edema, constipation, and urinary tract infections and interferes. It is not recommended early post-transplantation as it interferes with would

healing. The side effects of mTOR inhibitors are myelotoxicity, dyslipidemia, delayed wound healing, lung toxicity, and aphthous ulcers. Both agents are linked to enhanced nephrotoxicity if co-administered with standard dose cyclosporine. (Nelson et al., 2022)

Small molecules

Azathioprine

Azathioprine is a purine analogue that interferes with both DNA and RNA synthesis and ultimately inhibits de novo purine synthesis. It was first used as an immunosuppressive drug in transplantation in 1961. (Nakamura, 1993) It was routinely used as maintenance therapy until widely replaced with other agents such as mycophenolate mofetil due to its side effects. It can be used as a component of triple therapy with calcineurin inhibitor and a steroid for maintenance therapy. (Chocair et al., 2022; Clayton et al., 2012) Currently, it is recommended for use in patients who don't tolerate mycophenolate mofetil toxicity or patients planning pregnancy. (Nelson et al., 2022) The initial dose of azathioprine is 3-5 mg/kg then goes down to 1-1.5 mg/kg/day. (Opelz & Döhler, 2000) Common adverse effects of azathioprine that require switching to another agents are myelosuppression, hepatotoxicity, alopecia, serum sickness. Life threatening conditions like severe myelosuppression and pancreatitis have also been reported. (Anstey et al., 2004; Sheiko et al., 2017; Varma et al., 1996; Zhou et al., 2021)

Mycophenolate mofetil

The active metabolite of mycophenolate, mycophenolic acid inhibits IMP dehydrogenase, thereby depleting GMP, GTP and dGTP. The depletion of these nucleotides within the cells prevents T-cell and B-cell proliferation, the production of cytotoxic T cells and antibodies. These effects lead to the suppression of T-cell and B-cell mediated rejection.

(Dalal et al., 2009) A combination of tacrolimus, MMF and prednisolone is commonly used for de novo kidney transplant recipients and has been associated with excellent clinical outcomes relative to other regimens. The recommended starting dose of MMF for renal transplantation is 2 g daily. (Ruggenenti et al., 2021) Few studies recommend that 1 or 1.5 g daily are equivalent to 2 g while other studies reported that dosing at 1 g or less results in an increase in the incidence of rejection. (Dave et al., 2020) Mycophenolate mofetil has been associated with serious adverse effects such as increased risk of sepsis, CMV infection, bone marrow suppression, gastrointestinal side effects and leukopenia. In addition, it is teratogenic and should be avoided 6 weeks before pregnancy. (Nelson et al., 2022) Interference with erythropoiesis and pure red cell aplasia (PRCA) have been reported in patients treated with MMF in combination with other immunosuppressants. (Engelen et al., 2003)

Bortezomib

Bortezomib is a reversible inhibitor of the 26S proteasome and inhibits the degradation of ubiquitylated proteins which is a mechanism used by the cell to recycle abnormal and misfolded proteins. 26S proteasome protein found in all cells, however it is highly active in cells such as plasma cells that produce high quantities of protein. This is the basis for their use in transplantation. It has been evaluated in small clinical trials alone or in combination with other agents such as rituximab, IVIG and plasmapheresis. A study has shown that one cycle of four doses of bortezomib at dose of 1.3 mg/m^2 (IV, Day 1, 4, 8, 11) was superior to rituximab (500 mg IV) in maintaining kidney function and graft survival in patients who received plasmapheresis and IVIG. (Waiser et al., 2012) A desensitization combination regimen of four doses bortezomib, rituximab and 2 doses of IVIG increased

the probability of deceased kidney transplantation in highly sensitized patients. (Jeong et al., 2016) A recent study showed that a graft rescue regimen of 3-4 doses bortezomib in combination with plasmapheresis with or without IVIG improved clinical outcomes in patients who had early biopsy-proven AMR and was not inferior to previously proposed regimens employing rituximab, plasmapheresis, IVIG, ATG or immunoadsorption. (Kolonko et al., 2020)

Other experimental therapies

Anti-IL6 and IL6R antibodies

Tocilizumab (anti-IL6R) and clazakizumab (anti-IL6) have been clinically evaluated in phase I and phase II open label trials in kidney transplantation patients as rescue therapy for chronic AMR or as an add-on therapy to standard immunosuppression for desensitization in highly sensitized kidney recipients. (Choi et al., 2017; Jordan et al., 2022; Pearl et al., 2022; Vo et al., 2022) The rational for using anti-IL6 and anti-IL6R antibodies is that IL6 which is produced by plasma-blasts, is a potent stimulator of humoral immunity and conversion of plasma-blasts to plasma cells. The effects of IL6 include stimulation of IL21 secretion from Tfh cells and from Th17 cells. In addition, it promotes T cell differentiation to Th17 phenotype and IL17A, IL17F production. These effects are mediated through IL6R which is found on T and B cells. (Jordan et al., 2017) Studies in mice have shown that mice deficient in IL6 have reduced memory response. (Chen et al., 2018) In the first clinical trial, an open-label case study, tocilizumab was used at 8 mg/kg monthly, maximal dose 800 mg for 6–25 months IV infusion and offered to patients who had chronic AMR and DSAs that failed IVIG and rituximab standard therapy with or without plasmapheresis. The patients treated with tocilizumab had a 6-

year graft and patient survival of 80% and 91%, respectively. There was a significant reduction of DSAs at 2 years. In the second study, open-label study, clazakizumab (anti-IL6) was offered as a rescue therapy to a small cohort of 10 highly sensitized patients undergoing chronic AMR. Clazakizumab was given monthly at a dose of 25 mg subcutaneously for 12 months, with a 6-month protocol biopsy. There was a reduction in g+ptc and C4d inflammation scores, reductions in DSAs and there was a trend towards a stabilization of eGFR and prolongation of graft survival compared to patients with chronic AMR treated with standard care. (Jordan et al., 2022) The third trial, clazakizumab 25mg/ kg was given as add-on therapy to IVIG, and plasmapheresis continued for 6 to 12 months. Patients were transplanted with incompatible kidney any time after day 7 following the IVIG/plasmapheresis/clazakizumab and up to 270 days. There was a reduction in DSAs, de novo DSAs produced and an increase in Tregs and Bregs. (Vo et al., 2022) In the fourth trial, monthly tocilizumab stabilized kidney function in pediatric patients who suffered from AMR. (Pearl et al., 2022) A recent randomized phase II clinical trial evaluated the efficacy and safety of clazakizumab in patients with late AMR. Clazakizumab use was associated with an early decrease in DSA levels. In addition, clazakizumab modulated AMR activity, and slowed the decline of renal function. (Doberer et al., 2021) Several centers are currently conducting phase III clinical trials to evaluate the efficacy of clazakizumab in treatment of late and chronic AMR. (Eskandary et al., 2019; Nickerson et al., 2022)

<u>Therapies targeting Th17 cells</u>

Biologicals and small molecules targeting Th17 cells or Th17 secreted cytokines IL17 and IL21 are now evaluated in preclinical or clinical trials for many inflammatory and

autoimmune diseases, and some were recently approved. These therapies can be useful for the treatment of solid organ rejection and graft versus host disease (GVHD) based on the similarity in pathogenesis with these inflammatory conditions. (McDonald-Hyman et al., 2015) Two anti-IL17 antibodies ixekizumab and secukinumab; and the anti-IL17 receptor brodalumab were recently approved for the treatment of plaque psoriasis. (Wasilewska et al., 2016) Few animal studies in mice have investigated the role of IL17 in allogenic corneal graft rejection with inconsistent results. One study showed that anti-IL17 treatment can reverse late allogeneic corneal graft rejection. (Yin et al., 2015) Neutralization of IL17 in mice received an MHC II mismatched heart transplant improved signs of vasculopathy and prolonged graft survival and prevented accelerated rejection in Tbet$^{-/-}$ mice. (Yuan et al., 2008) Anti-IL21 antibodies are also investigated in phase I/II clinical trials for rheumatoid arthritis and phase II for Crohn's disease. A small molecule inhibitor of ROCK2, an enzyme required to produce IL17 and IL21, was effective in alleviating arthritis in animal studies and is now tested in phase II clinical trial for psoriasis. Small molecule inhibitors of RORγt, a transcription factor that regulates the expression on IL17, IL21 and IL22 cytokines, are currently evaluated in rheumatoid arthritis, psoriasis, systemic lupus, inflammatory bowel disease and graft versus host disease animal models. Anti-IL21 antibodies and ROCK2 inhibitors are believed to be useful for the treatment of GVHD due to the critical role of IL21 and ROCK2 in the pathogenesis of GVHD. On the other hand, anti-IL17 antibodies and RORγt inhibitors were previously suggested as new oral therapies for both GVHD and solid organ rejection. (McDonald-Hyman et al., 2015) Moreover, IL17 neutralization proved to exacerbate inflammatory bowel disease, which renders that therapeutic approach less attractive. On the contrary,

the inhibition of RORγt limited the intestinal inflammation in *C. rodentium* infected mouse model which makes RORγt more convenient compared to anti-IL17 in the treatment of inflammatory and autoimmune conditions. (Withers et al., 2016) Despite that there are no prior studies investigating the potential of RORγt inhibitors in the treatment of AMR, however the results of recent clinical trials on anti-IL6 and anti-IL6R antibodies can be used to establish the grounds for evaluating RORγt inhibitors in solid organ transplantation as it is previously known that IL6 is essential for T cell differentiation to Th17. The drawback of these studies was that they did not investigate the effects of anti-IL6 or anti-IL6R therapy on Th17 cells and their effect on specific classes of IgG as aforementioned. (Choi et al., 2017; Jordan et al., 2022)

RORγt inhibitors

Retinoic-acid- receptor related orphan receptors (RORs) comprise a group of nuclear receptors that is widely distributed in human tissues. The RORs forms are RORα (also known as RORA), RORβ (RORB), RORγ (also known as RORγ or RORC). The specific natural ligand(s) of the receptors are not definitely recognized, however, several recent studies reported that cholesterol, cholesterol biosynthesis intermediates, oxysterols, and retinoic acid are natural ligands of the receptors. The receptor forms are expressed differently in human tissues. RORα is expressed in the brain, liver, kidneys, lungs, skeletal muscles, and thymus. RORβ is expressed in brain and retina. RORγ is expressed in the thymus, heart, pancreas, testicles, and prostate. (Fabio et al., 2015; Huh & Littman, 2012) The isoform of RORγ that is expressed in thymus is referred to as RORγt. Both ROR-α and RORγt are expressed in Th17; however, the inhibition of RORγt is sufficient to achieve the desired effects. A previous study has shown that the inhibition of RORγt alone

completely blocks the differentiation of Th17. (Yang et al., 2008) The mechanism of action of RORγt inverse agonist is the inhibition of RORγt binding to DNA RORE region. Inhibition of RORγt-RORE binding leads to a downregulation of downstream genes such as IL17A, IL21 and IL22, Figure 1.1. (Sun et al., 2018) RORγ/RORγt ligand binding pocket bears similarities to RORα and they bind same natural ligands with similar affinity. (Wang et al., 2010) The inhibition of RORα will theoretically result in off target adverse effects as the two receptors were found to regulate housekeeping activities in various cells.
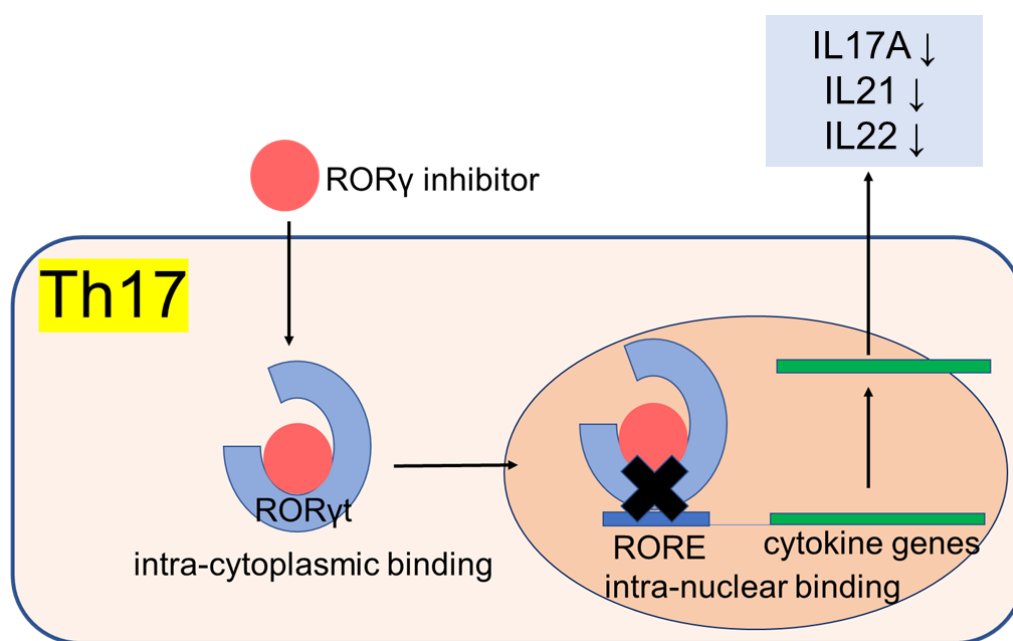

Figure 1.1. Mechanism of action of RORγt inhibitors

Studies have shown that RORα and RORβ null mice suffered severe developmental deformities. (Dussault et al., 1998; Jia et al., 2009) The ligand binding pocket of RORγt carries special characteristics in its cavity size, contour, and lipophilicity. The volume of the pocket is one of the largest among all the nuclear receptors. Compared to other nuclear receptors, there is a wide diversity in terms of the volume and size of the inverse agonists that were developed to modulate RORγt. Nuclear receptors' ligand binding

pockets are lipophilic with approximately 75% of the residues inside the pocket are hydrophobic residues. The volumes of ligand binding pockets of nuclear receptors are variable, and the ligands typically occupy >60% of the pocket volume which makes each nuclear receptor unique in its specificity and binding efficacy of ligands based on its volume and the distribution of the lipophilic and hydrophilic regions inside the pocket. The volume of RORγt and other nuclear receptors are pooled in table 1.1. (Benoit et al., 2004; Ingraham & Redinbo, 2005; Jin & Li, 2010; Madauss et al., 2004)
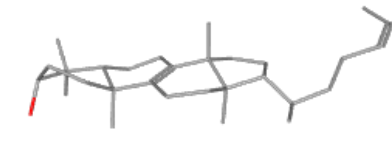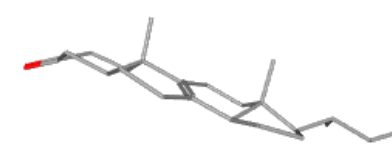
Table 1.1. Nuclear receptors ligand binding pocket volume
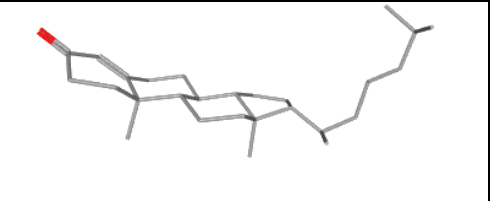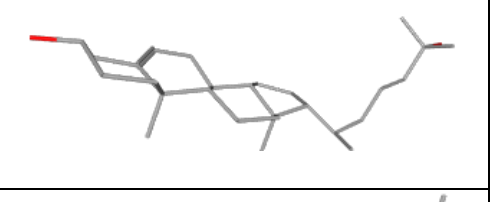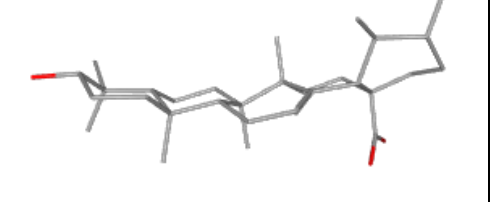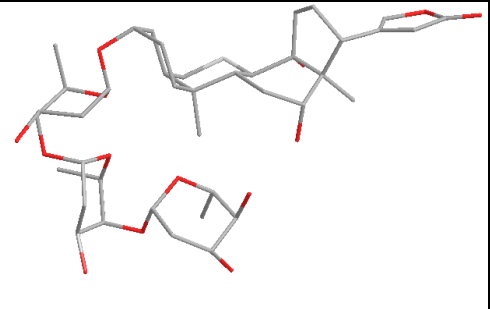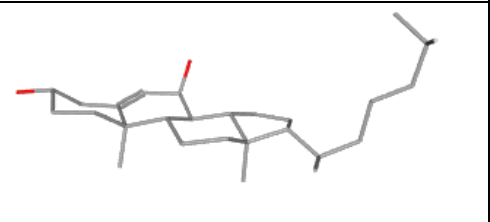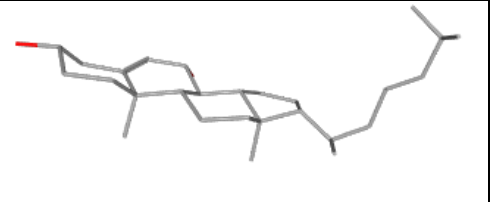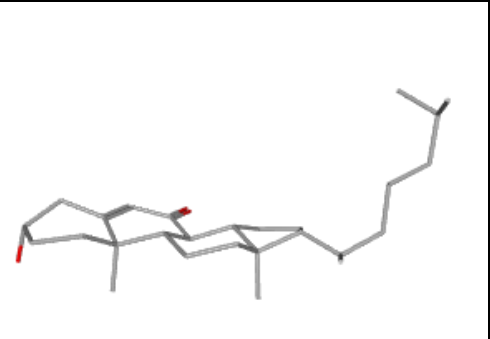
Nuclear receptor	Pocket volume apo	Pocket volume bound
Peroxisome proliferator-activated receptor (PPAR)γ	1600 $Å^3$	1600 $Å^3$
PPAR α (Pawlak et al., 2015)	1400 $Å^3$	1400 $Å^3$
PPARβ/δ	1300 $Å^3$	1300 $Å^3$
Pregnane X receptor (PXR)	1200-1600< $Å^3$	1200-1600< $Å^3$
Farnesoid X receptor (FXR) (Diao et al., 2018)	1081 $Å^3$	1081 $Å^3$
Liver X receptor (LXR)	700–800 $Å^3$	700–800 $Å^3$
RORγ (Li et al., 2017)	940 $Å^3$	940 $Å^3$
Constitutive androstane receptor (CAR)	675 $Å^3$	675 $Å^3$

Hepatocyte nuclear factor 4 alpha (HNF4α)	626 Å^3	626 Å^3
Thyroid hormone receptor (TR) β (Borngraeber et al., 2003)	600 to 700 Å^3	600 to 700 Å^3
Glucocorticoid receptor (GR)	540-1070 Å^3	540-1070 Å^3
Progesterone receptor	486-734 Å^3	486-734 Å^3
Hepatocyte Nuclear Factor 4 (HNF4γ)	370 Å^3	370 Å^3
Aryl hydrocarbon receptor (AhR) (Bisson et al., 2009)	201.5 Å^3	201.5 Å^3
Estrogen-related receptor α (ERRα)	100 Å^3	100 Å^3
REV-ERBβ	0 Å^3	500 Å^3

The lipophilic volume of RORγt ligand binding pocket constitutes >60% of the pocket volume, while hydrophilic basic and acidic volumes are <40%. (Li et al., 2017) Cholesterol, cholesterol derivatives, cholesterol precursors and several other sterols were identified as RORγ ligands. (Santori et al., 2015) Hydroxycholesterols such as 22-hydroxycholesterol, 25 hydroxycholesterol and 27 hydroxycholesterols are believed to be the natural substrates of RORγ. (Soroosh et al., 2014) The steroid conformations of most of the identified substrates are trans-trans-trans and they are mostly agonists, Table 1.2.

Table 1.2. Conformation and structure of natural ligands of RORγt

Ligand	Conformation	Bioactivity	Structure
coprostanol	cis-trans-trans	agonist (weak)	
cholesterol	trans-trans-trans	agonist	
lanthosterol	trans-trans-trans	agonist	
lanosterol	trans-trans-trans	agonist	
zymosterol	trans-trans-trans	agonist	
zymosterone	trans-trans-trans	agonist	
7-dehydro cholesterol	trans-trans-trans	agonist	

cholestenone	trans-trans-trans	agonist	
25-hydroxy cholesterol	trans-trans-trans	agonist	
ursolic acid	trans-trans-trans-cis	Inverse agonist	
digoxin	cis-trans-cis	Inverse agonist	
7alpha-hydroxy cholesterol	trans-trans-trans	agonist	
7 beta-hydroxy cholesterol	Trans-trans-trans	agonist	
7-keto cholsterol	Trans-trans-trans	agonist	

Several selective and nonselective inhibitors of the RORs have been identified in the last seven years. There is currently a fierce race between pharmaceutical companies to develop the first RORγt inhibitor for autoimmune diseases. **JTE-151** was the first RORγt inhibitor to enter Phase I trials for autoimmune disorders but was discontinued for undeclared reasons. Phase I clinical trials of topical **GSK 2981278** and oral **JTE-451** for treatment of plaque psoriasis, oral **TAK 828** for treatment of Crohn's disease and oral **ARN-6039** for treatment of multiple sclerosis were completed but results are not released yet. The oral **VTP-43742** entered phase II trials for psoriasis; however higher doses of **VTP-43742** (700mg) resulted in a reversible increase in serum transaminases in 4 study volunteers, which promoted the cancellation of further trials due to unwanted adverse effects. **VTP-45489** is announced as a backup to replace the **VTP-43742** in future clinical trials for the same indication. (Bronner et al., 2017; Gege, 2017) Different ROR-γt inhibitors are currently tested in preclinical studies for rheumatoid arthritis, autoimmune disease, psoriasis and inflammatory bowel disease. Hundreds of RORγt agonists and antagonists have been identified through multiple high throughput screenings using mainly four type of reporter cell lines namely 293T, Jurkat, Chinese hamster ovary and drosophila melanogaster RORγt reporter cell lines. (Ding et al., 2015; Huh et al., 2013; Huh et al., 2011) A series of compounds was discovered through a biochemical screening of the inhibitors of RORγt (LBD) binding to allosteric steroid receptor coactivator-1 (SRC-1) cofactor peptide. (Scheepstra et al., 2015) Medicinal scaffold hopping and direct chemical synthesis techniques were adopted by some pharmaceutical companies to produce their own RORγt inhibitors. (Gege, 2015; Hintermann et al., 2016; Wang et al., 2015) The status of many of the identified inhibitors is not known as most of the inverse

agonists are recently discovered and under investigation. Major pharmaceutical companies launched R&D programs, and many filed patent applications for RORγt inhibitors. Only a few articles were published on these programs mainly covering patented compounds. (Cyr et al., 2016) **MLR-248**, **MLR-367**, **GNE-3600**, **GSK805**, and Novartis imidazopyridine series are all newly discovered RORγt inhibitors that are now under development for treatment of several inflammatory conditions. The compounds suppress Th17 and inhibit IL17 production from PBMCs of healthy donors and patients suffering from inflammatory arthritis, inflammatory bowel diseases and autoimmune diseases. (Cyr et al., 2016; de Wit et al., 2016; Guendisch et al., 2017; Guntermann et al., 2017) Two of these compounds were found to induce thymic aberrations in mice. (Guendisch et al., 2017) This finding highlights a drawback of the RORγt inhibition as it was previously observed and lately confirmed that RORγt null mice develop lymphomas. (Liljevald et al., 2016; Ueda et al., 2002) This effect however is not considered a major hurdle in the way because the lymphomas developed in mouse models were not seen in humans with bi-allelic mutations in RORγt gene. (Okada et al., 2015) The current research in this area is dynamic and promising. For kidney transplantation patients it could provide them with an effective, yet tolerable medicine to be added to current immunosuppressive regimens to prevent or treat Th17 mediated rejection.

Article no.1

Title: Discovery, synthesis, and in vitro characterization of 2,3 derivatives of 4,5,6,7-tetrahydro-benzothiophene as potent modulators of retinoic acid receptor related orphan receptor γt

Authors: Ahmed Fouda[1,2], Sarita Negi[2], Oleg V. Zaremba[3], Rita S. Gaidar[4], Yurii S. Moroz[4,5], Eduard Rusanov[6,7], Steven Paraskevas[1,2,8,9], Jean Tchervenkov[1,2,8,9]

Affiliations:[1]Department of Experimental Surgery, McGill University, Montréal, Québec H3G 1A4, Canada; [2]Research Institute of the McGill University Health Centre, Montréal, Québec H3H 2R9, Canada;[3]Enamine Ltd, Kyïv 02660, Ukraine;[4]Chemspace LLC, Kyïv 02094, Ukraine;[5]Taras Shevchenko National University of Kyïv, Kyïv 01601, Ukraine; [6]Institute of Organic Chemistry, National Academy of Sciences of Ukraine, Kyïv 02094, Ukraine;[7]Department of Chemistry and Applied Biosciences; ETH Zürich, Zürich CH-8093, Switzerland;[8]Department of Surgery, McGill University, Montréal, Québec H3G 1A4, Canada;[9]McGill University Health Centre, Montréal, Québec H4A 3J1, Canada

Abstract: Retinoic acid receptor-related orphan receptor γt (RORγt) is a nuclear receptor that is expressed in a variety of tissues and is a potential drug target for the treatment of inflammatory and auto-immune diseases, metabolic diseases, and resistant cancer types. We herein report the discovery of 2,3 derivatives of 4,5,6,7-tetrahydro-benzothiophene modulators of RORγt. We also report the solubility in acidic/neutral pH, mouse/human/dog/rat microsomal stability, Caco-2, and MDR1-MDCKII permeabilities of a set of these derivatives. For this group of modulators, inverse agonism by steric clashes and push–pull mechanisms induce greater instability to protein conformation compared to agonist lock hydration. Independent of the two mechanisms, we observed a basal modulatory activity of the tested 2,3 derivatives of 4,5,6,7-tetrahydro-benzothiophene

toward RORγt due to the interactions with the Cys320-Glu326 and Arg364-Phe377 hydrophilic regions. The drug discovery approach reported in the current study can be employed to discover modulators of nuclear receptors and other globular protein targets.

Introduction

Retinoic acid receptor related orphan receptor gamma t (RORγt) ligand binding domain (LBD) is a 12-helix globular protein of a compelling drug target profile in cancer and autoimmune/inflammatory diseases (Ding et al., 2015; Ecoeur et al., 2019; Huh et al., 2011; Oh et al., 2016; Santori et al., 2015; Smith et al., 2016; Wang et al., 2016; Yoshida et al., 2016). The receptor has been extensively investigated in the past decade for its structural features, biological functions and most importantly for its candidacy as a drug target (Ding et al., 2015; Fulton et al., 2012; Huang et al., 2020; Huh et al., 2011; Kallen et al., 2017; Ranieri et al., 2020; Santori et al., 2015; Soroosh et al., 2014; Tan et al., 2013; Vonarbourg et al., 2010; Wang et al., 2016; Xiao et al., 2014). Several X-ray crystallography and NMR structural studies have identified numerous ligands, agonists, inverse agonists, and antagonists, with over 100 published crystal structures (Hintermann et al., 2016; Huang et al., 2020; Huh et al., 2011; Kallen et al., 2017; Li et al., 2017). These studies offer an opportunity for researchers to generate novel ligand design concepts. During development, most of the preclinical and clinical candidates were rejected based on safety and side effect profiles (Ding et al., 2015; Ecoeur et al., 2019; Guendisch et al., 2017; Liu et al., 2020; Soroosh et al., 2014; Xiao et al., 2014). Despite these unsuccessful trials the interest in developing RORγt modulators did not fade away and more studies were released reporting vastly diverse binding modes of new ligands that differ significantly in their chemical structure, in addition to the identification of

allosteric and sub-orthosteric pockets (Kallen et al., 2017; Scheepstra et al., 2015; Sun et al., 2018; Yuan et al., 2019). It has become apparent that both typical and so-called atypical ligands are much more diverse and can confer varied conformational changes at the structural level in terms of protein stability, helix-helix interactions, ligand binding domain (LBD) coactivator or corepressor recruitment. These are differentially reflected in biological function *in vivo* and comprise a large group of modulators with a corresponding range of potency and efficacy (Noguchi et al., 2018; Saen-Oon et al., 2019; Sun et al., 2018; Yuan et al., 2019). Crystallography studies on RORγt have revealed substantial structural information about the binding pocket and its key features (Huang et al., 2020; Kallen et al., 2017; Li et al., 2017; Noguchi et al., 2018). Orthosteric ligand binding pocket of RORγt carries special characteristics in its cavity size, contour, and lipophilicity. Its size is one of the largest among all nuclear receptors. The volume of the pocket is 940 Å^3 (Huang et al., 2020; Kallen et al., 2017; Li et al., 2017; Scheepstra et al., 2015). The lipophilic volume of the receptor is 575 Å^3(61 %), while hydrophilic, basic, and acidic volumes are 161 Å^3 (16%) and 178 Å^3 (19%) and 26 Å^3 (3%), respectively (Noguchi et al., 2018; Scheepstra et al., 2015). The pocket preserves plasticity regardless of the molecular volume occupied with agonists/inverse agonists, which vary in size from 200 to 800 g/mol (Huang et al., 2020; Kallen et al., 2017; Li et al., 2017). One of the key substructures of ligand pocket is the agonist lock His479-Tyr502-Phe509, which lays on the outer end of ligand binding pocket and the back wall of coactivator/corepressor binding pocket and is considered a key target for synthetic agonists (Fauber et al., 2013; Kallen et al., 2017; Saen-Oon et al., 2019; Sun et al., 2018; Yuan et al., 2019). The interruption/dissociation of the His479-Tyr502 hydrogen bond results in a subsequent

disruption of H11-H12 helix-helix interaction and eventually further impedes H12 coactivator interaction. On the other hand, conformational changes in H3 and H5 helices, which interface with both ligand binding pocket and the back wall of coactivator binding pocket, can disrupt protein-coactivator interaction. Such disruptions lead to the reduction or complete loss of RORγt activity (Huang et al., 2020; Kallen et al., 2017; Li et al., 2017; Saen-Oon et al., 2019; Sun et al., 2018; Yang et al., 2014; Yuan et al., 2019). Molecular dynamics simulation studies have shown that the chemical structure of an inverse agonist and its mode of binding can greatly affect protein dynamics and result in great variability in protein folding and conformation of the helices in solution (Saen-Oon et al., 2019; Sun et al., 2018; Yuan et al., 2019). Such changes can be crucial for activity and their early prediction can improve computer aided drug design and selection of candidates for further testing (Saen-Oon et al., 2019; Sun et al., 2018). Variabilities seen in the degree of water trapping during crystallization of RORγt ligand-protein complexes indicates a variability of pocket hydration induced by the binding of different agonists (Kallen et al., 2017; Saen-Oon et al., 2019). Hydration, on the other hand, can induce great distortion of RORγt folding that cannot be captured by crystallography (Saen-Oon et al., 2019). In a few examples, where the RMSDs of RORγt crystals greatly deviate (>3 Å) from their known average position, the deviation has been linked to the binding of larger inverse agonists (Huang et al., 2020; Kallen et al., 2017; Narjes et al., 2018). The effect of binding dynamics and pocket hydration cannot be captured in crystallography and MD simulation studies have become a useful tool to characterize and investigate the binding modes of agonists/inverse agonists (Huang et al., 2020). Similarly, the stabilization/disruption of the H11-H12 triangular net can be better judged during simulations (Saen-Oon et al., 2019).

Among the early identified ligands of RORγt orthosteric binding pocket are cholesterol derivatives. Hydroxycholesterols such as 22, 24, 25 and 27-hydroxycholesterols are believed to be natural ligands of RORγt. Steroid conformations of most of the identified ligands are *trans-trans-trans* and they behave as agonists (Kallen et al., 2017; Santori et al., 2015; Soroosh et al., 2014; Wang, Kumar, Crumbley, et al., 2010). 7α-hydroxycholesterol, 7β-hydroxycholesterol and 7-ketocholesterol were considered inverse agonists; however subsequent studies showed that they behave as agonists or partial agonists, like all *trans* cholesterol derivatives (Fabio et al., 2015; Soroosh et al., 2014; Wang, Kumar, Solt, et al., 2010). Cardiac glycosides and ursolic acid, on the other hand, are inverse agonists and have a *cis* conformation at ring A or at both ring A and D of the sterol core (Huh et al., 2011; Xu et al., 2011). The range of synthetic RORγt agonists/inverse agonists is large, and includes sulfonamides, pyrazole amides, biaryl amides, tertiary amines, benzoxazepines, tetrahydroquinoline sulfonamides, tetrahydro-naphthyridine derivatives, n-thiazolyl acetamides, quinoline sulfonamides, n-aryl sulfonyl indolines, phenyl (3-phenylpyrrolidin-3-yl) sulfones, hexafluoro isopropanol aryl sulfonamides, imidazopyridines, pyrimidines, quinazolinedione derivatives, thiazole-bis-amides, triazolopyridines, imidazolopyridines, carbazole carboxamides, diphenyl propanamides, 1,3,5-triazine derivatives, tetrahydrobenzo[4,5]thieno[2,3-d]pyrimidines, triazolopyridines, dihydroimidazole tethered imidazolinethiones, sulfoximines, phenyl glycinamides, oxadiazole substituted thiazoles, and n-indanyl benzamides (Amaudrut et al., 2019; Chao et al., 2015; Doebelin et al., 2016; Duan et al., 2019; Fauber et al., 2013; Fauber et al., 2015; Fukase et al., 2018; Gege et al., 2020; Gong et al., 2018; Hintermann et al., 2016; Huang et al., 2018; Huh et al., 2013; Kaitoh et al., 2017; Lao et al., 2019;

Nakajima et al., 2020; Nefzi et al., 2017; Olsson et al., 2016; Ouvry et al., 2018; Shirai et al., 2018; Steeneck et al., 2020; Sun et al., 2020; Tian et al., 2019; Tsuruoka et al., 2020; van Niel et al., 2014; T. Wang et al., 2015; Y. Wang et al., 2015; Wang et al., 2014; Yang et al., 2014). Herein we report the discovery of 4,5,6,7-tetrahydro-benzothiophene modulators of RORs. We show the results of *in vitro*/*in vivo* screening, molecular docking, and MD simulation studies that comprise a tailored drug discovery cycle suitable for nuclear receptors and similar globular protein drug targets. The cycle was adopted for the identification, evaluation, and optimization of novel 4,5,6,7 tetrahydro-benzothiophene modulators of RORγt in a contemporaneous fashion.

Results

Discovery workflow of 2,3 derivatives of 4,5,6,7 tetrahydro-benzothiophene and results of modeling steps are summarized in Figure2.1. The RORγt modulator molecular model was designed starting from 25-hydroxycholesterol (25HC) and using autodock vina for ideal pose prediction as shown in Figure 2.1A, 2.1B. Two-dimensional virtual screen using the molecular model as a fingerprint with Tanimoto coefficient cutoff of 0.7 returned a library of a thousand of 4,5,6,7 tetrahydro-benzothiophene based virtual hits. Two- and three-dimensional processing with Ligprep produced 1500 conformers. Ranking conformers based on their $RMSD_{scr/ref}$ from the best scoring conformer of the top ranked virtual hit in 2D screen, created three clusters (<1, 2-4 and >5 Å). The energy of conformers was 5-15 Kcal/mol in range, Figure 2.1C. A subsequent three-dimensional phase screen returned 167 virtual hits. Clustering those hits based on their $RMSD_{align}$, $RMSD_{scr/ref}$ and relative energy of conformer in binding position (ΔE_{bconf}) revealed that the $RMSD_{align}$ values for the hits were 0.3-1.7 Å. Additionally, there was a variability in binding modes,

and the $RMSD_{scr/ref}$ were 0-7 Å, while their ΔE_{bconf} ranged from 0-40kcal/mol, Figure 2.1D. Molecular docking of low $RMSD_{scr/ref}$, $RMSD_{align}$ and ΔE_{bconf} hits using glide HTVS and SP docking determined the top conformers that aligns with the original design and the ideal pose of the initial autodock vina screening, Figure 2.1E. 50ns MD simulations of selected hits showed stability of protein ligand complex in their binding poses, Figure 2.1F. The hits were more stable through the simulation compared to gsk2981278 in its proposed binding pose (Chen et al., 2021; Chen et al., 2022). Calculated ADME revealed drug like properties of many of the top hits, Figure 2.1G. The stepwise computer aided evaluation process resulted in a selected set of 23 virtual hits, which varied in MW from 350 to 515g/mol. The selected hits, except **3**, followed Lipinski's rule of five and had high oral bioavailability >0.55 and their calculated *i*logP (Daina et al., 2014), or logD (pH=7.4) was 0.4-5. TPSA was 80-140 Å^2. The predicted solubility of the hits ranged from poor to soluble using ESOL model logS (Delaney, 2004). Following synthesis, kinetic solubility evaluation results showed moderate solubility of the compounds except **2, 4** and **23** which had poor solubility (≤1µM, pH=7.4). Free energy perturbations (FEP) results showed slight differences in binding free energies ($\Delta\Delta G$) of the virtual hits (0.4-5kcal/mol). This was reflected by closely comparable experimental free binding energies (ΔG_{EXP}) in fluorescence polarization competitive RORγt binding assay against 25-NBD Cholesterol (25NC) and in time-resolved fluorescence energy transfer (TR-FRET) assay. Further, lipophilic efficiency (LipE) was calculated using logD and *i*logP (LipE$_{logD}$ and lipE$_{ilogP}$), Table 2.1.
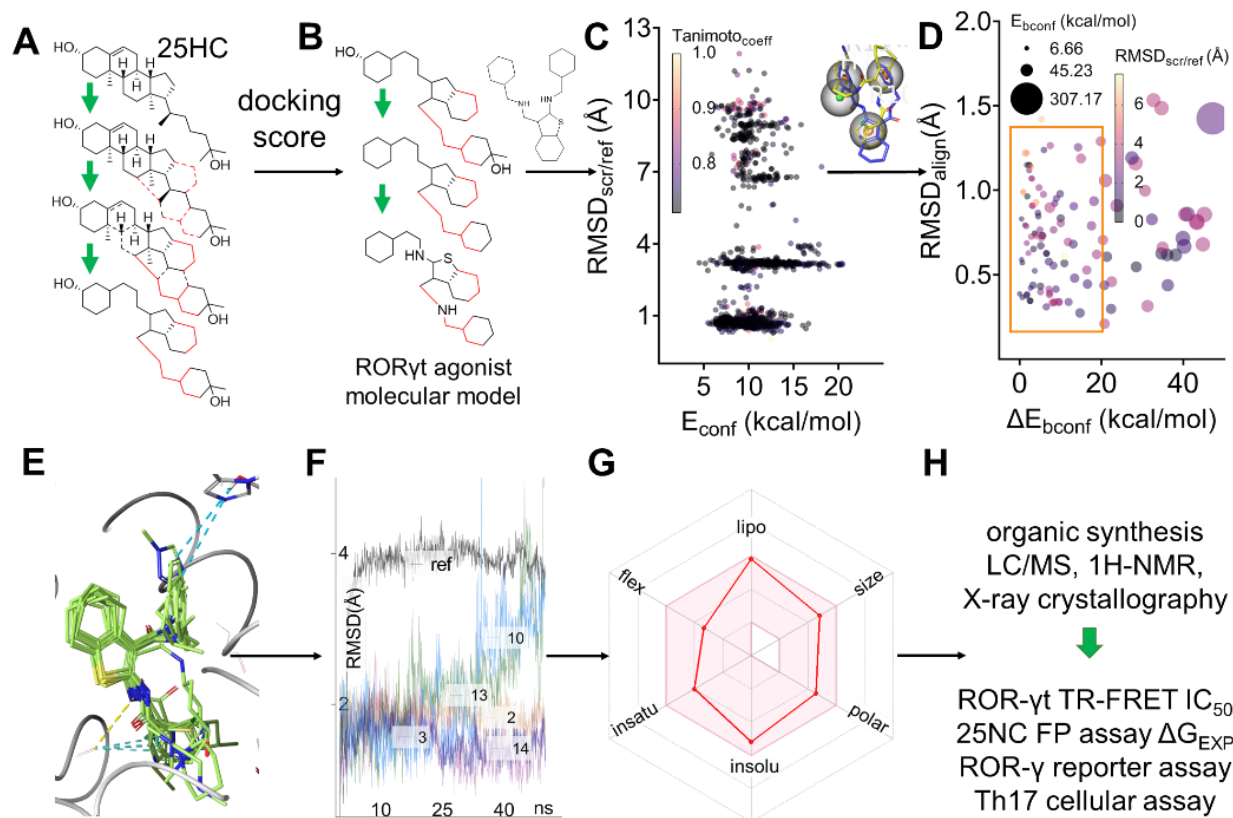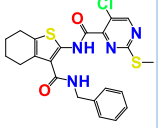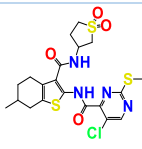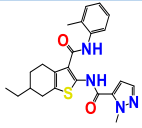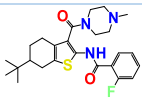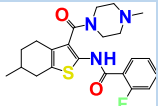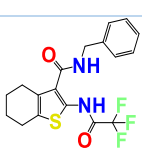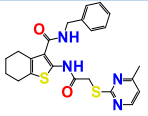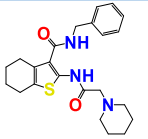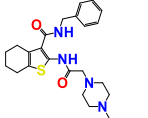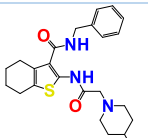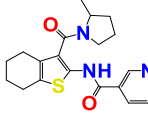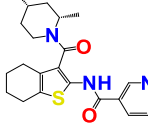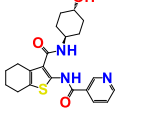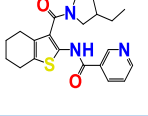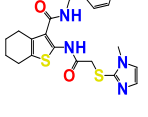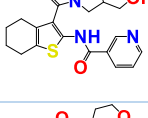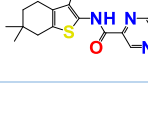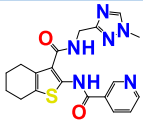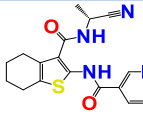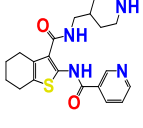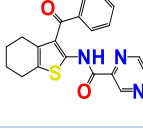
Figure 2.1. Discovery workflow of 2,3 derivatives of 4,5,6,7-tetrahydro-benzothiophene modulators of RORγt. (A,B) Linking and substitution starting from 25HC to design a fingerprint for 2D screening; (C) scatter plot of 1000 virtual hits showing maximum common structure rmsd$_{scr/ref}$ screening hit (scr) to the reference structure (ref), the energy of conformer (E$_{conf}$) and Tanimoto coefficient; (D) scatter plot of the hits of phase screen showing rmsd$_{scr/ref}$, relative energy of bound conformer ΔEb$_{conf}$, and rmsd$_{align}$; (E) predicted active poses of the top virtual hits inside the RORγt orthosteric ligand-binding pocket (PDB ID: 5APH) minimized without crystal water; (F) plots of short (50 ns) MD simulations of synthesis candidates chosen from HTVS, SP, and XP docking screens; (G) radar plot of the calculated ADME/PK properties of an optimized structure of one of the phase screen hits; and (H) synthesis and biological evaluation.

Table 2.1. Calculated physicochemical properties, kinetic solubility, docking scores, calculated, and experimental binding free energies, IC_{50} values in TR-FRET assay and lipophilic efficiency of 2,3 derivatives of 4,5,6,7-tetrahydro-benzothiophene modulators of RORγt.

ID	Structure	MW (g/mol)	$i$logP (Daina et al., 2014) /logD (pH=7.4)	TPSA (Ertl et al., 2000)	LogS (Delaney, 2004) /Solubility µM (pH=7.4) T= 298K UV-Vis	glide XP score	ΔG_{FEP} (kcal/mol) (pH=7.4) T=300K M±SE	ΔG_{EXP} (kcal/mol) (pH=7.4) T= 300K M±SD	TR-FRET IC_{50} (nM) (pH=7.4) T= 293K M±SD	LipE$_{i\log P}$ /LipE$_{\log D}$
1		477.59	4.01/4.65	80.89	-6.12/12.86	-7.71	-12.15±1.57	-12.49±0.29	1.63±0.01	5.09/4.45
2		473.01	3.79/5.45	137.52	-6.06/≤1	-11.53	-11.31±0.58	-11.63±1.15	0.40±0.00	4.68/3.02
3		515.07	3.13/3.28	180.04	-5.30/40.24	-8.05	-10.94±1.44	-9.75±0.43	4.45±0.20	3.97/3.82
4		422.54	3.34/4.72	104.26	-5.78/≤1	-11.1	-10.87±0.79	-11.38±0.66	1.47±0.14	4.95/3.57
5		457.60	4.09/5.06	80.89	-6.03/10.55	-7.57	-12.52±1.20	-10.72±0.34	3.80±0.24	3.72/2.75
6		415.52	3.63/3.59	80.89	-5.11/27.70	-9.52	-12.08±1.36	-10.20±0.91	2.46±0.11	3.80/3.84
7		382.40	2.62/4.43	86.44	-5.07/28.80	-9.45	N/A	-10.19±1.03	2.07±0.02	4.80/2.99

#	Structure									
8		452.59	3.61/4.92	137.52	-5.56/3.23	-8.79	-9.8±0.49	-10.21±0.99	0.69±0.04	3.83/2.52
9		411.56	3.08/4.33	89.68	-5.03/19.71	-10.92	-9.46±0.58	-10.28±0.58	2.15±0.04	4.41/3.16
10		426.57	3.39/3.06	92.92	-4.46/99.32	-11.37	-13.66±1.58	-12.51±1.00	1.17±0.00	5.72/6.05
11		425.59	3.26/4.57	89.68	-5.38/12.43	-11.1	-11.81±1.58	-10.19±0.02	4.50±0.15	4.16/2.85
12		369.48	2.93/3.68	90.54	-4.55/31.28	-10.01	-8.29±0.58	-7.57±0.75	3.51±0.08	2.58/1.83
13		397.53	3.30/4.45	90.54	-5.20/26.97	-9.49	-10.09±0.93	-12.69±0.80	0.23±0.00	5.94/4.79
14		399.51	2.45/3.08	119.56	-4.36/29.42	-8.56	-10.54±1.61	-12.73±0.29	1.76±0.11	6.82/6.19
15		383.51	3.00/4.05	90.54	-4.78/32.88	-7.01	-10.09±0.92	-10.39±0.87	5.66±0.27	4.57/3.52
16		440.58	3.45/4.44	129.56	-5.10/8.05	-9.31	-9.94±0.49	-11.53±1.86	8.98±0.76	3.89/2.90
17		385.48	2.69/2.60	110.77	-3.80/79.33	-7.05	-10.04±1.57	-6.16±0.04	45.82±2.31	4.98/5.07
18		400.49	2.42/3.00	112.66	-3.96/34.82	-6.96	-10.47±0.49	-7.78±0.56	20.14±0.96	2.07/1.49

#	Structure									
19		396.47	2.41/1.62	130.04	-3.75/93.59	-8.64	-13.32±1.07	-13.35±0.83	3.43±0.23	3.26/4.05
20		354.43	2.38/2.85	123.12	-3.83/90.93	-8.33	-10.31±0.78	-8.85±0.94	13.31±0.30	2.93/2.46
21		398.52	2.56/0.40	111.36	-4.07/84.70	-5.84	-13.75±1.31	-7.29±0.44	57.25±4.80	3.89/6.05
22		363.43	2.41/4.15	100.19	-4.82/18.34	-9.52	-10.06±1.44	-10.07±0.81	19.61±0.54	4.92/3.17
23		455.55	2.82/3.94	142.71	-5.47/≤1	-10.79	-8.44±0.91	-10.06±0.72	16.59±1.20	6.91/5.79
ref	gsk2981278	461.61	4.28/4.11	84.45	N/A	N/A	N/A	-11.22±0.90	1.71±0.16	3.89/4.06

2,3 derivatives of 4,5,6,7 tetrahydro-benzothiophene form non-covalent interactions with various residues of RORγt orthosteric ligand binding pocket. XP docking results show that the 23 compounds of the selected set vary slightly in their binding modes and alignment inside the pocket; however, they were all characterized by hydrogen bonds and/or water bridge contacts between their amide bridges and Cys320-Glu326, Arg364-Phe377 hydrophilic regions. The saturated tetrahydro-benzene ring sub-structures were buried in the hydrophobic region of the pocket. Examples of binding poses are shown in Figure 2.2A-D. With their aromatic rings linked to position 3 of 4,5,6,7 tetrahydro-benzothiophene through amide bridges, compounds **1**, **2**, **7-11**, **13**, **16** and **19** form a π–π bonds with His479 and Trp317. In addition, compound **19** forms a hydrogen bond with His479 through its triazole ring. Superposed binding poses of compounds **2**, **10** and **13** are shown in figure 2.2A. When compound **10**, in its predicted pose, was aligned with structurally

different natural and synthetic ligands 25HC, gsk2981278 and inverse agonist iag (Supplementary figure 1) described by Saen-Oon S, et al, 2019 (Saen-Oon et al., 2019), it showed good alignment with docked gsk2981278 and iag with RMSD <1 and <2 Å, respectively, based on selected atom pairs, Figure 2.2B. On the other hand, the ring substituents linked to position 2 of 4,5,6,7 tetrahydro-benzothiophene except compound **7**, formed hydrogen bond or were in proximity to form a water bridge with Gln286 such as in case of compounds **9**, **10** and **11** that formed hydrogen bonds between their piperidine nitrogen and Gln286. A deviation (> 2 A°) from the ideal pose occurred when the 4,5,6,7 tetrahydro-benzothiophene ring was substituted at position 6 with an alkyl group such as in case of compounds **3-6**, and **18.** This was not reflected by a reduction or an increase in activity in either TR-FRET or fluorescence polarization assay, Table 2.1. Superposition of compound **3** and **2** shows the extent of this deviation, where the 1,1 dioxide tetrahydro-thiophene ring of **3** forms a hydrogen bond with Gln286 while the methyl-thio-pyrimidine ring linked to position 2 of the 4,5,6,7 tetrahydro-benzothiophene forms a hydrogen bond with Phe377, Figure 2.2B. This was no effect on activity in TR-FRET of fluorescence polarization assay, Table 2.1. Reducing the length of the bridge linking ring substitution to position 3 of 4,5,6,7 tetrahydro-benzothiophene ring to one atom as in case of compounds **12**, **15**, **22** and **23** resulted in a deviation (>2 A°) from ideal pose and a reduction of the activity in non-cellular binding assays, Table 2.1. Similarly compounds **14** and **17** deviated from the ideal pose and there was no interaction with the agonist lock, however, they formed hydrogen bonds through their hydroxyl groups with Gln286. Their poses are stabilized by intramolecular hydrogen bond between their hydroxyl groups and the amide bridge of position 2 of 4,5,6,7 tetrahydro-benzothiophene. The activity of the

compound **14** in TR-FRET or fluorescence polarization was not lost in such pose despite that there was no significant interaction with the agonist lock from the ring linked to position 3 of 4,5,6,7 tetrahydro-benzothiophene or other substructures of the molecules, Table 2.1, Figure 2.2D. Compound **17**, on the other hand, which showed a lower docking score and increase in deviation (>2 A°) towards the hydrophobic region of the pocket. This was reflected by a reduced activity in both TR-FRET and fluorescence polarization assays, Table 2.1. Finally, increasing the amide bridge linked to position 2 of 4,5,6,7 tetrahydro-benzothiophene ring such as in case of compounds **8** and **16** had a slight effect on the binding poses and had no effect on the activity in the binding assays.
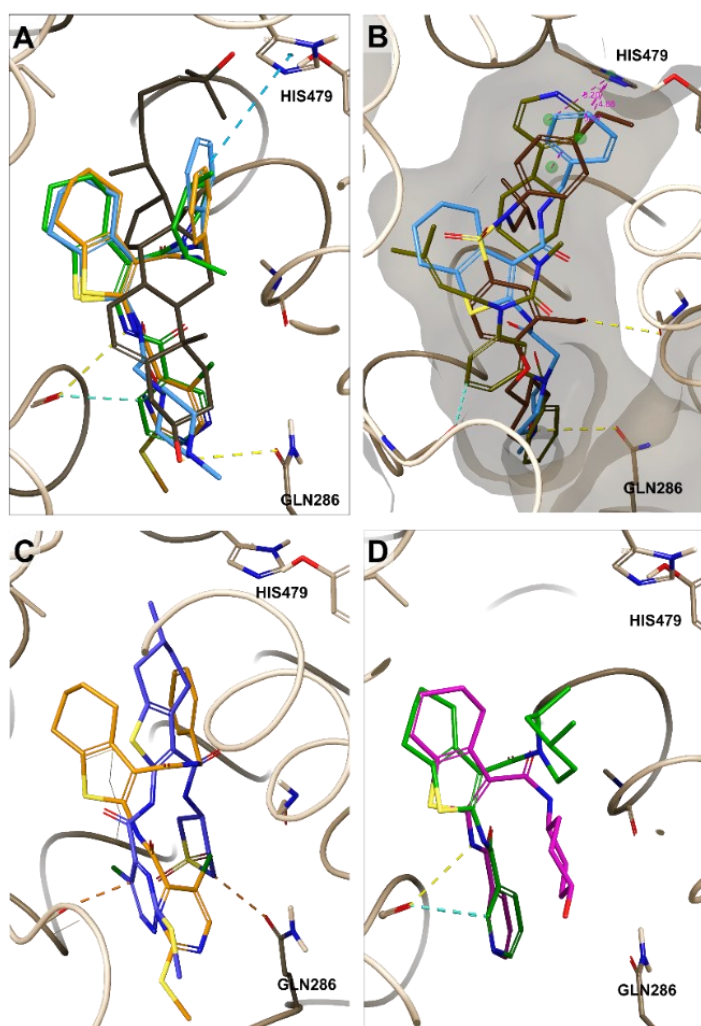
Figure 2.2. Predicted active poses of the 4,5,6,7-tetrahydro-benzothiophene derivatives superimposed with natural and synthetic ligands of RORγt (PDB ID: 5APH): (A) compounds 2 (orange), 10 (cyan), and 13 (green) (Ligrmsd <1 Å) in their active pose superimposed on 25HC; (B) 10 (cyan), superimposed on gsk2981278 and iag, forms a hydrogen bond with Gln286:δCO and π–π stacking between its phenyl group and His479; (C) 3 (cyan) superimposed on 2 (orange) and showing a deviation (Ligrmsd > 2 Å) of the predicted pose and forming hydrogen bond with Gln286:δCO through the 3-amide substitution ring and a hydrogen bond through the 2-amide substitution ring; (D) 14 (fuchsia) superimposed on 13 (green) showing a deviation of the 3-amide substitution ring and in proximity with Gln286:δCO and Hid323:CO (Ligrmsd = 1.77 Å).

The stability of 2,3 derivatives of 4,5,6,7 tetrahydro-benzothiophene ligand protein complexes with RORγt, from their initial binding poses shown in figure 2.2, was confirmed with 50 and 250 ns MD simulations. Compared to 25HC-, iag- and ago- (described by Saen-Oon S, et al, 2019) RORγt, **2**-, **3**-, **10**- and **14**- RORγt complexes were equally stable over the length of trajectory and the change in ligand protein RMSD was <1 Å. However, compound **13** moved away from its initial binding position <2 Å with no additional shift beyond that occurred at 40 ns, which was comparable with gsk2981278- RORγt complex, Figure 2.3A. The observed magnitude of H11-H12 atomic fluctuations in 4,5,6,7 tetrahydro-benzothiophene -RORγt complexes was 0.1- 0.5 Å higher compared to all the reference ligands, Figure 2.3B. The magnitude of fluctuations in H12 region is >1.5 Å in case of **3**-, **13**-, and **14**- RORγt complexes compared to apoprotein, and all ligand-protein complexes evaluated except 25HC-RORγt complex which showed an equally elevated fluctuation at the H12 region. Additionally, the observed magnitude of

fluctuations in H6-loop-H7 region, Leu391-Glu395 residues, of **2**- and **10**- RORγt complexes was 0.3-1 Å higher compared to apoprotein and all other simulated ligand-RORγt complexes, while the fluctuations in this region were only slightly elevated in case of **14**- RORγt complexes compared to apoprotein. Similarly, 25HC-, ago- and gsk2981278- RORγt complexes showed moderate increase of the magnitude of fluctuations 0.1-0.2 Å in H6-loop-H7 region compared to apoprotein. There was also a 0.2-0.3 Å reduction in magnitude of fluctuations of H6-loop-H7 region in trajectories of **3**- and **13**- RORγt complexes compared to apoprotein. Similarly, iag- RORγt complex showed a 0.2-0.3 Å reduction in fluctuations in H6-loop-H7 region compared to apoprotein. Metadynamics simulations based on CV distance from Gln286:δCO to His479:Nε (14-15 Å) revealed deep energy minima in pocket center in case of **2**-, **10**- and **13**- RORγt complexes compared to apoprotein. Those energy minima were shallow in case of RORγt ligand-protein complexes with **3** and **14** or completely absent for all reference compounds, Figure 2.3C, 2.3D. Radial distribution function (RDF) analysis of explicit water solvent around agonist lock Tyr502:OH showed an increase in hydration in case of 4,5,6,7 tetrahydro-benzothiophene-RORγt compared to apoprotein or ago-, iag- and gsk2981278- RORγt complexes. Similarly, the was an increase in the hydration around agonist lock of 2HC-RORγt compared to apoprotein, ago-, iag-, and gsk2981278- RORγt complexes. **13**- RORγt complex was the only among all the evaluated 4,5,6,7 tetrahydro-benzothiophene derivatives complexes with RORγt that showed higher hydration around the agonist lock compared to 25HC-RORγt complex. The hydration around Gln286:δCO hydrophilic center showed a reduction in case of **2**-, **3**-, **10**- and **14**- RORγt compared to apoprotein or ago- and iag- RORγt complexes. Similarly, the

hydration around Hid323:CO decreased in case of **2**-, **10**- and **13**- RORγt complexes compared to apoprotein and ago-RORγt complex. The hydration around Phe377:CO hydrophilic center decreased in case of **2**-, **3**-, **10**- and **14**- RORγt compared to all other reference ligand-RORγt complexes, Figure 2.3E. The results of RDF analysis of hydration shows that the pocket hydration patterns of **13**- RORγt complex was significantly different from the other four 4,5,6,7 tetrahydro-benzothiophene -RORγt complexes, Figure 2.3A-E, while differences in pocket hydration between those four -RORγt complexes were non-significant.
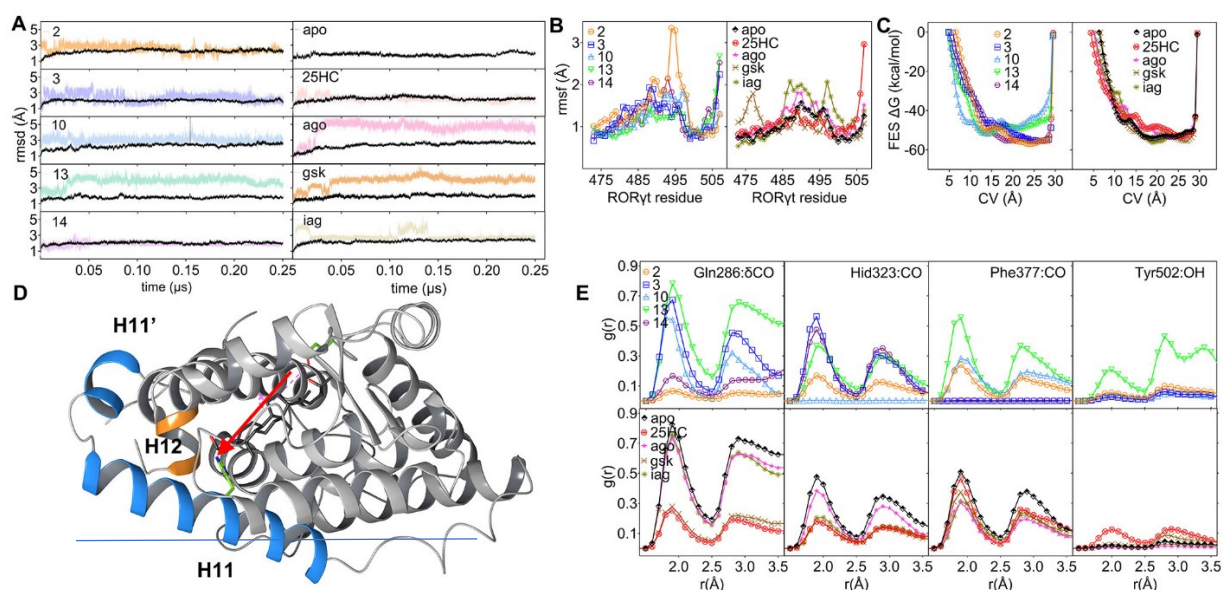
Figure 2.3. MD simulation studies performed on 2–, 3–, 10–, 13–, and 14–RORγt (PDB ID: 5APH) complexes: (A) rmsd plots of ligand fit protein superposed showing only small shifts for all compounds compared to reference RORγt agonists and inverse agonists; (B) rmsf of H11–H12 region showing an increase in atomic fluctuations for all the compounds 2–14 compared to reference ligands; (C) metadynamics simulation plots showing the change of free energy surface (FES) in terms of distance CV. Compounds 2–14 show deeper energy troughs in the pocket region compared to reference ligands; (D) 3D ribbon

diagram of RORγt showing H11–H12 region in blue and orange colors. CV distance direction from Gln286:δCO to His479:Nε (14–15 Å) is shown by a red arrow; (E) RDF of water around the three hydrophilic centers Gln286:δCO, Hid323:CO, Phe377:CO and the agonist lock Tyr502:OH of 2−, 3−, 10−, 13−, and 14−RORγt compared to apoprotein or 25HC−, ago−, iag−, and gsk2981278−RORγt complexes.

ADMET properties of 167 hits from 3D screening were calculated to exclude compounds that violate Lipinski rule of five. The 23 compounds were selected based on their docking scores, ligand-protein complex stability, drug-likeness, and synthetic feasibility. Compounds **1-23** can be obtained through amide formation from starting reactants, Scheme 1. Compound **1** was synthesized by amide formation of 3-carboxylic acid of 4,5,6,7 tetrahydro-benzothiophene 2-amide derivative and 1-benzylpiperazine in presence of 1-[bis(dimethylamino)methylene]-1*H*-1,2,3-triazolo[4,5-*b*]pyridinium 3-oxid hexafluorophosphate, N-[(dimethylamino)-1*H*-1,2,3-triazolo-[4,5-*b*]pyridin-1-ylmethylene]-N-methylmethanaminium hexafluorophosphate N-oxide (HATU) and N,N-diisopropylethylamine (DIPEA), Scheme 1. Compounds **2**, **12**, **14**, **15**, **17** and **19-21**, on the other hand, were obtained through amide formation reaction between their corresponding 2-amino 4,5,6,7 tetrahydro-benzothiophene 3-amide derivative and carboxylic acids in presence of 1-ethyl-3-(3-dimethylaminopropyl) carbodiimide (EDC) and dimethyl sulfoxide (DMSO), Scheme 1. Similarly, compound **3**, the 2-amide bond of 4,5,6,7 tetrahydro-benzothiophene 3-amide derivative was formed with the carboxylic acid in presence of HATU and DIPEA, Scheme 1. For compounds **4-6**, the 2-amide bond was formed between the corresponding 2-amino 4,5,6,7 tetrahydro-benzothiophene 3-amide derivatives and acyl chlorides in presence of NaOH, Scheme 1. In case of

compound **7**, the 2-amide bond was formed between 2-amino 4,5,6,7 tetrahydro-benzothiophene 3-amide derivative and trifluoroacetic anhydride (TFAA) at 60°C, Scheme 1. The 2-amide bond for compounds **8**, **9** and **11** were formed between the corresponding 2-amino 4,5,6,7 tetrahydro-benzothiophene 3-amide derivatives and carboxylic acids in presence of methane-sulfonyl chloride (MsCl) and triethylamine (NEt3), Scheme 1. Compound **10** was obtained from 2-amide formation of 2-amino 4,5,6,7 tetrahydro-benzothiophene 3-amide derivatives and carboxylic acid in presence of K2CO3, Scheme 1. The final amide formation reaction to derive compound **13**, was between the 3-carboxylic acid of 4,5,6,7 tetrahydro-benzothiophene 2-amide derivative and amine in presence of 1,1'-carbonyldiimidazole (CDI), Scheme 1. N-{3-[(2R,4R)-2,4-dimethylpiperidine-1-carbonyl]-4,5,6,7-tetrahydro-1-benzothiophen-2-yl}pyridine-3-carboxamide was separated from racemate by chiral chromatography. Enantiomeric excess was >98% for both compounds and (R)-configuration was confirmed by X-ray crystallographic analysis, Supporting information. Compound **16** was synthesized in presence of DIPEA and DMSO starting from of 2-amino 4,5,6,7-tetrahydro-benzothiophene 3-amide derivative and carboxylic acid, Scheme 1. Finally, compounds **18**, **22** and **23** were derived by amide formation between the corresponding 2-amino of 4,5,6,7-tetrahydro-benzothiophene 3-derivatives and carboxylic acids in presence of DIPEA and 2-chloro-1-methylpyridinium iodide at 100°C, Scheme 1.

Scheme 1. Synthesis scheme of compounds 1-23[a]

2,3 derivatives of 4,5,6,7 tetrahydrobenzothiophene
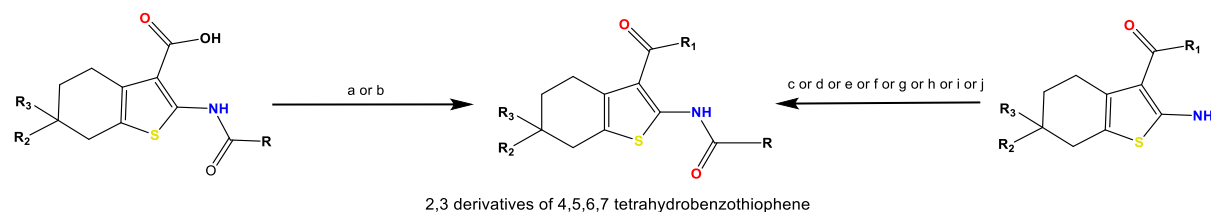
R= fluoro-$2\lambda^3$-benzene for **1**, **5** and **6**; 5-chloro-2-(methylthio)-$4\lambda^3$-pyrimidine for **2** and **3**; 1-methyl-1H-$5\lambda^3$-pyrazole for **4**; trifluoro-λ^3-methane for **7**; 4-methyl-2-(λ^1-sulfaneyl)pyrimidine for **8**; 1-(λ^3-methyl)piperidine for **9**; 1-(λ^3-methyl)-4-methylpiperazine for **10**; 1-(λ^3-methyl)-4-methylpiperidine for **11**; $3\lambda^3$-pyridine for **12-15**, **17**, **19-21**; 2-((λ^3-methyl)thio)-1-methyl-1*H*-imidazole for **16**; $2\lambda^3$-pyrazine for **18** and **22**; 5-methyl-2-(methylsulfonyl)-$4\lambda^3$-pyrimidine for 23. **R₁**= 1-benzyl-$4\lambda^2$-piperazine for **1**; benzyl-λ^2-azane for **2**, **7-11 and 16**; 3-(λ^2-azaneyl)tetrahydrothiophene 1,1-dioxide for **3**; o-tolyl-λ^2-azane for **4**; 1-methyl-$4\lambda^2$-piperazine for **5** and **6**; 2-methyl-$1\lambda^2$-pyrrolidine for **12**; (2*S*,4*S*)-2,4-dimethyl-$1\lambda^2$-piperidine for **13**; (1*r*,4*r*)-4-(λ^2-azaneyl)cyclohexan-1-ol for **14**; 3-ethyl-$1\lambda^2$-pyrrolidine for **15**; ($1\lambda^2$-pyrrolidin-3-yl)methanol for **17**; $4\lambda^2$-morpholine for **18**; 3-((λ^2-azaneyl)methyl)-1-methyl-1*H*-1,2,4-triazole for **19**; (*R*)-2-(λ^2-azaneyl)propanenitrile for **20**; 4-((λ^2-azaneyl)methyl)piperidine for **21**; $1\lambda^3$-benzene for **22** and **23**. **R₂**= H for **1**, **2**, **7-17**, and **19-23**; λ^3-methane for **3**, **6** and **18**; $1\lambda^3$-ethane for **4**; 2-methyl-$2\lambda^3$-propane for **5**. **R₃**= H for **1-17** and **19-23**; λ^3-methane for **18**.

*a*Reagents and conditions: (a) amine, DMF, HATU, DIPEA, rt, 32% for **1**; (b) amine, DMF, CDI, 70°C, 24% for **13**; (c) carboxylic acid, EDC, DMSO, rt, 58% for **2**, 67% for **12**, 63% for **14**, 65% for **15**, 59% for **17**, 57% for **19**, 67% for **20** and 63% for **21** ; (d) carboxylic acid, DMF, HATU, DIPEA, 50°C, 31% for **3**; (e) acyl chloride, NaOH, rt, 3% for **4**, 3% for **5** and 14% for **6**; (f) TFAA, 60°C, 52% for **7**; (g) carboxylic acid, dioxane, MsCl, NEt3, rt, 3% for **8**, 12% for **9**, 10% for **11**; (h) carboxylic acid, DMF, K2CO3, 50ºC, 42% for **10**; (i) carboxylic acid, DIPEA, DMSO, 100°C, 65% for **16**; (j) carboxylic acid, DIPEA and 2-chloro-1-methylpyridinium iodide at 100°C, 56% for **18**, 58% for **22**, 62% for **23**

In vitro potency of the compounds was evaluated in two binding assays TR-FRET and fluorescence polarization competitive assay. First, TR-FRET assay confirmed that 2,3 derivatives of 4,5,6,7 tetrahydro-benzothiophene are potent inverse agonists of RORγt, however there was no significant difference between the 23 compounds and their IC_{50} was in range 0.5-5 nM, Table 2.1. Experimental values were in good concordance with the SP docking scores. Lipophilicity, poor solubility or high TPSA of some compounds such as **1**, **2** and **16** did not have a significant impact on IC_{50} determined in TR-FRET assay. Secondly, fluorescence polarization assay confirmed the findings of TR-FRET. The experimental binding free energies (ΔG_{EXP}) of 2,3 derivatives of 4,5,6,7 tetrahydro-benzothiophene -RORγt complexes were comparable to XP docking scores and those obtained in FEP simulations (ΔG_{FEP}), Figure 2.4A, 2.4B. To confirm *in vitro* cellular binding, we tested compounds **2**, **3**, **10** and **13** in human GAL4-RORγ reporter assay that utilizes human cells that provide high-level expression of a hybrid human RORγ. In the reporter assay, N-terminal DNA binding domains (DBD) of the native RORγ receptor have been substituted with that of the yeast GAL4-DBD (Liu et al., 2021; Rauhamäki et al., 2018). Inverse agonists that bind to RORγ (LBD) decrease the affinity of GAL4-RORγ to DNA site. The IC_{50} measured in human GAL4-RORγ reporter assay of compounds **2**, **3**, **10** and **13** were 10 times lower compared ursolic acid (90 nM), Figure 2.4C.
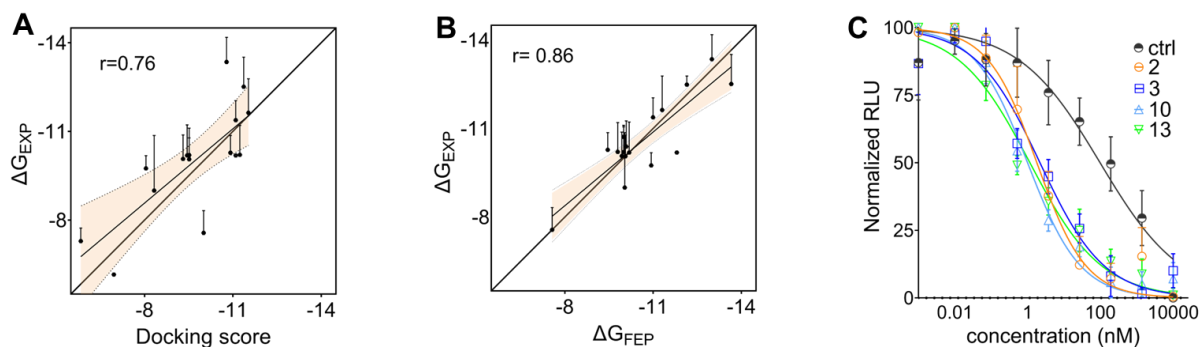
Figure 2.4. In vitro binding assay results: (A) linear regression of experimental binding free energies (ΔG_{EXP}) compared to Docking scores, R^2= 0.58, P<0.01; (B) ΔG_{EXP} compared to ΔG_{FEP}, R^2= 0.75, P<0.01; (C) concentration response GAL4-RORγ reporter assay of compound **2**, **3**, **10** ,**13** compared to ursolic acid (ctrl), IC_{50}= 0.75, 2.19, 0.82, 1.61 and 99.92 nM, respectively.

Furthermore, we performed an *in vivo* Th17 polarization assay to compare the effect of 2,3 derivatives of 4,5,6,7 tetrahydro-benzothiophene on IL17A production. Compounds **1-23** were tested for their ability to inhibit Th17 polarization of human peripheral blood mononuclear cells (PBMCs). PBMCs treated with compounds **2**, **9**, **10**, **13** and **14** showed the greatest reduction in IL17A+ cells compared to control (Figure 2.5A). Compound **3** showed a 30% reduction in percentage of IL17A+ cells (Figure 2.5A), compared to **2**, **10**, **13** and **14** which reduced IL17A+ cells by 40-60 %. Compounds **2**, **10** and **13** decreased IL17A and IL21 secretion from polarized PBMCs compared to vehicle, Figure 2.5B, 2.5C). We then sought to determine IC_{50} of compound **2** in Th17 polarization as a representative of the set of 2,3 derivatives of 4,5,6,7 tetrahydro-benzothiophene. The IC_{50} was 0.38 nM in the cellular assay compared to 0.39 nM in TR-FRET assay. We further tested compound **2** on Th17 polarization of PBMCs from multiple donors (n=9), which under the same experimental condition express different levels of IL17A. Compound **2** reduced the percentage of both IL17A+ and IL21+ cells from all donors by 20-40%, Figure 2.5D, 2.5E. There was no sign of cell death or decrease in cell viability when the cells were evaluated by flow cytometry. 2,3 derivatives of 4,5,6,7 tetrahydro-benzothiophene did not increase cell proliferation or apoptosis and did not affect the percentage of IFNγ+ or IL22+ T cells. The solubility of 12 compounds was further assessed in acidic pH (1.5 and 5). The

solubility of **1**, **6**, **10-13**, **16** and **17** was inversely proportional to changes in pH. Compound **3** was unstable in acidic pH as the maximum solubility decreased from 40 μM (pH=7.4), Table 2.1, to 9.72 μM (pH=5) to 1.7 μM (pH=1.5), Table 2.2. The solubility of **4** and **14** was not affected by pH changes, Table 2.2. Mouse/human/rat/dog microsomal stability studies showed that the intrinsic clearance (Cl_{in}) is high for compounds **1**, **11** and **16**; moderate for **2**, **3**, **6**, **10** and **13**; and low for **4**, **12** and **14**, Table 2.2. The determination of two direction Caco-2 permeability, like microsomal stability, revealed that the compounds are diverse in membrane permeability profiles where compounds **6**, and **12**, **13**, and **16** exhibited high permeability, while **1**, **2**, **10** and **17** were moderate and **3**, **4**, and **11** showed low permeability in A-B direction. Compounds **3** and **17** undergo active efflux, Table 2.2. Finally, MDR1-MDCKII permeabilities of **6**, **12**, **13** and **16** were high, while **1**, **2**, **3**, **4**, **10** and **17** were moderate. Compounds **11** and **14** showed low permeability in A-B direction. Compounds **3** and **17** undergo active efflux and are P-gp substrates, Table 2.2. The efflux ratio of compound **3** was decreased partially by verapamil in Caco-2 and completely blocked by cyclosporine A in MDR1-MDCKII cells, Table 2.2.
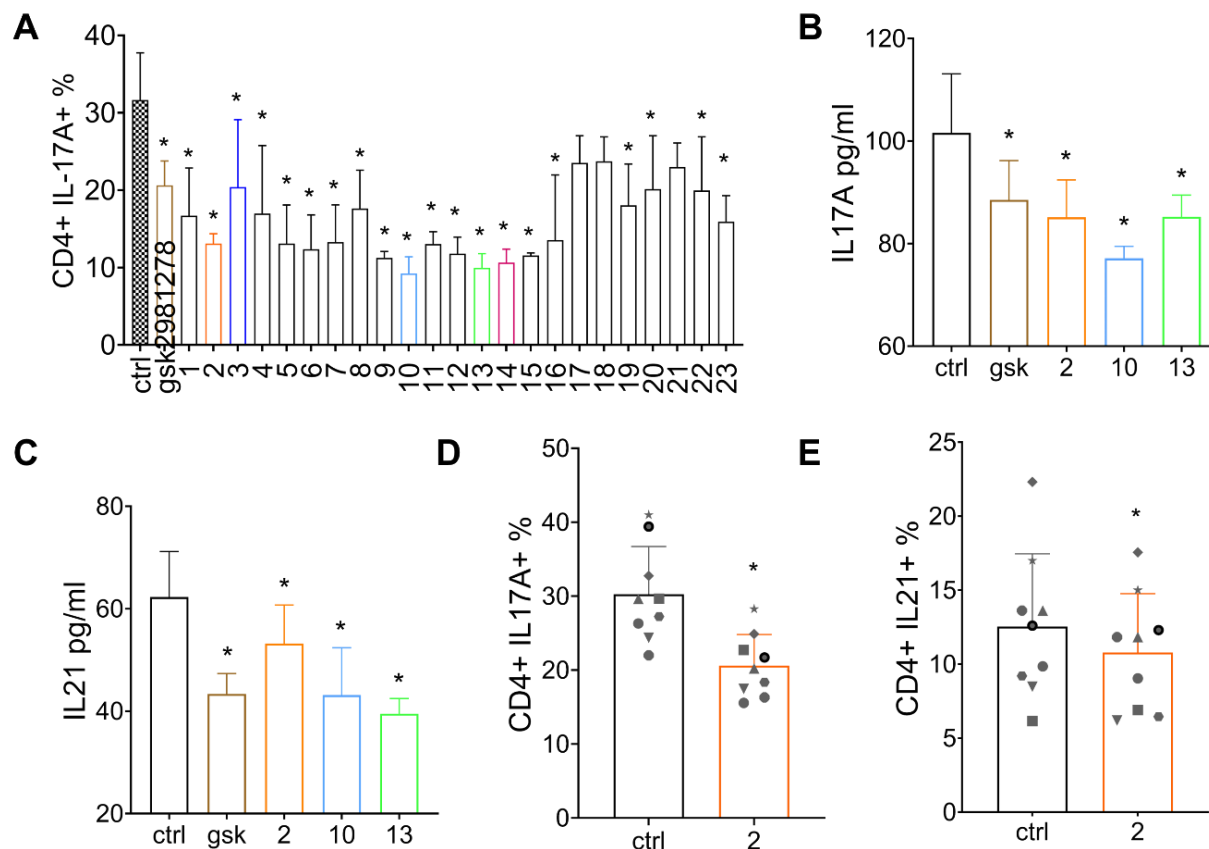
Figure 2.5. Th17 polarization assays: (A) effect of 10 nM of gsk2981278 and compounds **1-23** on Th17 polarization of PBMCs, *P<0.05 compared to vehicle (ctrl), one way ANOVA & Bonferroni's multiple comparisons test; (B) effect of 10 nM of gsk2981278 , **2**, **10** and **13** on levels of IL17A in the supernatant of Th17 polarized PBMCs compared to vehicle (ctrl), *<0.05, one way ANOVA and Dunnett's multiple comparisons test; (C) effect of 10 nM of gsk2981278, **10** and **13** on IL21 levels in the supernatant of Th17 polarized PBMCs compared to vehicle (ctrl), *P<0.05, one way ANOVA and Dunnett's multiple comparisons test; (D) effect of **2** (10 nM) on percentage of CD4+IL17A+ cells in Th17 polarization of PBMCs derived from multiple donors (n=9), *P<0.05 compared to ctrl, paired t-test; **(E)** effect of **2** (10 nM) on percentage of CD4+IL21+ cells in Th17 polarization of PBMCs derived from multiple donors (n=9), *P<0.05 compared to ctrl, paired t-test.

Table 2.2. Solubility, microsomal stability, Caco-2 and MDR1-MDCKII permeability of 2,3 derivatives of 4,5,6,7 tetrahydro-benzothiophene RORγt modulators

ID	solubility µM pH=5.0 T=298K UV-Vis	Solubility µM pH=1.6 T=298K LC/MS	Cl$_{in}$ (µl/min/mg) mouse/human/rat/dog	Caco-2 permeability			MDR1-MDCKII permeability		
				P$_{app}$ (AB), 10^{-6} cm/s M±SD	efflux	efflux verapa mil	P$_{app}$ (AB), 10^{-6} cm/s M±SD	efflux	efflux cyclos porine A
1	34	291	2015/1915/641/540	5.8±0.2	1.3	1.7	7.9±2.1	0.4	0.9
2	ND	ND	127/126/267/115	4.2±0.1	0.3	0.4	8.0±0.4	0.3	0.3
3	9.72	1.70	322/36/118/41	1.4±0.1	19.4	4.5	2.5±0.1	8.7	1.1
4	8.13	2.80	11/22/29/24	1.8±0.2	0.4	0.6	3.2±1.5	0.3	0.3
6	349.39	≥400	546/91/116/60	28.2±2.0	0.6	1.0	28.9±4.1	0.7	0.6
10	357.28	≥400	319/214/115/132	4.6±0.4	1.3	1.6	6.8±2.4	1.1	1.2
11	3.02	364	2345/510/942/260	1.2±0.3	0.3	1.2	1.3±0.2	0.8	0.7
12	391.51	≥400	71/67/97/53	34.2±2.2	0.8	0.9	29.0±4.7	0.8	0.8
13	23.72	≥200	414/404/507/369	26.7±1.3	0.9	1.2	26.7±3.4	0.7	1.0
14	33.70	16	50/35/5/16	2.0±0.5	0.9	1.0	1.2±0.1	1.3	0.9
16	13.56	267	2142/954/887/332	18.0±0.2	0.7	0.7	27.8±5.2	0.8	1.1
17	365.21	330	46/23/7/11	4.4±0.1	7.1	1.1	5.2±0.3	4.7	1.4

Discussion

In their pocket orientation, 2,3 derivatives of 4,5,6,7 tetrahydro-benzothiophene modulators of RORγt conform to structural features of previously discovered RORγt inverse agonists. The saturated tetrahydro-benzene ring structure is the hydrophobic pocket interacting moiety, the 3-amide ring substitution comprised the head group while the 2-amide ring substitution is the tail group. These structural features kept the ligand pose within RMSD <2 Å compared to reference ligands. On the other hand, the amide

arms that replace rings B and C of cholesterol core per initial design hypothesis, provided two hydrophilic surfaces that align in the two hydrophilic regions of the RORγt pocket at Hid323 and Phe377 regions. Those interactions stabilized the molecular complex in MD simulations and lowered the free energy surface of the pocket in this region of the ligand pocket. As such the 2,3-amide derivatives of 4,5,6,7 tetrahydro-benzothiophene complexes with RORγt were energetically more stable compared to RORγt complexes with other reference agonists/inverse agonists evaluated. Alkyl substitution of the tetrahydro-benzothiophene ring at position 6, resulted in a deviation from the active pose. In the case of one methyl or ethyl substitutions there was no effect on docking score and no reduction in activity in vitro. Substituting the tetrahydro-benzothiophene ring with a bulkier group such as in case of compound **5** resulted in a larger deviation (>3 A°) and a lower docking score; however, there was no reduction in activity *in vitro*. The addition of a second alkyl such as di-methyl substitution in the case of compounds **18** resulted in both a lower docking score and a reduction of in vitro activity. This can be explained by the preservation of the chair confirmation in case of a single substitution, while adding two alkyls forces the tetrahydro-benzene ring to adopt a boat or twisted boat confirmations and the creation of an additional perpendicular plane. In this case, the substitution can affect both the ligand entry and the stability of the ligand inside the pocket. It should be expected that a similar substitution at 4, 5 or 7 positions can lead to similar effects. As the results showed, the bridge length connecting ring substitution to position 3 of 4,5,6,7 tetrahydro-benzothiophene is another important determinant of the activity. In case the bridgeis one carbon long such as in case of compounds **22** and **23** the linked ring structures become sterically restricted and adopt a perpendicular confirmation with

respect to thiophene ring. As such, the ligand entry and pose are both affected. Extending the bridge beyond four atoms such as in case of compound **1** creates a similar perpendicular orientation of the substituent, however more distant to the tetrahydro-benzothiophene core. This modification does not seem to affect the entry; however, it affects the adoption of the ideal pose resulting in a lower docking score. SAR analysis shows that the adequate length of the bridge at position 3 is three atoms. A planar phenyl ring substitution linked to position 3 of the tetrahydro-benzothiophene ring through three atoms bridge, such as in case of compound **2** and **7-11**, showed a better affinity as determined by docking score, an increased stability as determined by MD simulation and higher potency in vitro. In those six compounds, ring planarity and bridge length allows for parallel or convex planes between the tetrahydro-benzothiophene and phenyl ring substitution. Such conformation allows for stacking and the reduction of PSA as calculated based on the atomic partitioning of B3LYP/6311G* wavefunctions (data not shown) compared to their TPSA. These π–π intramolecular interactions contribute to improved activity in cellular assays compared to the compounds with two-atom bridges such as **17**, **18**, **22** and **23**. An exception was compound **21**, which had flexible piperidine ring substitution. This substructure combined to a three-atom bridge led to the creation of an additional perpendicular plane like that seen in **1** and the compounds with two-atom bridges. On the other hand, compounds with two-atom bridges at position 3 were active when the substitution was a flexible unsaturated ring that can adopt a chair confirmation such as in case of compound **13**. Increasing the length of amide bridge at position 2 of 2,3 derivatives of 4,5,6,7 tetrahydro-benzothiophene which constitutes the tail group was less critical to affect the binding pose or *in vitro* activity. We increased the length of amide

bridge at position 2 of the tetrahydro-benzothiophene ring up to four atoms, such as in case of compounds **8** and **16** where the interactions with Gln286 and other residues at the pocket entry were maintained. Moreover, as we evaluated several ring substitutions linked to positions 2 and 3 of 2,3 derivatives of 4,5,6,7 tetrahydro-benzothiophene. Contrary to our initial assumptions incorporation of a hydroxyl group such as in case of compounds **14** and **17** resulted in a reduction of docking score and in vitro activity compared to **13** and **15**, respectively. These effects can be due to the intramolecular interactions between the hydroxyls and the amide bridges on position 2 as well as the N of the pyridine ring, because these interactions can change the distribution of dipole moment along the molecules, which affect their ability to form hydrogen bond interactions with the hydrophilic regions of the pocket through amide arms. Physicochemical studies revealed that all the evaluated 2,3 derivatives of 4,5,6,7 tetrahydro-benzothiophene except **2**, **3**, **4** and **23** have good solubility in neutral and acidic pH. They have diverse microsomal stability and Caco-2 permeability profiles that allow for a wide range of formulation options and organ specific targeting. Similarly, they have different potentials to cross blood brain barrier as determined by MDR1-MDCKII permeability, which allows for targeting the central nervous system disease conditions such as brain tumors and multiple sclerosis. In it worth mentioning that recovery values of compounds **2**, **4**, **10** and **11** in Caco-2 permeability assay were low (<80%) which can be attributed to the low solubility of compounds **2** and **4** or increased metabolism by Caco-2 cells for **10** and **11**, so the permeability values for those compounds are approximate. The structure metabolism relationship analysis, on the other hand, reveals that the compounds that had an alkyl substitution in position 6 of 2,3 derivatives of 4,5,6,7 tetrahydro-benzothiophene

were more stable in microsomal stability assay such as compound **3**, **4** and **6**. The hydroxyl substitutions and resulting intramolecular interactions also protected the compounds from microsomal metabolism such as in case of compound **14** and **17**. Increasing the length of amide bridge at position 3 such as in case of compound **1** or position 2 as in case of compound **16** resulted in an accelerated metabolism in microsomal stability assay. As aforementioned, these compounds adopt an open conformation because of the weak intramolecular interactions, where their ring substitutions at position 3 align to a perpendicular plane far from the thiophene ring due to increased bridge length. Such open confirmations increase compound's susceptibility to enzymatic cleavage of the amide bond. Compound **12** has improved stability and was effective in Th17 cellular assay, however this compound remains less attractive for clinical development. This is because of the small size of pyrrolidine ring substitution at position 3 renders compound **12** less target specific which is also the case for **20** with its propanenitrile. The same applies to compound **7** which is lacking a ring structure at the 2-position substitution with its trifluoromethyl group. Those three compounds maintain an activity towards RORγt; however, they are less specific in terms of target selectivity which we observed *in silico* off-target binding studies (data not shown). Additionally, they adopt other poses with orientations that differ significantly from the active pose. These findings collectively set forth the importance of central region of the pocket between Cys320-Glu326 and Arg364-Phe377 hydrophilic centers, where 2,3 derivatives of 4,5,6,7 tetrahydro-benzothiophene modulators of RORγt that occupy and strongly interact with this region showed a potent inverse agonist effect in vitro in both cell free and cellular assays. This potent inverse agonist effect was seen for all 2,3 derivatives of 4,5,6,7

tetrahydro-benzothiophene modulators of RORγt evaluated regardless of their conformity with the active pose defined by the compounds that interact with the agonist lock such as **1**, **2**, **9-11**, **13**, **16** and **19**. In our study, the availability of a fluorescent cholesterol 25NC provided a chance to perform the fluorescence polarization assay which is superior to other binding assays such as TR-FRET, SPR or SPA as it allows for ΔH and ΔS determination. 25NC was selected as a fluorescent tracer based on docking studies, molecular weight, and solubility profile. The availability of approximately seventy crystal structures of RORγt provided us with a large pool for sampling and testing with MD simulations with great accuracy, which renders molecular structure confirmation of binding poses unnecessary in our case; however, future studies employ X-ray crystallography can be performed to confirm the findings of the current study. In vivo chronic toxicity studies are required to understand the long-term effects of the modulators on body organs especially liver and lymphatic tissues which have been shown to be adversely affected by chronic administration of RORγt inverse agonist. Finally, in vivo evaluation of 2,3 derivatives of 4,5,6,7 tetrahydro-benzothiophene pharmacokinetics in rodents as well as RORγt disease animal models is a suitable next step. Compounds **10** and **13** are considered best lead candidates based on physicochemical properties and *in vitro* efficacy; however, metabolite profiling studies are required to identify the active metabolites of the two leads that can partially contribute to the activity towards RORγt. Such studies can give an explanation to the superior *in vitro* potency of compounds **10** and **13** despite their relatively high intrinsic clearance compared to other 2,3 derivatives of 4,5,6,7 tetrahydro-benzothiophene that were evaluated in this study.

Conclusions

We identified 2,3 derivatives of 4,5,6,7 tetrahydro-benzothiophene as potent modulators of RORγt. The modulators efficiently attenuate Th17 polarization and can be used *in vivo* to block T cells differentiation to Th17. The compounds can be developed to treat conditions associated with increased IL17A, IL21 and other cytokines regulated by RORγt. The compounds described in this study are bioavailable and can be developed for organ specific therapies and have low potential to penetrate blood brain barrier. The use of *in silico* studies in combination with in vitro studies provided an accelerated alternative to high throughput in vitro screening discovery and optimization studies. The efficiency of the approach is dependent on the availability of high-quality structural data of the target protein. Additionally, where multiple of such high-quality structure determination studies have been performed, adequately reviewed and publicly disclosed, we conclude that docking and MD simulations can effectively determine binding poses of new ligands without the need for a confirmation through NMR or X-ray crystallography studies.

Experimental section

In silico studies

2D fingerprint design: A review was conducted to collect data about the structure of positive hits identified in published RORα, γ, γt high throughput, medium throughput screening bioassays, counter screens, and final screens. All positive hits were ranked by potency and activity. Active hits were visually inspected to identify common structure features, 1) number of rings, 2) degree of branching, 3) linker length, 4) functional groups. The collected information was used to create intermediate design ideas starting from

25HC. The intermediate designs were tested by autodock vina against 3 RORγt crystal structures (**PDB ID**: 3KYT, 3L0L, 3L0J). Several rounds of substitutions were carried out to reach final design concepts, which were then used as screening fingerprints.

Virtual Screening: 2D screenings were performed using ChemSpider, REAL database, PubChem, Mcule and other databases that allow for structure search. Initial screens were based on 2D designs derived from 25HC linking and substitution and final screens were based on structures of compound 1 and 2. The minimum Tanimoto coefficient of similarity was set at 0.7 for all 2D screens. 3D screenings were done using phase screening and glide HTVS dockings (**PDB ID:** 5APH). A ligand binding hypothesis based on the pocket of the best resolution RORγt X-ray crystal (1.5 Å) that is currently published for RORγt (Olsson et al., 2016). Library enrichment and diversification was done at all stages by small rounds of 2D screenings of chemical catalogues of virtual and enumerated database of synthetically feasible molecules against selected scaffolds. The 23 compound sets were selected individually from small, clustered databases generated in parallel for each hit from phase screening or HTVS. Parallel rounds of screenings were performed using glide, ASE-dock, GBVI/WSA ΔG gold, London ΔG and autodock vina against RORγt (**PDB ID:** 5APH). $RMSD_{scr/ref}$ was based on maximum common structure. $RMSD_{align}$ was computed using PhaseScreen.

Molecular docking: All docking calculations were carried out with glide software using its standard precision (SP) and extra precision (XP) scoring functions. Compounds were processed with Ligprep, to generate 3D energy-minimized molecular structures with correct tautomeric states in OPLS3e force field. Epik was used to enumerate tautomers and protonation states at pH 7±2. RORγt (**PDB ID**: 5APH) was first pre-processed and

refined with protein preparation wizard to correct for deficiencies such as missing side chains, loops, hydrogen atoms; to check for protonation states of ionizable amino acids (at physiological pH); to flip wrongly assigned Asn and Gln side chains. The resulting structures were minimized with protein wizard for SP docking. Docking was performed using glide SP and XP docking. Results of the best docking pose are reported in SAR table. RMSD of docked poses was computed with maestro superposition utility or ligrmsd.

MD simulations: Initial screening 50 ns MD simulations were conducted in OPLS3e force field, Desmond 4.4 software. Longer simulations (250 ns) of ligand protein complexes were carried out in OPLS2005. Explicitly solvated (TIP3P) systems were simulated in the NPT ensemble in an orthorhombic box of sizes 79 Å × 56 Å × 75 Å. Systems were brought to neutrality with the addition of sodium and chlorine ions (physiologic pH, 0.15 M NaCl), minimized using a hybrid method of steepest decent and limited-memory algorithms. Simulations were performed under NPT ensemble implementing Berendsen thermostat/barostat methods, under constant temperature of 300 K, Nose-Hoover thermostat and Martyna-Tobias-Klein barostat algorithms to maintain 1atm of pressure, respectively. Short-range coulombic interactions were analyzed using a cut-off value 9 Å using short-range method. Smooth particle mesh Ewald method was used for handling long-range coulombic interactions. Tolerance value of $1e^{-9}$ was set for computations implemented by the SHAKE algorithm. Simulations were carried out for 25-HC, gsk2981278, **2**, **3**, **10**, **13** and **14** for 50 ns and 250 ns and trajectory sampling was done at 50 and 5 ps respectively.

FEP ligand mutation analysis: Free energy perturbation calculations were carried out using the GPU enabled FEP methodology, Desmond 6.9. REST algorithm was used for

locally enhanced sampling. Error estimates are based on standard deviation of repeat simulations and the mean unsigned error (MUE). Systems were assigned OPLS2005 force field, solvated in an orthogonal box of SPC water molecules with buffer width of 5 Å for complex and 10 Å for solvent simulations. Systems were brought to neutrality with the addition of sodium and chlorine ions (physiologic pH, 0.15 M NaCl). Systems were relaxed and equilibrated using Desmond relaxation protocol, consisting of a 100 ps energy-minimization with restraints on solute using Brownian dynamics NVT, then a 12 ps simulations at T=10 K using an NVT ensemble followed by a 12 ps simulation using NPT ensemble. Systems were equilibrated at room temperature for 24 ps using the NPT ensemble with restraints. A 240 ps room temperature NPT ensemble simulation, no restraints, was conducted. Finally, 5 ns hopping simulations were carried out in NPT ensemble, for both complex and solvent systems.

Metadynamics simulations: The solvated complex was loaded into metadynamics panel. The CV distance is defined between Gln286:δCO to His479:Nε. The Gaussian width and height are set to 0.05 Å and 0.03 kcal/mol, respectively and a wall was set at 30 Å. Systems were relaxed and equilibrated using Desmond relaxation protocol, consisting of a 100 ps energy-minimization with restraints on the solute heavy atoms using Brownian dynamics NVT, then a 12 ps NVT ensemble simulations at T = 10 K, small timesteps, and restraints on solute heavy atoms followed by a 12 ps simulation using NPT ensemble, similarly with restraints on solute heavy atoms. The solvated complexes were equilibrated at room temperature for 1ps using NPT ensemble with restraints. This was followed by 24 ps simulation at room temperature, NPT ensemble

with no restraints. Finally, a 25 ns metadynamics simulations were carried out in NPT ensemble.

Synthesis

Compounds **1-23** can be obtained through amide formation from starting reactants provided by Enamine Ltd, Kyiv, Ukraine. All compounds are >95% pure by HPLC analysis. HPLC/UPLC traces and 1H NMR spectra of example compounds are included in the supporting information. Analytical LC/MS instrument specifications: Agilent 1100 series LC/MSD system with DAD/ELSD and Agilent LC/MSD VL (G1956A), SL (G1956B) mass-spectrometer, Agilent 1200 series LC/MSD system with DAD/ELSD and Agilent LC/MSD SL (G6130A), SL (G6140A) mass-spectrometer. LC/MS data were obtained using positive/negative mode switching; column: SB-C18 1.8 μm 4.6x15mm rapid resolution cartridge ; mobile phase: A) acetonitrile, 0.1% formic acid, B) water, 0.1% formic acid; flow rate: 3 mL/min; gradient: 0 min – 100% B, 0.01 min – 100% B, 1.5 min - 0% B, 1.8 min - 0% B, 1.81 min - 100% B, injection volume: 1 μL; ionization mode: atmospheric pressure chemical ionization (APCI); scan range: m/z 80-1000. 1H NMR; the spectra were obtained using different spectrometers, mainly with an operating proton frequency of 400 MHz in DMSO-d6. Calibration was carried out according to internal standard DMSO = 2.5 ppm. **General synthetic procedure (Method 1):** An amine (100 mg), a carboxylic acid (1.1 mol eq. to the amine), and 0.5 mL of DMSO were placed into a 4 mL capped glass vial and the mixture was stirred for 30 min. Then EDC (1.2 mol eq. to the amine) was added, and the mixture was stirred for 1 hour. If the solution was transparent, the mixture was left overnight at room temperature; otherwise, the vial was placed in the ultrasonic bath and left overnight. The solution was filtered, and the solvent

and volatile components were evaporated under reduced pressure to give the crude product. The product was further purified by HPLC. **General synthetic procedure (Method 2):** An amine (100 mg), DIPEA (1.2 mol eq. to the amine), and DMSO (0.5 mL) were placed into a 4 mL capped glass vial and stirred for 30 min. After the addition of an alkyl halide (1.2 mol eq. to the amine), the vial was stirred for 1 hour at room temperature. Then the vial was placed into a thermostat (set to 100°C) for 9 hours. After cooling down the mixture was filtered; the solvent and volatile components were evaporated under reduced pressure to give the crude product. The product was further purified by HPLC. **General synthetic procedure (Method 3):** An amine (100 mg), a carboxylic acid (1.2 mol eq. to the amine), DIPEA (1.2 mol eq. to the amine), and acetonitrile (0.5 mL) were placed into a 4 mL capped glass vial, and stirred for 30 min. After the addition of 2-chloro-1-methylpyridine-1-ium iodide (1.44 mol eq. to the amine), the vial was stirred for 1 hour at room temperature and placed into a thermostat (set to 100°C) for 6 hours. After cooling down the mixture was filtered; solvent and volatile components were evaporated under reduced pressure to give the crude product. The product was further purified by HPLC.

N-(3-(4-benzylpiperazine-1-carbonyl)-4,5,6,7-tetrahydro-benzo[b]thiophen-2-yl)-2-fluorobenzamide **(1).** Step A: 2 M Aqueous NaOH solution (91 mL, 182 mmol) was added to a suspension of 2-amino-4, 5,6,7- tetrahydro-benzo[B]thiophene-3-carboxylic acid methyl ester 1 (13.1 g, 60.8 mmol) in EtOH (100 mL). The reaction mixture was heated to 60 °C and stirred for 4 hours. The temperature was raised to 80°C and the reaction was stirred overnight. The reaction was left stirring at 80°C for a further 7 hours and was then cooled to room temperature and stirred overnight. The reaction mixture was concentrated under reduced pressure to remove the EtOH. The aqueous solution was

washed with DCM (3x200 mL) and then acidified to pH 2 with concentrated hydrochloric acid. A brown solid was formed, filtered off, washed with water, and then with hexane. The solid was dried to afford the title compound (6 g, 50%) as a dark brown solid. Step B: 2-fluorobenzoic acid (500 mg, 3.5 mmol), (COCl)2 (10 mL) were heated at 50°C for 30 min. The reaction mixture was concentrated under reduced pressure. The residue was dissolved in 25 mL of dioxane. NaOH (3.5 mmol), and 10 mL of water were added at 0°C. 2-amino-4,5,6,7-tetrahydro-1-benzothiophene-3-carboxylic acid (3.5 mmol) was added, and the mixture was stirred at room temperature for 12 hours, and 2 mL of HCl was added. Then the precipitate was filtered and washed with water. Yield: 340 mg, 44%. Step C: 2-(2-fluorobenzamido)-4,5,6,7-tetrahydro-1-benzothiophene-3-carboxylic acid (340 mg, 1 mmol), HATU (1 mmol) and DIPEA (2 mmol) were dissolved in DMF (25mL). 1-benzylpiperazine (1mmol) was added, and the mixture was stirred for 24 hours at 50°C and cooled to room temperature. The reaction mixture was concentrated under reduced pressure to remove the DMF. 50 mL of water was added, 2 mL of HOAc was added, and the precipitate was filtered and washed with water. The product was purified with the use of HPLC. Yield: 149 mg, 32%. Yellow solid. Purity, >95% (assessed by LC/MS). LC/MS (APSI) m/z [M+H] calculated for $C_{25}H_{25}FN_3O_3S$: 478.2; found: 478.2.

***N-(3-(benzylcarbamoyl)-4,5,6,7-tetrahydrobenzo[b]thiophen-2-yl)-5-chloro-2-(methylthio) pyrimidine-4-carboxamide* (2). (Method1)** 2-amino-N-benzyl-4,5,6,7-tetrahydrobenzo[b] thiophene-3-carboxamide (100 mg), 5-chloro-2-(methylthio) pyrimidine-4-carboxylic acid (1.1 mol eq. to the amine), and 0.5 mL of DMSO were placed into a 4 mL capped glass vial and the mixture was stirred for 30 min. EDC (1.2 mol eq. to the amine) was added. The mixture was stirred for 1 hour and left overnight at room

temperature. The solution was filtered, and the solvent and volatile components were evaporated under reduced pressure to give the crude product. The product was further purified by HPLC. Yield: 58%; purity, >95% (assessed by LC/MS). 1H NMR (400 MHz, DMSO-d6) δ 13.07 (s, 1H), 8.91 (s, 1H), 8.05 (s, 1H), 7.50 – 7.12 (m, 5H), 4.48 (d, J = 5.7 Hz, 2H), 2.86 – 2.56 (m, 6H), 1.77 (s, 4H). LC/MS (APSI) m/z [M+H] calculated for $C_{25}H_{25}FN_3O_3S$: 473.2; found: 473.2.

***5-chloro-N-(3-{[(1,1-dioxidotetrahydro-3-thienyl)amino]-carbonyl}-6-methyl-4,5,6,7-tetrahydro-1-benzothien-2-yl)-2-(methylthio)-4-pyrimidine-carboxamide* (3).** Step A: 4-methylcyclohexan-1-one (5 g, 30 mmol) and methyl 2-cyanoacetate (5 g, 30 mmol) were mixed with NEt3 (20 mL) and Sulphur (powder, 2.5 g). The mixture was heated at 50°C for 24 hours, cooled and the reaction mixture was concentrated under reduced pressure. The residue was recrystallized from iPrOH, the precipitate was filtered, washed with iPrOH, and dried. Yield: 3 g, 35%. Step B: 2 M Aqueous NaOH solution (91 mL, 182 mmol) was added to a suspension of methyl 2-amino-6-methyl-4,5,6,7-tetrahydro-1-benzothiophene-3-carboxylate 1 (14 g, 60.8 mmol) in EtOH (100 mL). The reaction mixture was heated to 60°C and stirred for 4 hours. The temperature was raised to 80°C and the reaction was stirred overnight. The reaction was left stirring at 80°C for a further 7 hours and was then cooled to room temperature and stirred overnight. The reaction mixture was concentrated under reduced pressure to remove the EtOH. The aqueous solution was washed with DCM (3x200 mL) and then acidified to pH 2 with concentrated hydrochloric acid. A brown solid was formed, then filtered off, and washed with water, and hexane. Then the solid was dried to afford the title compound (4 g, 40%) as a dark brown solid. Step C: 2-amino-6-methyl-4,5,6,7-tetrahydro-1-benzothiophene-3-carboxylic acid

(500 mg, 2.4 mmol), HATU (2.4 mmol), and DIPEA (7.5 mmol) were dissolved in DMF (25 mL). 3-aminotetrahydrothiophene 1,1-dioxide hydrochloride (2.4 mmol) was added, and the mixture was stirred for 24 hours at 50°C and cooled to room temperature. The reaction mixture was concentrated under reduced pressure to remove the DMF, 50 mL of water was added, 2 mL of HOAc was added, and the precipitate was filtered and washed with water. The product was purified with the use of HPLC. Yield: 129 mg, 15%.

Step D: 2-amino-N-(1,1-dioxo- $1\lambda^6$ -thiolan-3-yl)-6-methyl-4,5,6,7-tetrahydro-1-benzothiophene-3-carboxamide (129 mg, 0.4 mmol), 5-chloro-2-(methylsulfanyl) pyrimidine-4-carboxylic acid (0.4 mmol), HATU (0.4 mmol) and DIPEA (0.8 mmol) were dissolved in DMF (15 mL). The mixture was stirred for 24 h at 50°C and cooled to room temperature. The reaction mixture was concentrated under reduced pressure to remove the DMF, 50 mL of water was added, 2 mL of HOAc was added, and the precipitate was filtered and washed with water. The product was purified with the use of HPLC. Yield: 62 mg, 31%. Brown solid. Purity, >95% (assessed by LC/MS). LC/MS (APSI) m/z [M+H] calculated for C25H25FN3O3S: 515.0; found: 515.0.

***N-(6-ethyl-3-{[(2-methylphenyl)amino]carbonyl}-4,5,6,7-tetrahydro-1-benzothien-2-yl)-1-methyl-1H-pyrazole-5-carboxamide* (4).** Step A: 2-cyano-N-(o-tolyl) acetamide (5 g, 30 mmol) and 4-ethylcyclohexan-1-one (2 g, 11.5 mmol) and 4-ethylcyclohexan-1-one (11.5 mmol) were mixed with NEt3 (10 mL) and Sulphur (powder, 1.5 g). The mixture was heated at 50°C for 24 hours, cooled, and the reaction mixture was concentrated under reduced pressure. The residue was recrystallized from iPrOH, the precipitate was filtered, washed with iPrOH, and dried. Yield: 1.4 g, 41%. Step B: 1-methyl-1H-pyrazole-5-carboxylic acid (100 mg, 0.8 mmol), (COCl)2 (10 mL) were heated at 50°C for 30 min.

The reaction mixture was concentrated under reduced pressure. The residue was dissolved in 25 mL of dioxane. NaOH (0.8 mmol) and 10 mL of water were added at 0°C. 2-amino-6-ethyl-N-(2-methylphenyl)-4,5,6,7-tetrahydro-1-benzothiophene-3-carboxamide (0.8 mmol) was added and the mixture was stirred at room temperature for 12 hours. 1 mL of HCl was added the precipitate was filtered and washed with water. The product was purified with the use of HPLC. Yield: 12 mg, 3%. Beige solid. Purity, >95% (assessed by LC/MS). LC/MS (APSI) m/z [M+H] calculated for C25H25FN3O3S: 423.2; found: 423.2.

N-{6-tert-butyl-3-[(4-methyl-1-piperazinyl)   carbonyl]-4,5,6,7-tetrahydro-1-benzothien-2-yl}-2-fluorobenzamide   (5).   Step A: 3-(4-methylpiperazin-1-yl)-3-oxopropanenitrile (2 g, 12 mmol) and 4-(tert-butyl) cyclohexan-1-one (12 mmol) were mixed with NEt3 (10 mL) and Sulphur (powder, 1.5 g). The mixture was heated at 50°C for 24 hours, cooled and the reaction mixture was concentrated under reduced pressure. The residue was recrystallized from iPrOH, the precipitate was filtered, washed with iPrOH, and dried. Yield: 2 g, 50%. Step B: 2-fluorobenzoic acid (100 mg, 0.7 mmol), (COCl)2 (10 mL) were heated at 50°C for 30 min. The reaction mixture was concentrated under reduced pressure. The residue was dissolved in 25 mL of dioxane. NaOH (0.7 mmol) and 10 mL of water were added at 0°C. 2-6-tert-butyl-3-(4-methylpiperazine-1-carbonyl)-4,5,6,7-tetrahydro-1-benzothiophene-2-amine (0.7 mmol) was added, and the mixture was stirred at room temperature for 12 hours, 1 mL of HCl was added the precipitate was filtered, washed with water. The product was purified with the use of HPLC. Yield: 11 mg, 3%. Yellow oil. Purity, >95% (assessed by LC/MS). LC/MS (APSI) m/z [M+H] calculated for C25H25FN3O3S: 458.2; found: 458.2.

2-fluoro-N-{6-methyl-3-[(4-methyl-1-piperazinyl) carbonyl]-4,5,6,7-tetrahydro-1-benzothien-2-yl} benzamide (6). Step A: 3-(4-methylpiperazin-1-yl)-3-oxopropanenitrile (5 g, 30 mmol) and 4-methylcyclohexan-1-one (5 g, 30 mmol) were mixed with NEt3 (20 mL) and Sulphur (powder, 2.5 g). The mixture was heated at 50°C for 24 hours, cooled and the reaction mixture was concentrated under reduced pressure. The residue was recrystallized from iPrOH, the precipitate was filtered, washed with iPrOH, and dried. Yield: 3.5 g, 40%. Step B: 2-fluorobenzoic acid (500 mg, 3.5 mmol), (COCl)2 (10 mL) were heated at 50°C for 30 min. The reaction mixture was concentrated under reduced pressure. The residue was dissolved in 25 mL of dioxane. NaOH (3.5 mmol) and 10 mL of water were added at 0°C. 6-methyl-3-(4-methylpiperazine-1-carbonyl)-4,5,6,7-tetrahydro-1-benzothiophen-2-amine (3.5 mmol) was added, and the mixture was stirred at room temperature for 12 hours. 2 mL of HCl was added, the precipitate was filtered, and washed with water. The product was purified with the use of HPLC. Yield: 25 mg, 14%. Yellow solid. Purity, >95% (assessed by LC/MS). LC/MS (APSI) m/z [M+H] calculated for C25H25FN3O3S: 416.2; found: 416.0.

N-benzyl-2-[(trifluoroacetyl)amino]-4,5,6,7-tetrahydro-1-benzothiophene-3-carboxamide (7). 2-amino-N-benzyl-4,5,6,7-tetrahydro-1-benzothiophene-3-carboxamide (100 mg, 0.35 mmol) was mixed with TFAA (20 mL) and the mixture was heated at 60°C for 5 hours. The reaction mixture was concentrated under reduced pressure and the residue was purified with the use of HPLC. Yield: 55 mg, 52%. Beige solid. Purity, >95% (assessed by LC/MS). LC/MS (APSI) m/z [M+H] calculated for C25H25FN3O3S: 383.1; found: 383.0.

N-benzyl-2-({[(4-methyl-2-pyrimidinyl)thio]acetyl}amino)-4,5,6,7-tetrahydro-1

benzothiophene-3-carboxamide (8). 2-[(4-methylpyrimidine-2-yl) sulfanyl] acetic acid

(0.35 mmol) was dissolved in dioxane (15 mL), MsCl (0.4 mmol), and NEt3 (0.4 mmol)

were added at 0°C. The mixture was stirred at room temperature for 1 hour. 2-amino-N-

benzyl-4,5,6,7-tetrahydro-1-benzothiophene-3-carboxamide (100 mg, 0.35 mmol) was

added and stirred for 12 hours at room temperature. The reaction mixture was

concentrated under reduced pressure. Yield: 2 mg, 3%. Brown solid. Purity, >95%

(assessed by LC/MS). LC/MS (APSI) m/z [M+H] calculated for C25H25FN3O3S: 453.1;

found: 453.0.

N-benzyl-2-[(1-piperidinylacetyl)   amino]-4,5,6,7-tetrahydro-1-benzothiophene-3-

carboxamide (9). 2-piperidine-1-ylacetic acid (0.35 mmol) was dissolved in dioxane (15

mL), MsCl (0.4 mmol), and NEt3 (0.4 mmol) were added at 0°C. The mixture was stirred

at room temperature for 1 hour, 2-amino-N-benzyl-4,5,6,7-tetrahydro-1-benzothiophene-

3-carboxamide (100 mg, 0.35 mmol) was added and stirred 12 hours at room

temperature. The reaction mixture was concentrated under reduced pressure. Yield: 16

mg, 12%. Brown solid. Purity, >95% (assessed by LC/MS). LC/MS (APSI) m/z [M+H]

calculated for C25H25FN3O3S: 412.2; found: 412.2.

N-benzyl-2-{[(4-methyl-1-piperazinyl)   acetyl]   amino}-4,5,6,7-tetrahydro-1-

benzothiophene-3-carboxamide   (10).   N-benzyl-2-(2-chloroacetamido)   -4,5,6,7-

tetrahydro-1-benzothiophene-3-carboxamide (compound 1) (3.63 g, 10 mmol), 1-

methylpiperazine (compound 2) (1.00 g, 10 mmol) were dissolved in 45 mL of DMF and

K2CO3 (2.07 g, 15 mmol) was added to the mixture. After that, the mixture was stirred

for 12 hours at 50°C. Then the mixture was cooled to room temperature and cold water

(250 mL) was added. The product was extracted with EtOAc (3x50 mL), washed with brine (3x50 mL), and the organic layer was dried with Na2SO4. The solvent was removed, and the residue was purified using HPLC. Brown oil. Yield: 42%; purity, >95% (assessed by LC/MS). 1H NMR (400 MHz, DMSO-d6) δ 11.84 (s, 1H), 7.95 (s, 1H), 7.32 (h, J = 6.6 Hz, 4H), 7.23 (t, J = 6.9 Hz, 1H), 4.46 (d, J = 5.8 Hz, 2H), 3.14 (s, 2H), 2.72 (d, J = 6.5 Hz, 2H), 2.60 (d, J = 6.6 Hz, 2H), 2.45 (s, 3H), 2.34 (s, 4H), 2.14 (s, 3H), 1.77 – 1.70 (m, 5H). LC/MS (APSI) m/z [M+H] calculated for $C_{25}H_{25}FN_3O_3S$: 427.2; found: 427.2.

N-benzyl-2-{[(4-methyl-1-piperidinyl) acetyl] amino}-4,5,6,7-tetrahydro-1-benzothiophene-3-carboxamide (11). 2-(4-methyl piperidine-1-yl) acetic acid (0.35 mmol) was dissolved in dioxane (15 mL), MsCl (0.4 mmol), and NEt3 (0.4 mmol) were added at 0°C. The mixture was stirred at room temperature for 1 hour, 2-amino-N-benzyl-4,5,6,7-tetrahydro-1-benzothiophene-3-carboxamide (100 mg, 0.35 mmol) was added and stirred 12 hours at room temperature. The reaction mixture was concentrated under reduced pressure. Yield: 15 mg, 10%. Light brown solid. Purity, >95% (assessed by LC/MS). LC/MS (APSI) m/z [M+H] calculated for $C_{25}H_{25}FN_3O_3S$: 426.2; found: 426.2.

N-(3-(2-methylpyrrolidine-1-carbonyl)-4,5,6,7-tetrahydro-benzo[b]thiophen-2-yl) nicotinamide (12). (Method 1) (2-amino-4,5,6,7-tetrahydrobenzo[b]thiophen-3-yl)(2-methylpyrrolidin-1-yl)methanone (100 mg), nicotinic acid (1.1 mol eq. to the amine), and 0.5 mL of DMSO were placed into a 4 mL capped glass vial and the mixture was stirred for 30 min. EDC (1.2 mol eq. to the amine) was added. The mixture was stirred for 1 hour and left overnight at room temperature. The solution was filtered, and the solvent and volatile components were evaporated under reduced pressure to give the crude product. The product was further purified by HPLC. Yield: 67%; purity, >95% (assessed by

LC/MS). 1H NMR (500 MHz, DMSO-d6) δ 11.33 (s, 1H), 10.95 (s, 1H), 8.96 (d, J = 2.3 Hz, 1H), 8.73 (d, J = 4.8 Hz, 1H), 8.20 – 8.14 (m, 1H), 2.64 (d, J = 6.3 Hz, 2H), 1.75 (s, 2H), 1.51 (s, 1H), 1.15 (s, 1H), 0.80 (s, 1H). LC/MS (APSI) m/z [M+H] calculated for C20H23N3O2S: 370.2; found: 370.2.

N-(3-((2R,4R)-2,4-dimethylpiperidine-1-carbonyl)-4,5,6,7-tetrahydrobenzo[b]thiophen-2-yl) nicotinamide (13).

Step A: methyl 2-amino-4,5,6,7-tetrahydro-1-benzothiophene-3-carboxylate (21.1g, 100mol) was dissolved in dry DMF (150 mL) followed by addition of HATU (100 mmol), pyridine-3-carboxylic acid (13.5g, 110 mmol) and DIPEA (300 mmol) at room temperature. The reaction mixture was stirred at ambient temperature for 12 hours. LC/MS analysis showed complete conversion and the mixture was concentrated under reduced pressure. The residue was redissolved in EtOAc (1 L), and the organic phase was washed with 0.1M HCl (aqueous) and brine, dried (MgSO4), and filtered. Evaporation of the solvent under reduced pressure gave compound 3 which was purified by chromatography. Yield: 65%. Step B: 2-(pyridine-3-amido)-4,5,6,7-tetrahydro-1-benzothiophene-3-carboxylic acid (50 mmol) and CDI (60 mmol) were dissolved in dry DMF (100 mL). The mixture was stirred at room temperature for 30 min and then at 70°C for 1 hour. Rac-(2R,4R) -2,4-dimethylpiperidine (60 mmol) was added. The mixture was heated with stirring for 12 hours at 50°C, cooled to room temperature and water (300 mL) was added. The residue was filtered out, washed with water (3x100 mL), dried at 60°C, and purified using HPLC. Yield: 38%. Step C: The mixture of rac-N-{3-[(2R,4R)-2,4-dimethylpiperidine-1-carbonyl]-4,5,6,7-tetrahydro-1-benzothiophen-2-yl}pyridine-3-carboxamide and 2-(pyridin-3-yl)-5,6,7,8-tetrahydro-4*H*-benzo[4,5]thieno[2,3-*d*][1,3]oxazin-4-one (25 mmol) and rac-(2R,4R)-2,4-

dimethylpiperidine (50 mmol) were dissolved in dry DMF (50 mL), the mixture was stirred at 100°C for 24 hours (LC\MS control). Reaction mixture was concentrated under reduced pressure. The residue was mixed with water (100 mL) and iPrOH (30 mL) was added. The mixture was stirred at room temperature for 2 hours, filtered, and washed with water (3x50 mL) and residue was purified using HPLC. Yield: 24%. Step D: For preparative separation, 120 mg of rac-N-{3-[(2R,4R)-2,4-dimethylpiperidine-1-carbonyl]-4,5,6,7-tetrahydro-1-benzothiophen-2-yl}pyridine-3-carboxamide was dissolved in methanol (0.9 mL), degassed by an ultrasonic bath. Yield: 37%. 1H NMR (400 MHz, DMSO-d6) δ 10.91 (d, J = 82.0 Hz, 1H), 9.01 (dd, J = 18.9, 2.3 Hz, 1H), 8.75 (d, J = 4.8 Hz, 1H), 8.22 (dd, J = 21.5, 8.2 Hz, 1H), 7.55 (dd, J = 8.0, 4.9 Hz, 1H), 4.13 (dd, J = 13.0, 6.9 Hz, 1H), 3.62 – 3.41 (m, 1H), 3.22 – 3.04 (m, 1H), 2.67 (d, J = 5.2 Hz, 3H), 2.34 (d, J = 7.7 Hz, 2H), 1.73 (ddd, J = 32.9, 16.5, 10.7 Hz, 8H), 1.14 (dd, J = 11.7, 6.6 Hz, 4H), 0.95 (d, J = 6.1 Hz, 1H), 0.84 (d, J = 6.5 Hz, 2H). LC/MS (APSI) m/z [M+H] calculated for $C_{25}H_{25}FN_3O_3S$: 398.0; found: 398.0.

***N-(3-(((1r,4r)-4-hydroxycyclohexyl)carbamoyl)-4,5,6,7-tetrahydrobenzo[b]thiophen-2-yl) nicotinamide* (14). (Method1)** 2-amino-N-((1r,4r)-4-hydroxycyclohexyl)-4,5,6,7-tetrahydrobenzo [b]thiophene-3-carboxamide (100 mg), nicotinic acid (1.1 mol eq. to the amine), and 0.5 mL of DMSO were placed into a 4 mL capped glass vial and the mixture was stirred for 30 min. EDC (1.2 mol eq. to the amine) was added. The mixture was stirred for 1 hour and left overnight at room temperature. The solution was filtered, and the solvent and volatile components were evaporated under reduced pressure to give the crude product. The product was further purified by HPLC. Yield: 63%; purity, >95% (assessed by LC/MS). 1H NMR (500 MHz, DMSO-d6) δ 12.15

(s, 1H), 9.03 (d, J = 2.3 Hz, 1H), 8.78 (s, 1H), 8.20 (dt, J = 8.1, 2.0 Hz, 1H), 7.61 (t, J = 6.3 Hz, 1H), 7.32 (s, 1H), 4.55 (d, J = 4.3 Hz, 1H), 3.80 – 3.63 (m, 1H), 2.66 (dt, J = 13.4, 6.0 Hz, 4H), 1.89 – 1.68 (m, 9H), 1.40 – 1.16 (m, 4H). LC/MS (APSI) m/z [M+H] calculated for $C_{25}H_{25}FN_3O_3S$: 400.2; found: 400.2.

N-(3-(3-ethylpyrrolidine-1-carbonyl)-4,5,6,7-tetrahydro-benzo[b]thiophen-2-yl)nicotinamide (15). (Method 1) (2-amino-4,5,6,7-tetrahydrobenzo[b]thiophen-3-yl)(3-ethylpyrrolidin-1-yl)methanone (100 mg), nicotinic acid (1.1 mol eq. to the amine), and 0.5 mL of DMSO were placed into a 4 mL capped glass vial and the mixture was stirred for 30 min. EDC (1.2 mol eq. to the amine) was added. The mixture was stirred for 1 hour and left overnight at room temperature. The solution was filtered, and the solvent and volatile components were evaporated under reduced pressure to give the crude product. The product was further purified by HPLC. Yield: 65%; purity, >95% (assessed by LC/MS). 1H NMR (500 MHz, DMSO-d6) δ 11.09 (s, 1H), 8.97 (s, 1H), 8.73 (dd, J = 4.7, 1.6 Hz, 1H), 8.22 – 8.13 (m, 1H), 7.55 (dd, J = 8.0, 4.9 Hz, 1H), 3.52 (s, 2H), 2.93 (d, J = 58.9 Hz, 1H), 2.64 (t, J = 6.0 Hz, 2H), 2.36 (s, 1H), 1.99 (s, 2H), 1.82 – 1.57 (m, 4H), 1.44 (t, J = 10.0 Hz, 1H), 1.30 (s, 3H), 0.80 (s, 2H). LC/MS (APSI) m/z [M+H] calculated for $C_{25}H_{25}FN_3O_3S$: 384.2; found: 384.2.

N-benzyl-2-(2-((1-methyl-1H-imidazol-2-yl)thio)acetamido)-4,5,6,7-tetrahydrobenzo[b] thiophene-3-carboxamide (16). (Method 2) 2-amino-N-benzyl-4,5,6,7-tetrahydrobenzo[b] thiophene-3-carboxamide (100 mg), DIPEA (1.2 mol eq. to the amine), and DMSO (0.5 mL) were placed into a 4 mL capped glass vial and stirred for 30 min. 2-((1-methyl-1H-imidazol-2-yl)thio)acetyl chloride (1.2 mol eq. to the amine) was added and the vial was stirred for 1 hour at room temperature. Then the vial was placed

into a thermostat (set to 100°C) for 9 hours. After cooling down the mixture was filtered; the solvent and volatile components were evaporated under reduced pressure to give the crude product. The product was further purified by HPLC. Yield: 65%; purity, >95% (assessed by LC/MS). 1H NMR (500 MHz, DMSO-d6) δ 11.75 (s, 1H), 8.03 (t, J = 6.0 Hz, 1H), 7.30 (d, J = 6.6 Hz, 4H), 7.22 (s, 1H), 7.17 (d, J = 1.4 Hz, 1H), 6.86 (d, J = 1.3 Hz, 1H), 4.44 (d, J = 5.9 Hz, 2H), 3.96 (s, 2H), 3.54 (s, 3H), 2.64 (s, 2H), 2.59 (d, J = 5.6 Hz, 2H), 1.70 (s, 4H). LC/MS (APSI) m/z [M+H] calculated for C25H25FN3O3S: 441.2; found: 441.2.

***N-(3-(3-(hydroxymethyl)pyrrolidine-1-carbonyl)-4,5,6,7-tetrahydrobenzo[b]thiophen-2-yl) nicotinamide* (17). (Method 1)** (2-amino-4,5,6,7-tetrahydrobenzo[b]thiophen-3-yl)(3-(hydroxymethyl)pyrrolidin-1-yl)methanone (100 mg), a carboxylic acid (1.1 mol eq. to the amine), and 0.5 mL of DMSO were placed into a 4 mL capped glass vial and the mixture was stirred for 30 min. EDC (1.2 mol eq. to the amine) was added. The mixture was stirred for 1 hour and left overnight at room temperature. The solution was filtered, and the solvent and volatile components were evaporated under reduced pressure to give the crude product. The product was further purified by HPLC. Yield: 59%; purity, >95% (assessed by LC/MS). 1H NMR (500 MHz, DMSO-d6) δ 11.10 (s, 1H), 8.97 (d, J = 2.3 Hz, 1H), 8.73 (dd, J = 4.8, 1.6 Hz, 1H), 8.18 (dt, J = 7.9, 1.9 Hz, 1H), 7.54 (dd, J = 8.0, 4.8 Hz, 1H), 4.63 (s, 1H), 3.52 (s, 1H), 2.63 (t, J = 5.9 Hz, 2H), 2.43 – 2.14 (m, 3H), 1.97 – 1.41 (m, 6H). LC/MS (APSI) m/z [M+H] calculated for C25H25FN3O3S: 386.2; found: 386.2.

***N-(6,6-dimethyl-3-(morpholine-4-carbonyl)-4,5,6,7-tetrahydrobenzo[b]thiophen-2-yl) pyrazine-2-carboxamide* (18). (Method 3)** (2-amino-6,6-dimethyl-4,5,6,7-

tetrahydrobenzo[b] thiophen-3-yl)(morpholino)methanone (100 mg), pyrazine-2-carboxylic acid (1.2 mol eq. to the amine), DIPEA (1.2 mol eq. to the amine), and acetonitrile (0.5 mL) were placed into a 4 mL capped glass vial, and stirred for 30 min. After the addition of 2-chloro-1-methylpyridine-1-ium iodide (1.44 mol eq. to the amine), the vial was stirred for 1 hour at room temperature. Then the vial was placed into a thermostat (set to 100°C) for 6 hours. After cooling down the mixture was filtered; the solvent and volatile components were evaporated under reduced pressure to give the crude product. The product was further purified by HPLC. Yield: 56%; purity, >95% (assessed by LC/MS). 1H NMR (500 MHz, DMSO-d6) δ 10.94 (s, 1H), 9.27 (d, J = 1.5 Hz, 1H), 8.95 (d, J = 2.4 Hz, 1H), 8.83 (dd, J = 2.5, 1.5 Hz, 1H), 3.63 – 3.35 (m, 9H), 3.12 (d, J = 8.0 Hz, 1H), 2.45 (d, J = 15.5 Hz, 4H), 1.49 (t, J = 6.4 Hz, 2H), 1.23 (q, J = 7.3 Hz, 6H), 0.97 (s, 7H). LC/MS (APSI) m/z [M+H] calculated for C25H25FN3O3S: 401.2; found: 401.2.

***N-(3-(((1-methyl-1H-1,2,4-triazol-3-yl)methyl)carbamoyl)-4,5,6,7-tetrahydrobenzo[b]thiophen -2-yl)nicotinamide* (19). (Method 1)** 2-amino-N-((1-methyl-1H-1,2,4-triazol-3-yl)methyl)-4,5,6,7-tetrahydrobenzo[b]thiophene-3-carboxamide (100 mg), nicotinic acid (1.1 mol eq. to the amine), and 0.5 mL of DMSO were placed into a 4 mL capped glass vial and the mixture was stirred for 30 min. EDC (1.2 mol eq. to the amine) was added. The mixture was stirred for 1 hour and left overnight at room temperature. The solution was filtered, and the solvent and volatile components were evaporated under reduced pressure to give the crude product. The product was further purified by HPLC. Yield: 57%; purity, >95% (assessed by LC/MS). LC/MS (APSI) m/z [M+H] calculated for C25H25FN3O3S: 397.0; found: 397.0.

(S)-N-(3-((1-cyanoethyl)carbamoyl)-4,5,6,7-tetrahydro-benzo[b]thiophen-2-yl)nicotinamide **(20).** **(Method** **1)** (R)-2-amino-N-(1-cyanoethyl)-4,5,6,7-tetrahydrobenzo[b]thiophene-3-carboxamide (100 mg), nicotinic acid (1.1 mol eq. to the amine), and 0.5 mL of DMSO were placed into a 4 mL capped glass vial and the mixture was stirred for 30 min. EDC (1.2 mol eq. to the amine) was added. The mixture was stirred for 1 hour and was left overnight at room temperature. The solution was filtered, and the solvent and volatile components were evaporated under reduced pressure to give the crude product. The product was further purified by HPLC. Yield: 67%; purity, >95% (assessed by LC/MS). LC/MS (APSI) m/z [M+H] calculated for $C_{25}H_{25}FN_3O_3S$: 355.0; found: 355.0.

N-(3-((piperidin-4-ylmethyl)carbamoyl)-4,5,6,7-tetrahydro-benzo[b]thiophen-2-yl) ***nicotinamide*** **(21).** **(Method** **1)** 2-amino-N-(piperidin-4-ylmethyl)-4,5,6,7-tetrahydrobenzo[b] thiophene-3-carboxamide (100 mg), nicotinic acid (1.1 mol eq. to the amine), and 0.5 mL of DMSO were placed into a 4 mL capped glass vial and the mixture was stirred for 30 min. EDC (1.2 mol eq. to the amine) was added. The mixture was stirred for 1 hour and left overnight at room temperature. The solution was filtered, and the solvent and volatile components were evaporated under reduced pressure to give the crude product. The product was further purified by HPLC. Yield: 63%; purity, >95% (assessed by LC/MS). 1H NMR (500 MHz, DMSO-d6) δ 9.09 (d, J = 2.1 Hz, 1H), 8.54 (d, J = 4.7 Hz, 1H), 8.20 (dd, J = 7.9, 2.1 Hz, 1H), 7.41 (dd, J = 7.9, 4.8 Hz, 1H), 3.25 – 3.13 (m, 4H), 2.85 – 2.69 (m, 3H), 2.52 (d, J = 6.5 Hz, 2H), 1.79 (t, J = 10.4 Hz, 3H), 1.71 – 1.62 (m, 4H), 1.31 (q, J = 13.6, 12.9 Hz, 2H). LC/MS (APSI) m/z [M+H] calculated for $C_{25}H_{25}FN_3O_3S$: 399.2; found: 399.2.

N-(3-benzoyl-4,5,6,7-tetrahydrobenzo[b]thiophen-2-yl)pyrazine-2-carboxamide

(22). (Method 3) (2-amino-4,5,6,7-tetrahydrobenzo[b]thiophen-3-yl)(phenyl)methanone (100 mg), pyrazine-2-carboxylic acid (1.2 mol eq. to the amine), DIPEA (1.2 mol eq. to the amine), and acetonitrile (0.5 mL) were placed into a 4 mL capped glass vial, and stirred for 30 min. After the addition of 2-chloro-1-methylpyridine-1-ium iodide (1.44 mol eq. to the amine), the vial was stirred for 1 hour at room temperature, then placed into a thermostat (set to 100°C) for 6 hours. After cooling down the mixture was filtered; the solvent and volatile components were evaporated under reduced pressure to give the crude product. The product was further purified by HPLC. Yield: 58%; purity, >95% (assessed by LC/MS). 1H NMR (500 MHz, DMSO-d6) δ 12.58 (s, 1H), 9.31 (s, 1H), 8.96 (d, J = 2.5 Hz, 1H), 8.81 (d, J = 2.6 Hz, 1H), 7.63 – 7.45 (m, 5H), 2.70 (t, J = 6.4 Hz, 2H), 1.96 (t, J = 6.1 Hz, 2H), 1.73 (t, J = 5.9 Hz, 2H), 1.50 (d, J = 7.6 Hz, 2H). LC/MS (APSI) m/z [M+H] calculated for C25H25FN3O3S: 364.0; found: 364.0.

N-(3-benzoyl-4,5,6,7-tetrahydrobenzo[b]thiophen-2-yl)-5-methyl-2-(methylsulfonyl) pyrimidine-4-carboxamide **(23).** **(Method 3)** (2-amino-4,5,6,7-tetrahydrobenzo[b]thiophen-3-yl)(phenyl)methanone (100 mg), 5-methyl-2-(methylsulfonyl)pyrimidine-4-carboxylic acid (1.2 mol eq. to the amine), DIPEA (1.2 mol eq. to the amine), and acetonitrile (0.5 mL) were placed into a 4 mL capped glass vial, and stirred for 30 min. After the addition of 2-chloro-1-methylpyridine-1-ium iodide (1.44 mol eq. to the amine), the vial was stirred for 1 hour at room temperature. Then the vial was placed into a thermostat (set to 100°C) for 6 hours. After cooling down the mixture was filtered; the solvent and volatile components were evaporated under reduced pressure to give the crude product. The product was further purified by HPLC. Yield: 62%;

purity, >95% (assessed by LC/MS). 1H NMR (500 MHz, DMSO-d6) δ 12.82 (s, 1H), 9.21 (s, 1H), 7.63 – 7.45 (m, 5H), 3.57 (s, 3H), 2.70 (s, 5H), 1.94 (s, 2H), 1.72 (s, 2H), 1.50 (s, 2H). LC/MS (APSI) m/z [M+H] calculated for $C_{25}H_{25}FN_3O_3S$: 456.1; found: 456.1.

TR-FRET co-activator recruitment assay: Five µL of each compound in an assay buffer is added to 15µL of detection mix for 20µL total assay volume (50 mM tris-HCl pH=7.0, 150 mM NaCl, 50 mM KCl, 5 mM MgCl2, 1 mM DTT, 0.1% BSA, 0.001% triton X); 1.5 nM GST-RORγt (LBD) expressed in insect cells (Creative Biomart, Shirley, NY, USA); 90 nM biotinylated RIP140 coactivator peptide (biotinyl-NH-Ahx-NSHQKVTLLQLLLGHKNEEN-CONH2); 50 nM SA-APC; 1.5 nM Eu-anti GST IgG. Reactions were read with EnSpire plate reader, (excitation: 320 nm, emission A: 615 nm; emission B: 699 nm) to measure emission ratio acceptor/donor. Final compound concentrations range from 0.004 nM to 100 µM. 100% activity is represented by average DMSO controls. Zero% activity is average of two wells of 100 µM gsk2981278 controls.

FP competitive binding assay: Competition assays were performed with 10 nM full length RORγ, expressed in HEK293T cells, (Origene technologies inc., Rockville, MD, USA) loaded with 5 nM 25NC. The mixture was then incubated with increasing concentrations of compounds (0.004 nM to 100 µM). Parallel and perpendicular fluorescence intensity were measured with synergy 2 plate reader (Excitation 497 nm, emission 551 nm) and polarization reported in milli polarization. Ki values were determined by Cheng-Prusoff equation (Yung-Chi & Prusoff, 1973). ΔH and ΔS were determined by Van't Hoff equation. ΔG was determined by Gibbs free energy equation (Rossi & Taylor, 2011).

RORγ reporter assay: RORγ reporter assay kit, INDIGO biosciences, was used to measure the inhibitory activity of compounds compared to standard RORγ inverse agonist ursolic acid. 200 µL of reporter cells were dispensed into each well of the assay plate. The cells were preincubated for 4-6 hours. Following the pr-incubation period, culture media were discarded and 200 µL/well of the prepared 1x concentration treatment media are added. Following 24-hour incubation, treatment media were discarded, and luciferase detection reagent were added to each well. The intensity of light emission in units of relative light units (RLU) from each assay well was quantified using a plate-reading luminometer.

Th17 polarization: PBMCs were plated in complete RPMI-1640 medium (10% FBS), and incubated at 37°C in a humidified, 5% CO_2 atmosphere, treated with CD3/CD28 (2 µl: 80000 cells) for 12 days in presence of IL6 10 ng/mL, IL1B 10 ng/mL, TGFβ 10 ng/mL, and IL23 10 ng/mL. Compounds were added to the cells at day 12 for 48 hours. On day 14, cells were treated with cell stimulation cocktail for 5 hours at the end of 48 hours incubation. PBMCs were stained cells with live/dead (455 UV) viability dye. Anti-human antibodies for IL17A, RORγt, IL21, IL22 and IFNγ were added to wells at 1:1000 concentration in permeabilization buffer. Cell viability and intracellular cytokines were analyzed by flowcytometry.

Kinetic solubility: Compound dilutions were prepared in duplicates in phosphate-buffered saline (PBS, pH=7.4), 100 mM citrate buffer (pH=5.0) or fasted state simulated gastric fluid (FaSSGF, pH=1.6) with 2% DMSO. The dilutions in PBS were allowed to equilibrate at 25°C on a thermostatic shaker for two hours and then filtered through HTS filter plates. The filtrates of test compounds were diluted 2-fold with acetonitrile with 2%

DMSO before measuring. Compound dilutions in 50% acetonitrile/PBS were prepared (2% final DMSO) to generate calibration curves. Ondansetron was used as a reference compound to control proper assay performance. For PBS and citrate buffer solubility, 200 µL of each sample was transferred to a 96-well plate and measured by UV spectrometer/reader in the 260-300 nm range, absolute absorbance unit values for the minimum and maximum concentration points within the 0-3 OD range. For FaSSGF solubility, samples were analyzed using HPLC system coupled with a tandem mass spectrometer.

Microsomal stability: Microsomal incubations were carried out in 96-well plates in 5 aliquots of 30 µL each (one for each time point). Liver microsomal incubation medium comprised of phosphate buffer (100 mM, pH=7.4), MgCl2 (3.3 mM), NADPH (3 mM), glucose-6-phosphate (5.3 mM), glucose-6-phosphate dehydrogenase (0.67 units/mL) with 0.42 mg of liver microsomal protein per mL. In the control reactions the NADPH-cofactor system was substituted with phosphate buffer. Compounds (2 µM) were incubated with microsomes at 37°C, shaking at 100rpm. Each reaction was performed in duplicates. Five time points over 40 mins were analyzed. Reactions were stopped by adding methanol containing internal standard, followed by protein sedimentation by centrifuging. Supernatants were analyzed using HPLC system coupled with tandem mass spectrometer. Intrinsic clearance (Cl_{in}) was determined in plot of ln (AUC) versus time, using linear regression analysis according to equation:$Clin = \frac{0.693}{t1/2} \times \frac{\text{µL incubation}}{\text{mg microsomes}}$

Caco-2 permeability: Caco-2 cells were suspended in the DMEM complete medium to a final concentration 6×10^5 cells/mL. 0.4 mL of cell suspension was added to each well of HTS 24 multi-well insert system and 25mL of pre-warmed DMEM complete medium was

added to the feeder tray. The plates were incubated for 6-10 days before the transport experiments, then placed in a sterile 24-well transport analysis plates. The inserts were washed with PBS after medium aspiration. Ketoprofen, atenolol, quinidine, and digoxin were used as reference compounds. To determine the rate of compounds transport in apical (A)-to basolateral (B) direction, 0.3 mL of compounds solutions in transport buffer (Hank's BSS (9.5 g/L), NaHCO3 (0.35 g/L), 0.81 mM MgSO4, 1.26 mM CaCl2, 25 mM HEPES, pH=7.4) were added into the filter wells and 1 mL of transport buffer was added to transport analysis plate wells. To determine transport rates in B-A direction, 1 mL of compound solutions were added into the wells of the transport analysis plate, the wells in the filter plate were filled with 0.3 mL of buffer (apical compartment). P-gp mediated transport of the compounds was assessed by determining the bidirectional transport in the presence or absence of verapamil. Plates were incubated for 90 mins at 37°C under continuous shaking. Aliquots were taken from the donor and receiver compartments for LC-MS/MS analysis. Samples were mixed with acetonitrile followed by protein sedimentation by centrifuging. Supernatants were analyzed using HPLC system coupled with a tandem mass spectrometer.

MDR1-MDCKII permeability: Canine MDR1 knock-out, human MDR1 knock-in MDCKII cells (MDR1-MDCKII) (Sigma-Aldrich, Saint Louis, MO, USA) were cultured in 75 cm^2 flasks to 80-90% confluency in a humidified atmosphere at 37°C and 5% CO2. Cells were detached with trypsin/EDTA solution and resuspended in the cell culture medium to a final concentration of 4 × 105 cells/mL. Then, 400 µL of the cell suspension was added to each well of the HTS multiwell insert system and 25 mL of prewarmed complete medium was added to the feeder tray. Confluent MDR1-MDCKII monolayers expressing

P-gp were obtained after 4 - 5 days post seeding. The integrity of the cell monolayers was determined by measuring the trans-epithelial electrical resistance (TEER, $\Omega \times cm^2$) using an epithelial voltammeter. A mature MDR1-MDCKII cell monolayer exhibited TEER values > 100 $\Omega \times cm^2$. 24-well insert plate was removed from its feeder tray and placed in a new sterile 24-well transport analysis plate. The inserts were washed with PBS after medium aspiration. To determine the rate of compounds transport in apical (A)-to-basolateral (B) direction, 300 µL of the test compound dissolved in transport buffer (9.5 g/L Hanks' BSS and 0.35 g /L NaHCO3 with 0.81 mM MgSO4, 1.26 mM CaCl2, 25 mM HEPES, pH adjusted to 7.4) was added into the filter wells; 1000 µL of transport buffer was added to transport analysis plate wells. Ketoprofen, atenolol, digoxin, and quinidine were used as reference compounds. To determine transport rates in the basolateral (B) to apical (A) direction, 1000 µl of the test compound solutions were added into the wells of the transport analysis plate, and the wells in the filter plate were filled with 300 µl of buffer (apical compartment). The final concentration of the test compounds was 10 µM. The effect of the inhibitor on the P-gp-mediated transport of the tested compounds was assessed by determining the bidirectional transport in the presence or absence of cyclosporine A. The MDR1-MDCKII cells were preincubated for 30 mins at 37°C with 10 µM of cyclosporine A in both apical and basolateral compartments. After removal of the preincubation medium, the test compounds (final concentration 10 µM) with cyclosporine A (10 µM) in transport buffer were added in donor wells, while the receiver wells were filled with the appropriate volume of transport buffer with 10 µM cyclosporine A respectively. The plates were incubated for 90 mins at 37°C under continuous shaking at 100 rpm. After this, 75 µL aliquots were taken from the donor and receiver compartments

for LC-MS/MS analysis. All samples were mixed with 2 volumes of acetonitrile followed by protein sedimentation by centrifuging at 10000 rpm for 10 mins. Supernatants were analyzed using HPLC system coupled with tandem mass spectrometer.

Acknowledgements

Abbreviations

25HC 25-hydroxycholesterol

25NC 25-NBD cholesterol

APCI atmospheric pressure chemical ionization

APSI appearance potential soft ionization

CDI   1,1′-carbonyldiimidazole

Clin   intrinsic clearance

DBD   DNA-binding domains

DIPEA   N,N-diisopropylethylamine

Ebconf   energy of conformer (pocket bound)

Econf   energy of conformer

EDC   1-ethyl-3-(3-dimethylaminopropyl) carbodiimide

FEP   free-energy perturbations

FES   free-energy surface

FP   fluorescence polarization

G   Gibbs energy

GEXP experimental Gibbs energy

GFEP FEP calculated Gibbs energy

HATU 1-[bis(dimethylamino)methylene]-1H-1,2,3-triazolo[4,5-b]pyridinium 3-oxid

hexafluorophosphate, N-[(dimethylamino)-1H-1,2,3-triazolo-[4,5-b]pyridin-1-

ylmethylene]-N-methylmethanaminium hexafluorophosphate N-oxide

HTVS high-throughput virtual screening

LipE   lipophilic efficiency

LipEilogP   lipophilic efficiency based on ilogP

LipElogD   lipophilic efficiency based on log D

MDR1-MDCKII   canine MDR1 knock-out, human MDR1 knock-in MDCKII

MsCl   methane-sulfonyl chloride

MUE   mean unsigned error

NEt3   triethylamine

RDF   radial distribution function

RLU   relative light units

rmsf   root-mean-square fluctuation

RORγt   retinoic acid receptor-related orphan receptor γt

SP   standard precision

TPSA topological polar surface area

TR-FRET   time-resolved fluorescence energy transfer

XP   extra precision

References

Amaudrut, J., Argiriadi, M. A., Barth, M., Breinlinger, E. C., Bressac, D., Broqua, P., Calderwood, D. J., Chatar, M., Cusack, K. P., Gauld, S. B., Jacquet, S., Kamath, R. V., Kort, M. E., Lepais, V., Luccarini, J.-M., Masson, P., Montalbetti, C., Mounier, L., Potin, D., . . . Wallace, C. D. (2019). Discovery of novel quinoline sulphonamide derivatives as potent, selective and orally active RORγ inverse agonists. *Bioorg. Med. Chem. Lett.*, *29*(14), 1799-1806.

Chao, J., Enyedy, I., Van Vloten, K., Marcotte, D., Guertin, K., Hutchings, R., Powell, N., Jones, H., Bohnert, T., Peng, C.-C., Silvian, L., Hong, V. S., Little, K., Banerjee, D., Peng, L., Taveras, A., Viney, J. L., & Fontenot, J. (2015). Discovery of biaryl carboxylamides as potent RORγ inverse agonists. *Bioorg. Med. Chem. Lett.*, *25*(15), 2991-2997.

Chen, L., Su, M., Jin, Q., Wang, W., Wang, C.-G., Assani, I., Wang, M.-X., Zhao, S.-F., Lv, S.-M., Wang, J.-W., Sun, B., Li, Y., & Liao, Z.-X. (2021). Discovery of

Chromane-6-Sulfonamide Derivative as a Potent, Selective, and Orally Available Novel Retinoic Acid Receptor-Related Orphan Receptor γt Inverse Agonist. *Journal of Medicinal Chemistry*, *64*(21), 16106-16131.

Chen, L., Su, M., Wu, X.-Z., Wang, D.-Z., Kang, Y.-y., Wang, C.-G., Assani, I., Wang, M.-X., Zhao, S.-F., Lv, S.-M., Wang, J.-W., Sun, B., Li, Y., Jin, Q., Huang, R.-Z., & Liao, Z.-X. (2022). Discovery of 2H-chromone-4-one based sulfonamide derivatives as potent retinoic acid receptor-related orphan receptor γt inverse agonists. *European Journal of Medicinal Chemistry*, *229*, 114065.

Daina, A., Michielin, O., & Zoete, V. (2014). iLOGP: A Simple, Robust, and Efficient Description of n-Octanol/Water Partition Coefficient for Drug Design Using the GB/SA Approach. *Journal of Chemical Information and Modeling*, *54*(12), 3284-3301.

Delaney, J. S. (2004). ESOL: Estimating Aqueous Solubility Directly from Molecular Structure. *Journal of Chemical Information and Computer Sciences*, *44*(3), 1000-1005.

Ding, Q., Zhao, M., Bai, C., Yu, B., & Huang, Z. (2015). Inhibition of RORgammat activity and Th17 differentiation by a set of novel compounds. *BMC Immunol*, *16*, 32.

Doebelin, C., Patouret, R., Garcia-Ordonez, R. D., Chang, M. R., Dharmarajan, V., Kuruvilla, D. S., Novick, S. J., Lin, L., Cameron, M. D., Griffin, P. R., & Kamenecka, T. M. (2016). N-Arylsulfonyl Indolines as Retinoic Acid Receptor-Related Orphan Receptor γ (RORγ) Agonists. *ChemMedChem*, *11*(23), 2607-2620.

Duan, J. J. W., Lu, Z., Jiang, B., Stachura, S., Weigelt, C. A., Sack, J. S., Khan, J., Ruzanov, M., Galella, M. A., Wu, D.-R., Yarde, M., Shen, D.-R., Shuster, D. J.,

Borowski, V., Xie, J. H., Zhang, L., Vanteru, S., Gupta, A. K., Mathur, A., . . . Dhar, T. G. M. (2019). Structure-based Discovery of Phenyl (3-Phenylpyrrolidin-3-yl)sulfones as Selective, Orally Active RORγt Inverse Agonists. *ACS Med. Chem. Lett., 10*(3), 367-373.

Ecoeur, F., Weiss, J., Kaupmann, K., Hintermann, S., Orain, D., & Guntermann, C. (2019). Antagonizing Retinoic Acid-Related-Orphan Receptor Gamma Activity Blocks the T Helper 17/Interleukin-17 Pathway Leading to Attenuated Pro-inflammatory Human Keratinocyte and Skin Responses. *Front Immunol, 10*, 577.

Ertl, P., Rohde, B., & Selzer, P. (2000). Fast Calculation of Molecular Polar Surface Area as a Sum of Fragment-Based Contributions and Its Application to the Prediction of Drug Transport Properties. *Journal of Medicinal Chemistry, 43*(20), 3714-3717.

Fabio, Huang, P., Serge, Eugene, David, Brad, Keber, R., Lorbek, G., Konijn, T., Brittany, Rozman, D., Horvat, S., Rahier, A., Reina, Rastinejad, F., W, & Dan. (2015). Identification of Natural RORγ Ligands that Regulate the Development of Lymphoid Cells. *Cell Metabolism, 21*(2), 286-298.

Fauber, B. P., De Leon Boenig, G., Burton, B., Eidenschenk, C., Everett, C., Gobbi, A., Hymowitz, S. G., Johnson, A. R., Liimatta, M., Lockey, P., Norman, M., Ouyang, W., René, O., & Wong, H. (2013). Structure-based design of substituted hexafluoroisopropanol-arylsulfonamides as modulators of RORc. *Bioorganic & Medicinal Chemistry Letters, 23*(24), 6604-6609.

Fauber, B. P., Gobbi, A., Robarge, K., Zhou, A., Barnard, A., Cao, J., Deng, Y., Eidenschenk, C., Everett, C., Ganguli, A., Hawkins, J., Johnson, A. R., La, H., Norman, M., Salmon, G., Summerhill, S., Ouyang, W., Tang, W., & Wong, H.

(2015). Discovery of imidazo[1,5-a]pyridines and -pyrimidines as potent and selective RORc inverse agonists. *Bioorg. Med. Chem. Lett.*, *25*(15), 2907-2912.

Fukase, Y., Sato, A., Tomata, Y., Ochida, A., Kono, M., Yonemori, K., Koga, K., Okui, T., Yamasaki, M., Fujitani, Y., Nakagawa, H., Koyama, R., Nakayama, M., Skene, R., Sang, B.-C., Hoffman, I., Shirai, J., & Yamamoto, S. (2018). Identification of novel quinazolinedione derivatives as RORγt inverse agonist. *Bioorg. Med. Chem.*, *26*(3), 721-736.

Fulton, L. M., Carlson, M. J., Coghill, J. M., Ott, L. E., West, M. L., Panoskaltsis-Mortari, A., Littman, D. R., Blazar, B. R., & Serody, J. S. (2012). Attenuation of acute graft-versus-host disease in the absence of the transcription factor RORgammat. *J Immunol*, *189*(4), 1765-1772.

Gege, C., Albers, M., Kinzel, O., Kleymann, G., Schlueter, T., Steeneck, C., Hoffmann, T., Xue, X., Cummings, M. D., Spurlino, J., Milligan, C., Fourie, A. M., Edwards, J. P., Leonard, K., Coe, K., Scott, B., Pippel, D., & Goldberg, S. D. (2020). Optimization and biological evaluation of thiazole-bis-amide inverse agonists of RORγt. *Bioorg. Med. Chem. Lett.*, *30*(12), 127205.

Gong, H., Weinstein, D. S., Lu, Z., Duan, J. J. W., Stachura, S., Haque, L., Karmakar, A., Hemagiri, H., Raut, D. K., Gupta, A. K., Khan, J., Camac, D., Sack, J. S., Pudzianowski, A., Wu, D.-R., Yarde, M., Shen, D.-R., Borowski, V., Xie, J. H., . . . Dhar, T. G. M. (2018). Identification of bicyclic hexafluoroisopropyl alcohol sulfonamides as retinoic acid receptor-related orphan receptor gamma (RORγ/RORc) inverse agonists. Employing structure-based drug design to

improve pregnane X receptor (PXR) selectivity. *Bioorg. Med. Chem. Lett.*, *28*(2), 85-93.

Guendisch, U., Weiss, J., Ecoeur, F., Riker, J. C., Kaupmann, K., Kallen, J., Hintermann, S., Orain, D., Dawson, J., Billich, A., & Guntermann, C. (2017). Pharmacological inhibition of RORgammat suppresses the Th17 pathway and alleviates arthritis in vivo. *PLoS One*, *12*(11), e0188391.

Hintermann, S., Guntermann, C., Mattes, H., Carcache, D. A., Wagner, J., Vulpetti, A., Billich, A., Dawson, J., Kaupmann, K., Kallen, J., Stringer, R., & Orain, D. (2016). Synthesis and Biological Evaluation of New Triazolo- and Imidazolopyridine RORgammat Inverse Agonists. *ChemMedChem*, *11*(24), 2640-2648.

Huang, M., Bolin, S., Miller, H., & Ng, H. L. (2020). RORγ Structural Plasticity and Druggability. *International Journal of Molecular Sciences*, *21*(15), 5329.

Huang, Y., Yu, M., Sun, N., Tang, T., Yu, F., Song, X., Xie, Q., Fu, W., Shao, L., & Wang, Y. (2018). Discovery of carbazole carboxamides as novel RORγt inverse agonists. *Eur. J. Med. Chem.*, *148*, 465-476.

Huh, J. R., Englund, E. E., Wang, H., Huang, R., Huang, P., Rastinejad, F., Inglese, J., Austin, C. P., Johnson, R. L., Huang, W., & Littman, D. R. (2013). Identification of Potent and Selective Diphenylpropanamide RORγ Inhibitors. *ACS Med. Chem. Lett.*, *4*(1), 79-84.

Huh, J. R., Leung, M. W., Huang, P., Ryan, D. A., Krout, M. R., Malapaka, R. R., Chow, J., Manel, N., Ciofani, M., Kim, S. V., Cuesta, A., Santori, F. R., Lafaille, J. J., Xu, H. E., Gin, D. Y., Rastinejad, F., & Littman, D. R. (2011). Digoxin and its derivatives

suppress TH17 cell differentiation by antagonizing RORgammat activity. *Nature*, *472*(7344), 486-490.

Kaitoh, K., Toyama, H., Hashimoto, Y., & Fujii, S. (2017). Design and synthesis of 1,3,5-triazine derivatives as novel inverse agonists of nuclear retinoic acid receptor-related orphan receptor-γ. *Heterocycles*, *95*(1, Spec. Issue), 547-556.

Kallen, J., Izaac, A., Be, C., Arista, L., Orain, D., Kaupmann, K., Guntermann, C., Hoegenauer, K., & Hintermann, S. (2017). Structural States of RORgammat: X-ray Elucidation of Molecular Mechanisms and Binding Interactions for Natural and Synthetic Compounds. *ChemMedChem*, *12*(13), 1014-1021.

Lao, C., Zhou, X., Chen, H., Wei, F., Huang, Z., & Bai, C. (2019). 5,6,7,8-Tetrahydrobenzo[4,5]thieno[2,3-d]pyrimidine derivatives as inhibitors of full-length RORγt. *Bioorg. Chem.*, *90*, 103077.

Li, X., Anderson, M., Collin, D., Muegge, I., Wan, J., Brennan, D., Kugler, S., Terenzio, D., Kennedy, C., Lin, S., Labadia, M. E., Cook, B., Hughes, R., & Farrow, N. A. (2017). Structural studies unravel the active conformation of apo RORgammat nuclear receptor and a common inverse agonism of two diverse classes of RORgammat inhibitors. *J Biol Chem*, *292*(28), 11618-11630.

Liu, Q., Batt, D. G., Weigelt, C. A., Yip, S., Wu, D.-R., Ruzanov, M., Sack, J. S., Wang, J., Yarde, M., Li, S., Shuster, D. J., Xie, J. H., Sherry, T., Obermeier, M. T., Fura, A., Stefanski, K., Cornelius, G., Khandelwal, P., Tino, J. A., . . . Dhar, T. G. M. (2020). Novel Tricyclic Pyroglutamide Derivatives as Potent RORγt Inverse Agonists Identified using a Virtual Screening Approach. *ACS Medicinal Chemistry Letters*, *11*(12), 2510-2518.

Liu, S., Liu, D., Shen, R., Li, D., Hu, Q., Yan, Y., Sun, J., Zhang, F., Wan, H., Dong, P., Feng, J., Zhang, R., Li, J., Zhang, L., & Tao, W. (2021). Discovery of a novel RORγ antagonist with skin-restricted exposure for topical treatment of mild to moderate psoriasis. *Scientific Reports*, *11*(1), 9132.

Nakajima, R., Oono, H., Sugiyama, S., Matsueda, Y., Ida, T., Kakuda, S., Hirata, J., Baba, A., Makino, A., Matsuyama, R., White, R. D., Wurz, R. P., Shin, Y., Min, X., Guzman-Perez, A., Wang, Z., Symons, A., Singh, S. K., Mothe, S. R., . . . Shuto, S. (2020). Discovery of [1,2,4]Triazolo[1,5-a]pyridine Derivatives as Potent and Orally Bioavailable RORγt Inverse Agonists. *ACS Med. Chem. Lett.*, *11*(4), 528-534.

Narjes, F., Xue, Y., von Berg, S., Malmberg, J., Llinas, A., Olsson, R. I., Jirholt, J., Grindebacke, H., Leffler, A., Hossain, N., Lepistoe, M., Thunberg, L., Leek, H., Aagaard, A., McPheat, J., Hansson, E. L., Baeck, E., Taangefjord, S., Chen, R., . . . Hansson, T. G. (2018). Potent and Orally Bioavailable Inverse Agonists of RORγt Resulting from Structure-Based Design. *J. Med. Chem.*, *61*(17), 7796-7813.

Nefzi, A., Marconi, G. D., Ortiz, M. A., Davis, J. C., & Piedrafita, F. J. (2017). Synthesis of dihydroimidazole tethered imidazolinethiones and their activity as novel antagonists of the nuclear retinoic acid receptor-related orphan receptors (RORs). *Bioorg. Med. Chem. Lett.*, *27*(7), 1608-1610.

Noguchi, M., Nomura, A., Doi, S., Yamaguchi, K., Hirata, K., Shiozaki, M., Maeda, K., Hirashima, S., Kotoku, M., Yamaguchi, T., Katsuda, Y., Crowe, P., Tao, H., Thacher, S., & Adachi, T. (2018). Ternary crystal structure of human RORγ ligand-

binding-domain, an inhibitor and corepressor peptide provides a new insight into corepressor interaction. *Scientific Reports*, 8(1), 17374.

Oh, T. G., Wang, S. M., Acharya, B. R., Goode, J. M., Graham, J. D., Clarke, C. L., Yap, A. S., & Muscat, G. E. O. (2016). The Nuclear Receptor, RORgamma, Regulates Pathways Necessary for Breast Cancer Metastasis. *EBioMedicine*, *6*, 59-72.

Olsson, R. I., Xue, Y., von Berg, S., Aagaard, A., McPheat, J., Hansson, E. L., Bernstroem, J., Hansson, P., Jirholt, J., Grindebacke, H., Leffler, A., Chen, R., Xiong, Y., Ge, H., Hansson, T. G., & Narjes, F. (2016). Benzoxazepines Achieve Potent Suppression of IL-17 Release in Human T-Helper 17 (TH17) Cells through an Induced-Fit Binding Mode to the Nuclear Receptor RORγ. *ChemMedChem*, *11*(2), 207-216.

Ouvry, G., Bihl, F., Bouix-Peter, C., Christin, O., Defoin-Platel, C., Deret, S., Feret, C., Froude, D., Hacini-Rachinel, F., Harris, C. S., Hervouet, C., Lafitte, G., Luzy, A.-P., Musicki, B., Orfila, D., Parnet, V., Pascau, C., Pascau, J., Pierre, R., . . . Hennequin, L. F. (2018). Sulfoximines as potent RORγ inverse agonists. *Bioorg. Med. Chem. Lett.*, *28*(8), 1269-1273.

Ranieri, V. M., Pettila, V., Karvonen, M. K., Jalkanen, J., Nightingale, P., Brealey, D., Mancebo, J., Ferrer, R., Mercat, A., Patroniti, N., Quintel, M., Vincent, J. L., Okkonen, M., Meziani, F., Bellani, G., MacCallum, N., Creteur, J., Kluge, S., Artigas-Raventos, A., . . . Group, I. S. (2020). Effect of Intravenous Interferon beta-1a on Death and Days Free From Mechanical Ventilation Among Patients With Moderate to Severe Acute Respiratory Distress Syndrome: A Randomized Clinical Trial. *JAMA*, 18(1), 536.

Rauhamäki, S., Postila, P. A., Lätti, S., Niinivehmas, S., Multamäki, E., Liedl, K. R., & Pentikäinen, O. T. (2018). Discovery of Retinoic Acid-Related Orphan Receptor γt Inverse Agonists via Docking and Negative Image-Based Screening. *ACS Omega*, *3*(6), 6259-6266.

Rossi, A. M., & Taylor, C. W. (2011). Analysis of protein-ligand interactions by fluorescence polarization. *Nature protocols*, *6*(3), 365-387.

Saen-Oon, S., Lozoya, E., Segarra, V., Guallar, V., & Soliva, R. (2019). Atomistic simulations shed new light on the activation mechanisms of RORγ and classify it as Type III nuclear hormone receptor regarding ligand-binding paths. *Scientific Reports*, *9*(1), 17249.

Santori, F. R., Huang, P., van de Pavert, S. A., Douglass, E. F., Jr., Leaver, D. J., Haubrich, B. A., Keber, R., Lorbek, G., Konijn, T., Rosales, B. N., Rozman, D., Horvat, S., Rahier, A., Mebius, R. E., Rastinejad, F., Nes, W. D., & Littman, D. R. (2015). Identification of natural RORgamma ligands that regulate the development of lymphoid cells. *Cell Metab*, *21*(2), 286-298.

Scheepstra, M., Leysen, S., Van Almen, G. C., Miller, J. R., Piesvaux, J., Kutilek, V., Van Eenennaam, H., Zhang, H., Barr, K., Nagpal, S., Soisson, S. M., Kornienko, M., Wiley, K., Elsen, N., Sharma, S., Correll, C. C., Trotter, B. W., Van Der Stelt, M., Oubrie, A., . . . Brunsveld, L. (2015). Identification of an allosteric binding site for RORγt inhibition. *Nature Communications*, *6*(1), 8833.

Shirai, J., Tomata, Y., Kono, M., Ochida, A., Fukase, Y., Sato, A., Masada, S., Kawamoto, T., Yonemori, K., Koyama, R., Nakagawa, H., Nakayama, M., Uga, K., Shibata, A., Koga, K., Okui, T., Shirasaki, M., Skene, R., Sang, B. C., . . . Yamamoto, S. (2018).

Discovery of orally efficacious RORγt inverse agonists, part 1: Identification of novel phenylglycinamides as lead scaffolds. *Bioorg. Med. Chem.*, *26*(2), 483-500.

Smith, S. H., Peredo, C. E., Takeda, Y., Bui, T., Neil, J., Rickard, D., Millerman, E., Therrien, J. P., Nicodeme, E., Brusq, J. M., Birault, V., Viviani, F., Hofland, H., Jetten, A. M., & Cote-Sierra, J. (2016). Development of a Topical Treatment for Psoriasis Targeting RORgamma: From Bench to Skin. *PLoS One*, *11*(2), e0147979.

Soroosh, P., Wu, J., Xue, X., Song, J., Sutton, S. W., Sablad, M., Yu, J., Nelen, M. I., Liu, X., Castro, G., Luna, R., Crawford, S., Banie, H., Dandridge, R. A., Deng, X., Bittner, A., Kuei, C., Tootoonchi, M., Rozenkrants, N., . . . Sun, S. (2014). Oxysterols are agonist ligands of RORgammat and drive Th17 cell differentiation. *Proc Natl Acad Sci U S A*, *111*(33), 12163-12168.

Steeneck, C., Gege, C., Kinzel, O., Albers, M., Kleymann, G., Schlueter, T., Schulz, A., Xue, X., Cummings, M. D., Fourie, A. M., Leonard, K. A., Scott, B., Edwards, J. P., Hoffmann, T., & Goldberg, S. D. (2020). Discovery and optimization of new oxadiazole substituted thiazole RORγt inverse agonists through a bioisosteric amide replacement approach. *Bioorg. Med. Chem. Lett.*, *30*(12), 127174.

Sun, N., Ma, X., Zhou, K., Zhu, C., Cao, Z., Wang, Y., Xu, J., & Fu, W. (2020). Discovery of novel N-sulfonamide-tetrahydroquinolines as potent retinoic acid receptor-related orphan receptor γt inverse agonists for the treatment of autoimmune diseases. *Eur. J. Med. Chem.*, *187*, 111984.

Sun, N., Yuan, C., Ma, X., Wang, Y., Gu, X., & Fu, W. (2018). Molecular Mechanism of Action of RORgammat Agonists and Inverse Agonists: Insights from Molecular Dynamics Simulation. *Molecules*, *23*(12), 3181.

Tan, Z., Jiang, R., Wang, X., Wang, Y., Lu, L., Liu, Q., Zheng, S. G., Sun, B., & Ryffel, B. (2013). RORgammat+IL-17+ neutrophils play a critical role in hepatic ischemia-reperfusion injury. *J Mol Cell Biol*, *5*(2), 143-146.

Tian, J., Sun, N., Yu, M., Gu, X., Xie, Q., Shao, L., Liu, J., Liu, L., & Wang, Y. (2019). Discovery of N-indanyl benzamides as potent RORγt inverse agonists. *Eur. J. Med. Chem.*, *167*, 37-48.

Tsuruoka, R., Yoshikawa, N., Konishi, T., & Yamano, M. (2020). Asymmetric Synthesis of a 5,6,7,8-Tetrahydro-1,6-naphthyridine Scaffold Leading to Potent Retinoid-Related Orphan Receptor γt Inverse Agonist TAK-828F. *J. Org. Chem.*, *85*(16), 10797-10805.

van Niel, M. B., Fauber, B. P., Cartwright, M., Gaines, S., Killen, J. C., Rene, O., Ward, S. I., de Leon Boenig, G., Deng, Y., Eidenschenk, C., Everett, C., Gancia, E., Ganguli, A., Gobbi, A., Hawkins, J., Johnson, A. R., Kiefer, J. R., La, H., Lockey, P., . . . Wong, H. (2014). A reversed sulfonamide series of selective RORc inverse agonist. *Bioorg. Med. Chem. Lett.*, *24*(24), 5769-5776.

Vonarbourg, C., Mortha, A., Bui, V. L., Hernandez, P. P., Kiss, E. A., Hoyler, T., Flach, M., Bengsch, B., Thimme, R., Holscher, C., Honig, M., Pannicke, U., Schwarz, K., Ware, C. F., Finke, D., & Diefenbach, A. (2010). Regulated expression of nuclear receptor RORgammat confers distinct functional fates to NK cell receptor-expressing RORgammat(+) innate lymphocytes. *Immunity*, *33*(5), 736-751.

Wang, J., Zou, J. X., Xue, X., Cai, D., Zhang, Y., Duan, Z., Xiang, Q., Yang, J. C., Louie, M. C., Borowsky, A. D., Gao, A. C., Evans, C. P., Lam, K. S., Xu, J., Kung, H. J., Evans, R. M., Xu, Y., & Chen, H. W. (2016). ROR-gamma drives androgen receptor expression and represents a therapeutic target in castration-resistant prostate cancer. *Nat Med*, *22*(5), 488-496.

Wang, T., Banerjee, D., Bohnert, T., Chao, J., Enyedy, I., Fontenot, J., Guertin, K., Jones, H., Lin, E. Y., Marcotte, D., Talreja, T., & Van Vloten, K. (2015). Discovery of novel pyrazole-containing benzamides as potent RORγ inverse agonists. *Bioorg. Med. Chem. Lett.*, *25*(15), 2985-2990.

Wang, Y., Cai, W., Cheng, Y., Yang, T., Liu, Q., Zhang, G., Meng, Q., Han, F., Huang, Y., Zhou, L., Xiang, Z., Zhao, Y.-G., Xu, Y., Cheng, Z., Lu, S., Wu, Q., Xiang, J.-N., Elliott, J. D., Leung, S., . . . Lin, X. (2015). Discovery of Biaryl Amides as Potent, Orally Bioavailable, and CNS Penetrant RORγt Inhibitors. *ACS Med. Chem. Lett.*, *6*(7), 787-792.

Wang, Y., Cai, W., Zhang, G., Yang, T., Liu, Q., Cheng, Y., Zhou, L., Ma, Y., Cheng, Z., Lu, S., Zhao, Y.-G., Zhang, W., Xiang, Z., Wang, S., Yang, L., Wu, Q., Orband-Miller, L. A., Xu, Y., Zhang, J., . . . Lin, X. (2014). Discovery of novel N-(5-(arylcarbonyl)thiazol-2-yl)amides and N-(5-(arylcarbonyl)thiophen-2-yl)amides as potent RORγt inhibitors. *Bioorg. Med. Chem.*, *22*(2), 692-702.

Wang, Y., Kumar, N., Crumbley, C., Griffin, P. R., & Burris, T. P. (2010). A second class of nuclear receptors for oxysterols: Regulation of RORα and RORγ activity by 24S-hydroxycholesterol (cerebrosterol). *Biochimica et Biophysica Acta (BBA) - Molecular and Cell Biology of Lipids*, *1801*(8), 917-923.

Wang, Y., Kumar, N., Solt, L. A., Richardson, T. I., Helvering, L. M., Crumbley, C., Garcia-Ordonez, R. D., Stayrook, K. R., Zhang, X., Novick, S., Chalmers, M. J., Griffin, P. R., & Burris, T. P. (2010). Modulation of Retinoic Acid Receptor-related Orphan Receptor α and γ Activity by 7-Oxygenated Sterol Ligands. *Journal of Biological Chemistry*, *285*(7), 5013-5025.

Xiao, S., Yosef, N., Yang, J., Wang, Y., Zhou, L., Zhu, C., Wu, C., Baloglu, E., Schmidt, D., Ramesh, R., Lobera, M., Sundrud, M. S., Tsai, P. Y., Xiang, Z., Wang, J., Xu, Y., Lin, X., Kretschmer, K., Rahl, P. B., . . . Kuchroo, V. K. (2014). Small-molecule RORgammat antagonists inhibit T helper 17 cell transcriptional network by divergent mechanisms. *Immunity*, *40*(4), 477-489.

Xu, T., Wang, X., Zhong, B., Nurieva, R. I., Ding, S., & Dong, C. (2011). Ursolic Acid Suppresses Interleukin-17 (IL-17) Production by Selectively Antagonizing the Function of RORγt Protein. *Journal of Biological Chemistry*, *286*(26), 22707-22710.

Yang, T., Liu, Q., Cheng, Y., Cai, W., Ma, Y., Yang, L., Wu, Q., Orband-Miller, L. A., Zhou, L., Xiang, Z., Huxdorf, M., Zhang, W., Zhang, J., Xiang, J.-N., Leung, S., Qiu, Y., Zhong, Z., Elliott, J. D., Lin, X., & Wang, Y. (2014). Discovery of Tertiary Amine and Indole Derivatives as Potent RORγt Inverse Agonists. *ACS Medicinal Chemistry Letters*, *5*(1), 65-68.

Yoshida, N., Kinugasa, T., Miyoshi, H., Sato, K., Yuge, K., Ohchi, T., Fujino, S., Shiraiwa, S., Katagiri, M., Akagi, Y., & Ohshima, K. (2016). A High RORgammaT/CD3 Ratio is a Strong Prognostic Factor for Postoperative Survival in Advanced Colorectal

Cancer: Analysis of Helper T Cell Lymphocytes (Th1, Th2, Th17 and Regulatory T Cells). *Ann Surg Oncol*, *23*(3), 919-927.

Yuan, C. M., Chen, H. H., Sun, N. N., Ma, X. J., Xu, J., & Fu, W. (2019). Molecular dynamics simulations on RORgammat: insights into its functional agonism and inverse agonism. *Acta Pharmacol Sin*, *40*(11), 1480-1489.

Yung-Chi, C., & Prusoff, W. H. (1973). Relationship between the inhibition constant (KI) and the concentration of inhibitor which causes 50 per cent inhibition (I50) of an enzymatic reaction. *Biochemical Pharmacology*, *22*(23), 3099-3108.

… *to article no. 2*

In the study titled "discovery, synthesis, and in vitro characterization of 2,3 derivatives of 4,5,6,7-tetrahydro-benzothiophene as potent modulators of RORγt" we presented the drug discovery work of the project. In this first study we answered the first and second objectives of global study. In this part we identified a class of novel RORγt inverse agonists, and we elected 23 virtual structures for synthesis and evaluation in vitro. This study provided us with information about the relative potency and stability of the 23 compounds and their important physicochemical properties such as their solubility. Based on the results of that study we eventually narrowed down our best candidates for in vivo testing to 3 compounds and evaluated them in a sensitized mouse model of skin transplantation in a study titled "RORγt inverse agonist TF-S14 inhibits Th17 cytokines and prolongs skin allograft survival in sensitized mice" In this study, to test the hypothesis that **RORγt inverse agonists can prevent and treat AMR in highly sensitized transplantation recipients**, which is the third objective of our global study, we first evaluated two out of three RORγt modulators namely compound **1** and **2** in additional Th17, Th1 and Tregs polarization assays against reference compounds such as tacrolimus, sirolimus and dexamethasone. Based on these experiments we replaced compound **1** with compound **13** to be evaluated in vivo in mouse model of skin transplantation along with compound **2**. We performed additional Th17 polarization experiments to compare the Th17 polarization potential between highly sensitized, non-sensitized transplantation candidates and healthy volunteers. Furthermore, we evaluated the effect of compounds **2** and **13** on Th17 polarization in highly sensitized transplantation candidates. We finally selected compound **13** which we named **TF-S14** for in vivo characterization in a sensitized murine model of skin transplantation. In these

experiments we transplanted C57BL/ mice with BALB/c mice skin grafts. These in vitro and in vivo experiments were designed for hypothesis testing to know whether RORγt inverse agonists can treat graft rejection in a sensitized mouse model of skin transplantation. In the study we present in the following section, not only the effects of RORγt inverse agonists on Th17 cells were measured, but we also measured their effects on other immune cells. The cells include macrophages, neutrophils, ILC3 cells, and B cells. In addition, we measured the levels of DSAs in mice sera. Furthermore, we performed a histopathological examination of the skin grafts and the spleens of the recipient mice. In the following section we present the results of these experiments, and we discuss these results and finally present our conclusions which constitute the answer to the main question of the study or the study hypothesis. The diagram below illustrates the progress in answering the objectives of the global study.
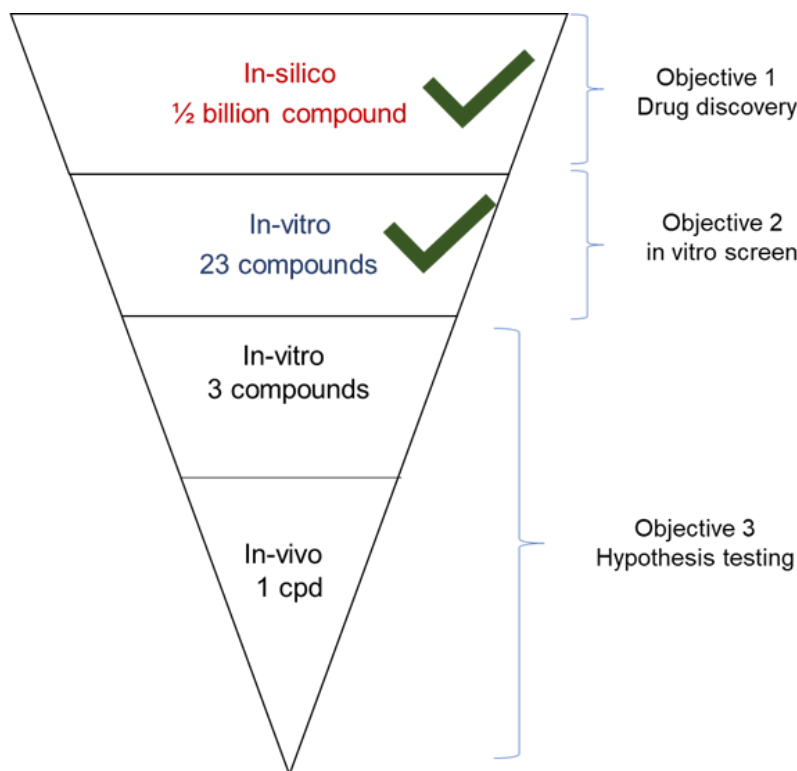
Article no. 2

Title: RORγt inverse agonist TF-S14 inhibits Th17 cytokines and prolongs skin allograft survival in sensitized mice

Authors: Ahmed Fouda[1,2,3*], Mohamed Taoubane Maallah[1,2,3], Araz Kouyoumdjian[2,3,4], Sarita Negi[2], Steven Paraskevas[1,2,3,4], Jean Tchervenkov[1,2,3,4*].

Affiliations: [1]Division of Surgical and Interventional Sciences, Department of Surgery, McGill University, Montréal, Québec, H3G 1A4, Canada; [2]Research Institute of the McGill University Health Centre, Montréal, Québec, H3H 2R9, Canada; [3]McGill University Health Centre, Montréal, Québec, H4A 3J1, Canada; [4]Division of General Surgery, Department of Surgery, McGill University, Montréal, Québec, H3G 1A4, Canada.

Abstract: Chronic antibody mediated rejection (AMR) is the major cause of solid organ graft rejection. Th17 contributes to AMR through the secretion of IL17A, IL21 and IL22. These cytokines promote neutrophilic infiltration, B cell proliferation and donor specific antibodies (DSAs) production. In the current study we investigated the role of Th17 in transplant sensitization. Additionally, we investigated the therapeutic potential of novel inverse agonists of the retinoic acid receptor-related orphan receptor gamma t (RORγt) in the treatment of skin allograft rejection in sensitized mice. Our results show that RORγt inverse agonists reduce cytokine production in human Th17 cells in vitro. In mice, we demonstrate that the RORγt inverse agonist TF-S14 reduces Th17 signature cytokines in vitro and in vivo and leads to blocking neutrophilic infiltration to skin allografts, inhibition of the B-cell differentiation, and the reduction of de novo IgG3 DSAs production. Finally, we show that TF-S14 prolongs the survival of a total mismatch grafts in sensitized mice. In conclusion, RORγt inverse agonists offer a therapeutic intervention through a novel mechanism to treat rejection in highly sensitized patients.

Introduction

Kidney disease is the ninth leading cause of death in high income countries. The disease was long considered a terminal illness until both dialysis and kidney transplantation became widely practiced worldwide. Either peritoneal dialysis or hemodialysis poses a considerable burden on the patient and requires specialized laborious care (Garcia et al., 2012). Transplantation, on the other hand, is considered the treatment of choice for end stage kidney disease, as it decreases the mortality, the morbidity and health-care costs compared to dialysis (Tonelli et al., 2011). In Canada and USA, patients with kidney disease can get a kidney donation either from living or deceased donors within 3-5 years waiting time. However, 16% of kidney transplantation candidates are highly sensitized as defined by a high calculated panel reactive antibody (cPRA > 80%). These patients are at a higher risk of developing AMR. Highly sensitized patients stay on the waiting lists for longer periods until a perfect donor match is allocated (Gebel et al., 2016). Although, both cellular and humoral immunity can be involved in allograft rejection. T cell mediated cellular rejection is currently fully preventable, however, humoral, or commonly known as AMR is difficult to prevent, even when the prevention of the acute form is achieved for short period it cannot be maintained for long term (Zachary & Leffell, 2014). Chronic AMR can progress in an indolent fashion resulting in a slow accumulation of small injuries to the donated organ over time, which in many instances cannot be predicted with current diagnostic methods (Loupy et al., 2012). This type of rejection is now considered the major cause of renal graft rejection (Djamali et al., 2014; Lachmann et al., 2017). An increase in Th17 phenotype was observed in (transplantation patients with chronic allograft dysfunction (Chung et al., 2015). This observation suggests a close relationship

between Th17 activation and AMR progression; however, this relationship is not well investigated. Several studies showed that Th17 and Tfh17 cells induce proliferation of B cells, antibody production and antibody class switching directly through the action of IL17A inside the germinal centers in chronic inflammatory and autoimmune disease characterized by the production of autoantibodies (Ghali et al., 2017; Hsu et al., 2008; Mitsdoerffer et al., 2010). In solid organ transplantation, apart from the Tfh17 model inside the germinal centers, tissue resident Th17 are believed to trigger the development of a tertiary lymphoid tissue following allotransplantation, which mediate B-cell differentiation, alloantibody production and antibody class switching outside the germinal center (Deteix et al., 2010; Zhang & Reed, 2016). Those findings highlight the pathogenic role of Th17 cells, IL17A and IL21 cytokines in AMR. Therapeutic targeting of IL17A and IL21 has been evaluated in clinical trials for a variety of inflammatory and autoimmune indications, and anti-IL17A monoclonal antibodies were recently approved for psoriasis. On the other hand, targeting RORγt the master regulator of Th17 cells, was suggested as new therapy for solid organ rejection (McDonald-Hyman et al., 2015). Previous research has shown that RORγt is a critical transcription factor for the secretion of IL17A (Ivanov et al., 2006; Tuzlak et al., 2021). RORγt inhibitors are particularly interesting as they can be used as oral medications of favorable adverse effects profile to substitute currently used oral immunosupressants (McDonald-Hyman et al., 2015). Several studies have investigated the role of IL17A+ cells and Th17 in graft rejection in partial or full antigenic MHC class I and MHC class II mismatch mouse models of transplantation which mimics human incompatible transplantation (Agorogiannis et al., 2012; Vokaer et al., 2010; Yuan et al., 2008). Prior sensitization to the donor antigens can be done by performing two successive

transplantations to the same recipient from different mouse species such as two skin transplantations, splenocytes injection followed by skin transplantation or a skin transplantation followed by a vascularized organ transplantation (Eichwald et al., 1966; Sicard et al., 2012; Zhao et al., 2018). In such models the rejection to the vascularized organ mimics AMR (Sicard et al., 2012; Zhao et al., 2018). In the current study we evaluated the anti-rejection immunomodulatory effect of RORγt inverse agonist TF-S14 on Th17 mediated cellular and AMR response in a sensitized mouse model of skin transplantation (Eichwald et al., 1966; Fouda et al., 2023). In our model of sensitized mice, we pre-sensitized C57BL/6 mice to BALB/C donor antigens to develop DSAs to mimic highly sensitized patients with cPRA=100%. We show that RORγt inverse agonists decrease the production of IL17A, IL21 and IL22 in vitro and in vivo. We also show that TF-S14 increases total mismatch skin graft survival in pre-sensitized mice, attenuates Th17 mediated leukocytic infiltration to the graft and decreases de novo production of IgG3 DSAs. These effects are beneficial and can be further investigated to provide a new therapy to combat rejection in highly sensitized transplantation candidates.

Results

Effect of RORγt inverse agonists on Th17, Th1 and Treg polarization of human PBMCs

To compare the PBMCs to Th17 transformation between two transplantation candidate categories based on cPRA classification, namely, the highly sensitized whose cPRA > 80% and the non-sensitized transplantation candidates whose cPRA < 20%, we cultured the PBMCs from these two classes and from healthy volunteers (n=3-5 per category) under Th17 polarization condition and measured the fractions of RORγt^{hi}/, IL17A+/,

IL21+/, and IL22+/CD4+ on day 0, 7, 10 and 16. On days 0 and 7 the differences in the percentages of the IL17A+/, IL21+/ or IL22+/CD4+ cells were not significant between the three groups. On the other hand, the percentage of RORγt^{hi}/CD4+ cells was higher in PBMCs derived from highly sensitized compared to non-sensitized transplantation candidates on day 7 (Fig. 3.1a). On day 10 and 16 in addition to RORγt^{hi}, both the IL17A+/ and IL21+/CD4+ fractions of CD4 cells were higher in highly sensitized compared to either non-sensitized transplantation candidates or healthy volunteers (Fig. 3.1b, 3.1c). To evaluate the effect of RORγt inverse agonists on human PBMCs to Th17 polarization, three 2,3 derivatives of 4,5,6,7-tetrahydro-benzothiophene RORγt inverse agonists, that we described in a recent report, were selected based on their potency in IL17A inhibition (Fouda et al., 2023). The three compounds TF-S1, TF-S2 and TF-S14 showed similar results in cell free TR-FRET binding assays (Fig. 3.1d-3.1f). TF-S1 and TF-S2 were tested at three doses for their effect on Th17 signature cytokines in a 16-days human to Th17 polarization. The addition of TF-S1 and TF-S2 at 15, 150 or 750 nM in the last 48 h of culture incubation reduced the fractions of IL17A+/ and IL21+/CD4+ compared to vehicle treated cultures. In addition, TF-S2 at 15, 150 or 750 nM reduced IL22+/CD4+ fraction compared to vehicle, while TF-S1 reduced IL22+/CD4+ fraction at 750nM only (Fig. 3.1g-3.1i, Supplementary Fig. 3.1a). Cyclosporine A reduced the percentage of IL21+/CD4+ and increased the percentage of IL22+/CD4+ cells. The results confirm the findings that have been reported before (Abikhair et al., 2016; Kim et al., 2005). On the other hand, dexamethasone reduced the fraction of IL21+/CD4+ cells which result confirms a recently reported findings about the effects of dexamethasone on Tfh cells and IL21 mRNA and protein expression (Shen et al., 2021). Additionally, dexamethasone reduced

IL17A+/CD4+ at the highest concentration tested (Fig. 3.1g). Further we tested the two compounds in Th1 and Tregs polarization assays to determine their effects on both cell types. In a 3-days Th1 polarization experiment TF-S1 and TF-S2 had no effect on IFNγ+/CD4+ compared to dexamethasone of cyclosporine A (Fig. 3.1j, Supplementary Fig. 3.1b). In a 6-days Treg polarization assay the two compounds had no effect on percentage of Tregs when compared to the Treg inhibitor tacrolimus or the inducer sirolimus. The identification was based on fraction of CD127^{lo}CD25^{hi}FOXP3+/CD4+ cells (Fig 1k, Supplementary Fig. 3.1c). Despite their superior effects in vitro, however the two compounds were not selected for further evaluation because of the poor stability of TF-S1 and poor solubility of TF-S2. Additional 2,3 derivatives of 4,5,6,7-tetrahydro-benzothiophene were further tested in Th17 polarization assay and cell free binding assays (Fouda et al., 2023).

Effect of RORγt inverse agonists on Th17 polarization of human PBMCS from highly sensitized kidney transplantation candidates

To evaluate the effect of TF-S2 and TF-S14 on RORγt expression and Th17 signature cytokines IL17A as well as IL21 and IL22 expression in Th17 polarized PBMCs from highly sensitized kidney transplantation candidates, we added either TF-S2, TF-S14 or GSK2981278 reference RORγt inverse agonist to 14-days Th17-polarized human PBMCs from 7 transplantation candidates who had a cPRA >95%. The RORγt inverse agonists were added to the culture media at a concentration of 15 nM for 48 h. On day 16, following a 5-h PMA/ionomycin stimulation, we measured the fractions of RORγt^{hi}/, IL17A+/, IL21+/ and IL22+/CD4+ cells. The RORγt inverse agonists GSK2981278, TF-S2 and TF-S14 reduced the RORγt protein expression in CD4+ T cells

compared to the vehicle control as measured by mean fluorescence intensity (MFI) (Fig. 3.2a, Supplementary Fig. 2a). In addition, all the tested RORγt inverse agonists reduced the percentages of RORγt^{hi}/, IL17A+/, IL21+/ and IL22+/CD4+ in Th17-polarized human PBMCs compared to vehicle control (Fig. 3.2b-3.2f, Supplementary Fig. 2b).
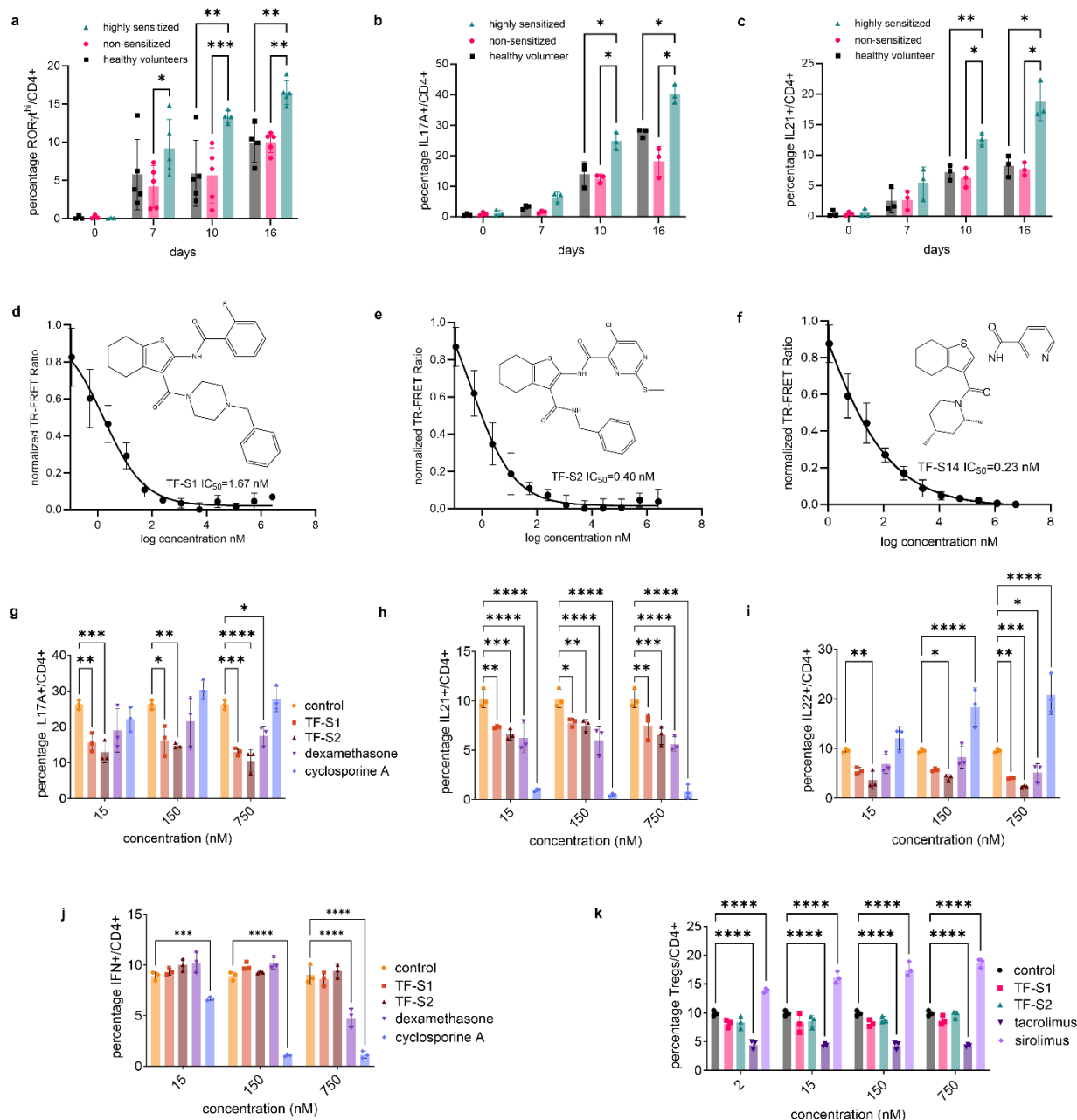
Fig. 3.1: In vitro Th17 polarization time course of human PBMCs from highly sensitized kidney transplantation candidates and the effect of RORγt inverse agonists on cytokine production from Th17, Th1 and Treg cells. PBMCs from highly sensitized, non-sensitized transplantation candidates and healthy volunteers were polarized for 0, 7, 10, 16 days then stimulated with PMA/ionomycin/monensin/prefoldin cocktail for 5 h. The percentages of RORγt^{hi}/ (**a**), IL17A+/ (**b**) and IL21+/CD4+ cells (**c**) were measured by flow cytometry. Dose-response curves of TR-FRET assay of RORγt-LBD: serial dilutions of compounds TF-S2, TF-S10, TF-S14 were incubated with 1.5 nM GST−RORγt (LBD); 90 nM biotinylated RIP140 coactivator peptide; 50 nM streptavidin-APC; 1.5 nM Eu-anti GST. The data are represented as percentage TR-FRET ratio. IC$_{50}$ of TF-S1, TF-S2 and TF-S14 were 1.67, 0.40 and 0.23 nM, respectively (**d–f**). Effect of TF-S1, TF-S2, cyclosporine A and dexamethasone on Th17 polarization: the percentages of IL17A+/ (**g**), IL21+/ (**h**) and IL22+/CD4+ cells (**i**) were measured by flow cytometry. Effect of TF-S1, TF-S2, cyclosporine A and dexamethasone on human PBMCs to Th1 polarization: the percentage of IFNγ+/CD4+ cells was measured on day 3 by flow cytometry (**j**). Effect of TF-S1, TF-S2, sirolimus and tacrolimus on human PBMCSs to Treg polarization: the percentage of CD127^{lo}CD25^{hi}FOXP3+/CD4+ was measured on day 6 by flow cytometry (**k**). Data are presented as mean ± SD, *$p < 0.05$, **$p < 0.01$, ***$p < 0.005$, ****$p < 0.001$, two-way ANOVA and Tukey's test, $n = 3$–5 per group.

Moreover, to determine the effect of the RORγt inverse agonists on non-Th17 signature cytokines, we measured the percentage of IFNγ+/CD4+ and no difference was found between vehicle control and RORγt inverse agonists treated Th17-polarized

human PBMCs (Fig. 3.2f). However, the ratio of Th17/Th1 (IL17A+CD4+/IFNγ+CD4+ cells) was reduced in RORγt inverse agonists treated compared to vehicle treated Th17-polarized human PBMCs control cultures (Fig. 3.2g). Finally, RORγt inverse agonists decreased the concentration of the secreted IL17A and IL21 cytokines in the culture media of Th17-polarizaed human PBMCs collected on day 16 following PMA/ionomycin stimulation (Fig. 3.2h, 3.2i).
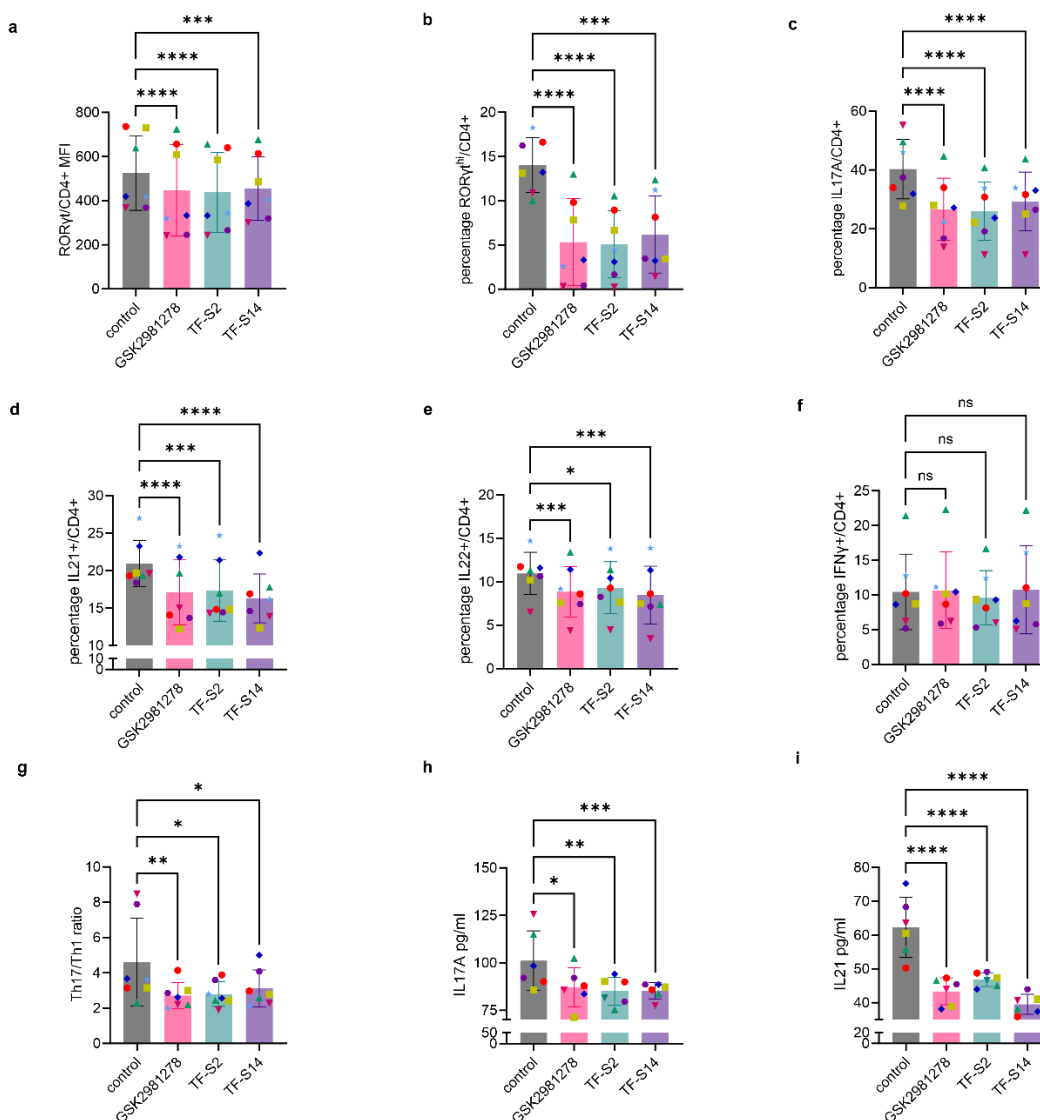

Fig. 3.2: Effect of RORγt inverse agonists TF-S2 and TF-S14 on Th17 polarization of human PBMCs collected from highly sensitized transplantation candidates.

PBMCs from highly sensitized kidney transplantation candidates were treated with CD3/CD28 magnetic beads for 16 days in presence of IL6 10 ng/ml, IL1β 10 ng/ml, TGFβ 10 ng/ml, and IL23 10 ng/ml. Culture medium was changed every 3 days for the whole duration. GSK298128 (15 nM), TF-S2 (15 nM), TF-S14 (15 nM) or vehicle were added to the polarized cells on day 14 for 48 h and at the end of incubation cells were stimulated with PMA/ionomycin/monensin/prefoldin cocktail for 5 h. RORγt$_{BV650}$ MFI of CD4+ cells (**a**), the percentages of RORγt^{hi}/ (**b**), IL17A+/ (**c**), IL21+/ (**d**), IL22+/ (**e**) and IFNγ+/CD4+ (**f**) were measured with flow cytometry. The ratio of Th17/Th1 was measured by dividing the percentage of IL17+/CD4+ by the percentage of IFNγ+/CD4+ cells (**g**). The concentration of IL17A and IL21 secreted in the culture media were both measured in supernatant using ELISA (**h**, **i**). Data are presented as mean ± SD, *$p < 0.05$, **$p < 0.01$, ***$p < 0.005$, ****$p < 0.001$, two-way ANOVA and Tukey's test, $n = 6$–7 per group.

RORγt inverse agonist TF-S14 prolongs the survival of skin allograft in BALB/C-sensitized C57BL/6 mouse model

To evaluate the effect of RORγt inverse agonist TF-S14 in vivo, we developed a BALB/C-sensitized C57BL/6 mouse, hereafter referred to as "sensitized", model of complete mismatch full thickness BALB/C skin transplantation. In this model three IP doses of BALB/C cell suspension were given over a 2-week period to C57BL/6 mice before the transplantation with a BALB/C mouse dorsal skin graft (Fig. 3.3a). To validate the model, we performed a Th17 polarization of T cells derived from the sensitized mice. The percentages of RORγt^{hi}/, IL17A+/, IL21+/ and IL22+/CD4+ were higher in BALB/C-sensitized compared to non-sensitized C57BL/6 mice (Fig. 3.3b-3.3e, Supplementary Fig. 3). In addition, we evaluated the effect of adding TF-S14 (15 nM) on Th17 polarization of

T cells isolated from sensitized and non-sensitized mice. TF-S14 decreased the percentages of RORγt^{hi}/, IL17A+/, IL21+/ and IL22+/CD4+ in Th17 polarized T cells isolated from the splenocytes of sensitized mice compared to vehicle control (Fig. 3.3b-3.3e). Similarly, TF-S14 decreased the percentages of IL17A+/ and IL21+/CD4+ in Th17 polarized T cells from non-sensitized mice compared to vehicle control (Fig. 3.3c, 3.3d, Supplementary Fig. 3). In vivo TF-S14 IP administration to sensitized mice transplanted with BALB/C skin grafts, at a daily dose of 1 mg/kg alone or in combination with tacrolimus 0.5 mg/kg improved the surgical wound inflammation ASEPESIS score for mice (Kick et al., 2019) compared to no treatment (NT) or tacrolimus 0.5 mg/kg treatment alone, respectively (Fig. 3.3f, 3.3g). In another experiment, the histological evaluation of BALB/C skin grafts that were isolated on day 5 post-transplantation and stained with hematoxylin and eosin, revealed that daily treatment of the sensitized mice with IP injections of RORγt inverse agonist TF-S14 at doses of 1, 10 or 100 mg/kg alone or in combination with tacrolimus 0.5 mg/kg resulted in the reduction or absence of neutrophilic infiltration to the skin grafts compared to a diffuse neutrophilic infiltration in BALB/C skin grafts isolated from NT sensitized mice or those treated daily with tacrolimus at a dose of 0.5 mg/kg following the transplantation surgery (Fig. 3.3h). Furthermore, the daily IP injection of TF-S14 at doses of 1, 10 or 100 mg/kg prolonged the graft median survival time (MST) in sensitized mice to 13.5, 15 and 15 days, respectively, compared to a graft MST of 6 days in NT sensitized mice group. Similarly, the daily administration of the combination of TF-S14 at doses of 1, 10 or 100 mg/kg with tacrolimus 0.5 mg/kg increased the graft MST in sensitized mice to 18.5, 18 and 19 days, respectively, compared to a graft MST of 7 days in tacrolimus 0.5 mg/kg only treated sensitized mice group (Fig. 3.3i-3.3k).
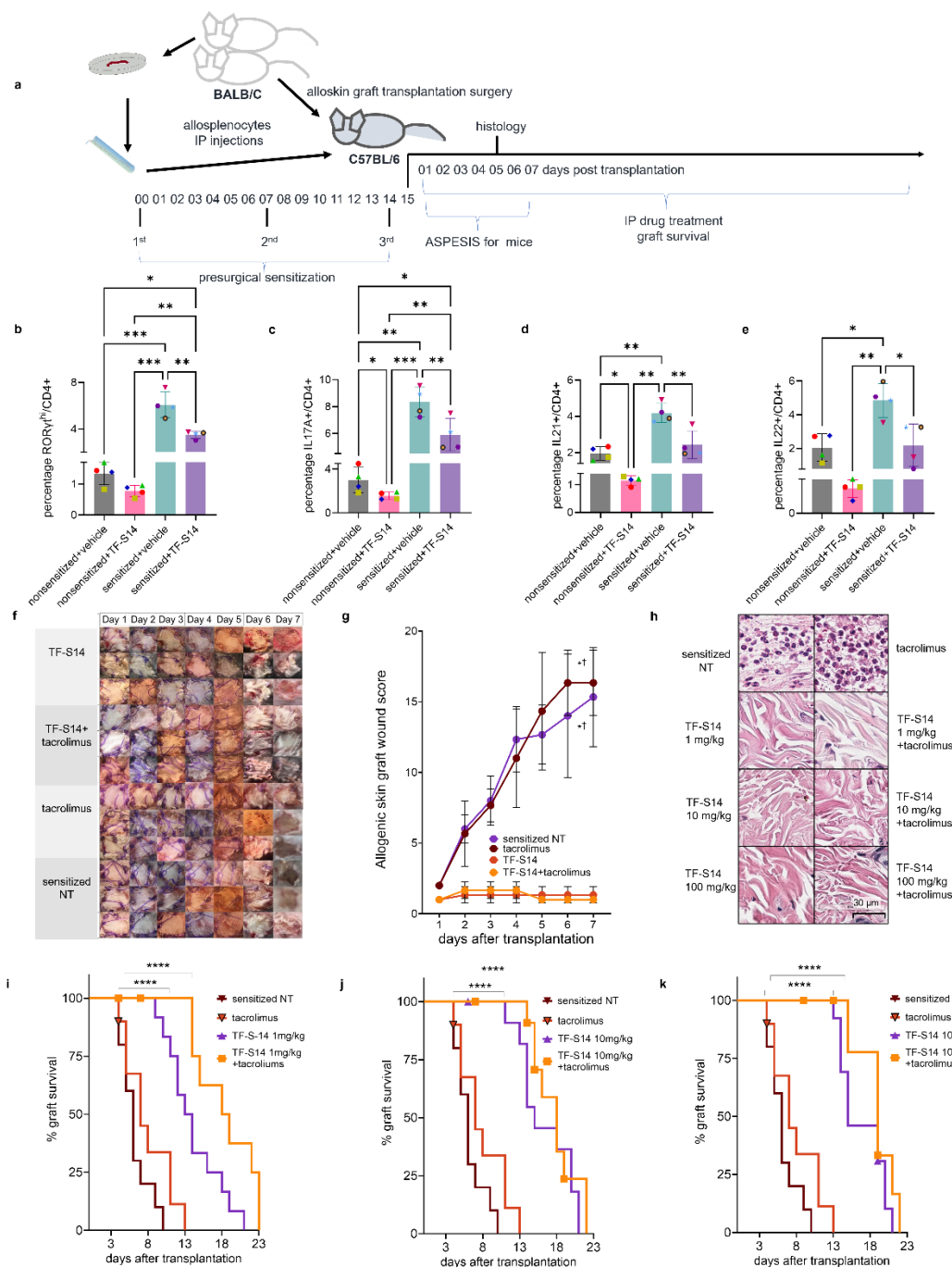
Fig. 3.3: Effect of RORγt inverse agonist TF-S14 on sensitized mice T-cell to Th17 polarization, allograft survival and histological features of full thickness BALB/C skin transplantation to BALB/C-sensitized C57BL/6 mice. C57BL/6 were sensitized by three IP injections of BALB/C splenocytes (10^7) on day 0, 7 and 14. On day 15 mice

were transplanted with 12 × 12 mm BALB/C dorsal skin grafts (**a**). The sensitization was assessed by polarizing T cells isolated from splenocytes of non-sensitized and sensitized mice to Th17 phenotype for 4 days in the presence or absence of TF-S14 (15 nM), followed by stimulation with PMA/ionomycin/monensin/prefoldin cocktail for 5 h. The percentages of RORγt^{hi}/CD4+ (**b**), IL17A+/CD4+ (**c**), IL21+/CD4+ (**d**) and IL22+ (**e**) were measured by flow cytometry. Data are presented as mean ± SD, *$p < 0.05$, **$p < 0.01$, ***$p < 0.005$, REML and Tukey's tests, $n = 4$ per group. Following skin BALB/C allograft surgery, pre-sensitized C57BL/6 mice were assigned into sensitized no treatment (NT), tacrolimus (0.5 mg/kg), TF-S14 (1mg/kg) or TF-S14 (1mg/kg) and tacrolimus (0.5 mg/kg) combination daily treatment groups. The allografts were inspected daily, and area (12 × 12 mm) were imaged with 12 megapixels camera (**f**). The graft area was scored for swelling (1–5), redness (1–5), presence of serous exudate (1–5), presence of purulent exudate (2–10) and loss of hair (2–10) to determine ASPESIS wound score for mice over time. Data are presented as mean ± SD, *†$p < 0.05$ compared to sensitized NT and tacrolimus treated groups, respectively, Friedman one-way ANOVA and Dunn's test, $n = 3$ per group (**g**). Histopathology photomicrographs of skin allografts isolated on day 5 post-transplantation (H&E, ×40) show that grafts from mice treated with TF-S14 1, 10 or 100 mg/kg alone or in combination with tacrolimus 0.5 mg/kg have low neutrophilic infiltration in <10% of graft area compared to high neutrophilic infiltration (>10%) in sensitized NT mice (**h**), $p < 0.05$, Kruskal–Wallis one-way ANOVA and Dunn's test, $n = 3–4$ per group. Graft survival assessed daily until complete necrosis or graft loss (**i**–**k**). Data are presented in Kaplan–Meier survival curve, ****$p < 0.001$, Log-rank (Mantel–Cox) test, $n = 8–12$ per group.

TF-S14 RORγt inverse agonist decreases IL17A protein expression in spleen and tissue resident leukocytes

To measure the effect of TF-S14 on the immune system following daily administration to transplanted sensitized mice. Th17/Tfh17 signature cytokine protein expression was measured in splenocytes from transplanted sensitized mice treated daily with IP injection of TF-S14 at doses of 1, 10 or 100 mg/kg alone or in combination with tacrolimus 0.5 mg/kg using flow cytometry following a 5-h PMA/ionomycin activation. The percentage of IL17A+/CD4+ cells were reduced in all TF-S14 treated compared to NT controls. There was no difference between the three doses tested (1, 10 and 100 mg/kg) on the IL17A+/CD4 fraction in spleen. Similarly, the combination of TF-S14 at doses of 1, 10 or 100 mg/kg with tacrolimus 0.5 mg/kg, administered daily following transplantation surgery, decreased IL17A+/CD4+ fraction in splenocytes from combination treated compared to tacrolimus 0.5 mg/kg treated sensitized mice (Fig. 3.4a, 3.4b). In addition, RORγt inverse agonist TF-S14 treatment reduced the expression of IL17A and RORγt in Ly6G+ neutrophils and Ly6G+ neutrophil like monocytes (Fig. 3.4c-3.4f). At the graft level, there was a decrease in the infiltration of Ly6G+ neutrophils in the grafts that were collected on day 5 from the mice treated with RORγt inverse agonist TF-S14 at doses of 10 and 100 mg/kg alone or in combination with tacrolimus 0.5 mg/kg compared to NT controls (Fig. 3.4g, 3.4h). Similarly, TF-S14 treatment at doses of 10 and 100 mg/kg alone or in combination with tacrolimus 0.5 mg/kg reduced IL17A+ lymphocytic infiltration to the grafts compared to those isolated from NT sensitized mice (Fig. 3.4i, 3.4j). Neither the neutrophilic nor lymphocytic infiltration in tacrolimus only treated mice was different from those infiltrations seen in NT controls (Fig. 3.4g–3.4j). Th17 and IL17A+

lymphocytes were smaller in size and cytoplasmic IL17A granules were less dense compared to those found in the grafts isolated from NT or tacrolimus 0.5 mg/kg treated sensitized mice (Supplementary Fig. 4a, 4b). In TF-S14 plus tacrolimus treated mice, the skin grafts that survived beyond 13 days showed thinning of hypodermis and fibrosis of dermis and epidermis (Supplementary Fig. 4c). IL17A expression, in CD169+ macrophages and CD169+ macrophage like monocytes, was reduced in the splenocytes isolated from TF-S14 treated compared to NT or tacrolimus treated sensitized mice (Fig. 3.4k, 3.4l).

RORγt inverse agonist TF-S14 decreases antibody class switching, B cell differentiation and de novo IgG3 DSAs

To determine the effects of RORγt inhibition on B cells. We measured both IgM and IgG3 immunoglobulins to determine the effect of RORγt inverse agonists administration of antibody class switching from IgM to IgG3. This was based on previous reports that showed that Th17 promotes IgG1, IgG2a, IgG2b and IgG3 subtypes production in B cells, while IL17A specifically promotes IgG2 and IgG3 subtypes (Mitsdoerffer, M. et al., 2010). Our results show that TF-S14 1, 10, 100 mg/kg treated mice had lower IgG3+IGM+/CD19+CD138+ mature B cells compared to NT sensitized or tacrolimus 0.5 mg/kg treated sensitized mice (Fig. 3.5a, 3.5b). In addition, TF-S14 treatment at doses of 10 mg/kg and 100 mg/kg reduced the percentage of IgM^{hi}/CD19+CD138+ cells, compared to NT sensitized mice (Fig. 3.5a, 3.5c). Moreover, TF-S14 treatment to sensitized mice decreased serum IgG3 content (Fig. 3.5d). However, the treatment didn't decrease the total IgG concentration in mice sera in TF-S14 treated compared to NT sensitized mice, however sensitized mice from all groups had high concentrations of total

IgG compared to non-sensitized mice (Fig. 3.5e). The IgM to IgG3 class switching was observed in the spleen sections using immunofluorescence staining of IgM+, IgG+ and ly6G+ cells (Fig. 3.5f). There was a decrease in IgG3+ cell clusters which was confirmed by the reduction of IgG3$_{Alexa\ Fluor\ 594}$ MFI in the spleen section from TF-S14 treated sensitized mice groups compared to vehicle or tacrolimus treated groups (Fig. 3.5g).
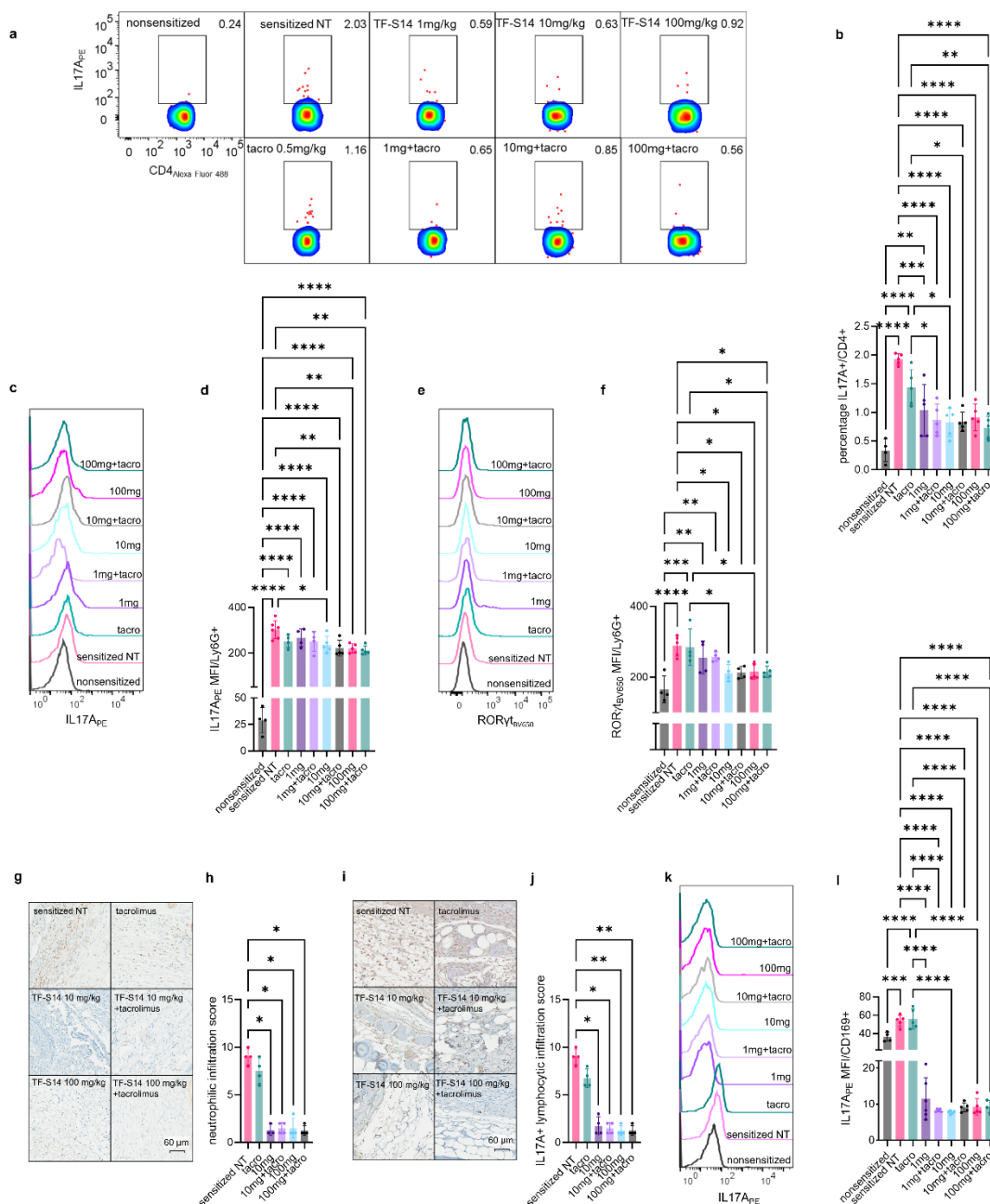
Fig. 3.4: Effect of RORγt inverse agonist TF-S14 on IL17A production in splenic CD4+ T cells, CD169+ macrophages, Ly6G+ neutrophils and graft infiltrating leukocytes following full thickness BALB/C skin transplantation to BALB/C-sensitized C57BL/6 mice. Splenocytes were isolated from NT sensitized control, tacrolimus 0.5 mg/kg (tacro), TF-S14 1, 10 or 100 mg alone and or in combination with tacrolimus 0.5 mg/kg treated mice on the day of rejection. The splenocytes were activated with PMA/Ionomycin/monensin/prefoldin cocktail and percentage of IL17A+/CD4+ (**a**, **b**), RORγt$_{BV650}$ MFI (**c**, **d**), IL17A$_{PE}$ MFI of Ly6G+ cells (**e**, **f**) were measured by flow cytometry. Data are presented as mean ± SD, $*p < 0.05$, $**p < 0.01$, $***p < 0.005$, $****p < 0.001$, one-way ANOVA and Tukey's test, $n = 4$–6 per group. Histopathology photomicrographs show BALB/C skin allografts ($n = 3$–4 per group) that were isolated on day 5 post-transplantation and stained with anti-ly6G (brown), ×40 (**g**, **h**) or anti-IL17A (brown), ×40 (**i**, **j**). The percentage area of Ly6G+ neutrophilic and IL17A+ lymphocytic infiltrations were scored from 1 (<10%) to 10 (>90%) of the graft area. Data are presented as mean ± SD, $*p < 0.05$, $**p < 0.01$, Kruskal–Wallis one-way ANOVA and Dunn's test, $n = 3$–4 per group. IL17A$_{PE}$ MFI in CD169+ cells was measured by flow cytometry (**k**, **l**). Data are presented as mean ± SD, $*p < 0.05$, $**p < 0.01$, $***p < 0.005$, $****p < 0.001$, one-way ANOVA and Tukey's test, $n = 4$–6 per group.

RORγt inverse agonist TF-S14 decreases ILC3 fraction in splenocytes of sensitized mice

Previous work showed that *Rorc$^{-/-}$* mice had fewer splenic Lin−CD117+CD127+ ILC3 compared to *Rorc$^{+/+}$* (wild-type) mice (Magri et al., 2014). To determine the effect of RORγt inhibition on ILC3 we compared the percentage of CD117+CD127+/Lin-

population in TF-S14 treated, tacrolimus treated, NT sensitized and non-sensitized mice. The ILC3/Lin- fraction was higher in tacrolimus treated compared to NT sensitized mice. TF-S14 RORγt inverse agonist alone or in combination with tacrolimus reduced the ILC3 fraction compared to tacrolimus 0.5 mg/kg only treated sensitized mice and restored the ILC3 levels to the normal levels seen in non-sensitized mice (Fig. 3.5h, 3.5i).
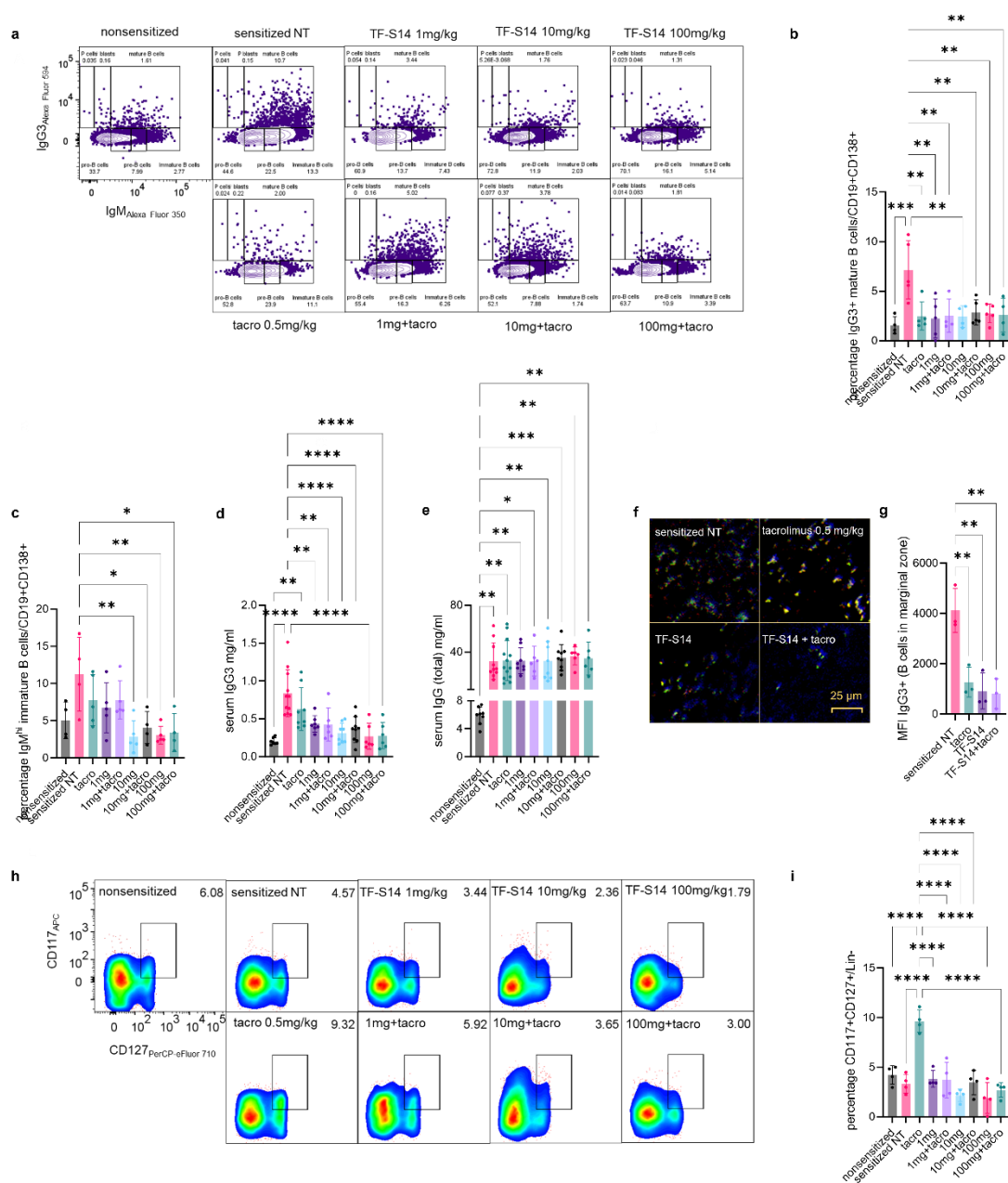
Fig. 3.5: Effect of RORγt inverse agonist TF-S14 on B-cell differentiation, IgM to IgG3 class switching, ILC3 fraction, serum IgG/IgG3 content following full thickness BALB/C skin transplantation to BALB/C-sensitized C57BL/6 mice. Splenocytes were isolated from sensitized NT control, tacrolimus 0.5 mg/kg (tacro), TF-S14 1, 10 or 100 mg alone and combination treated mice on the day of rejection and activated using anti-IgM/anti-IgG3. The percentage of mature B cells IgG3+IgM+/CD19+CD138+ and immature B cells IgM^{hi}IgG3−/CD19+CD138+ were measured by flow cytometry (**a**–**c**). The content of IgG and IgG3 were measured in mice sera with ELISA (**d**, **e**). Photomicrographs show spleen sections that were stained with anti-IgG3 (red), anti-IgM (blue), anti-Ly6G (green), showing increase in IgG3 cells in the spleens in vehicle or tacrolimus treated mice compared to TF-S14 alone or in combination with tacrolimus 0.5 mg/kg (**f**, **g**). Splenocytes were stained with ILC3 phenotyping surface markers and the percentage of CD117+CD127+/Lin− cells was measured by flow cytometry (**h**, **i**). Data are presented as mean ± SD, *$p < 0.05$, **$p < 0.01$, ***$p < 0.005$, ****$p < 0.001$, one-way ANOVA and Tukey's test, $n = 3$–13 per group.

Discussion

The role of Th17 and other IL17A producing cells in heart and skin graft rejection have been deliberated before in many studies (Chung et al., 2012; Chung et al., 2011; Hsieh et al., 2001; Yuan et al., 2008). However, the correlation between prior sensitization state and leukocyte predisposition to transformation to IL17A+ phenotypes was not studied before. We showed in a preliminary report that Th17 phenotype is present in the peripheral blood of highly sensitized kidney transplantation candidates (Kandeva et al., 2010). In the current study, we found a positive correlation between prior sensitization

status and IL17A+CD4+ T cells in an in vitro Th17 polarization of human PBMCs. Previous studies have shown that Th17 is involved in both cellular rejection and AMR (Chung et al., 2012; Chung et al., 2011). The hallmark of Th17 mediated cellular rejection is the acute massive neutrophilic infiltration of the grafts (Agorogiannis et al., 2012), which we observed during graft rejection in sensitized mice. This is mediated through IL17A, and other cytokines secreted from Th17 (Agorogiannis et al., 2012; Zhang & Reed, 2016). Our findings show that in addition to its production in T cells, IL17A was also produced by other leukocytes such as neutrophils and macrophages as we found in the splenocytes of sensitized mice. Both neutrophils and macrophages have been shown to produce IL17A (Hasan et al., 2013; Song et al., 2008). The increase in IL17A+ neutrophils and macrophages in sensitized mice compared to non-sensitized mice indicates intercellular positive feedback where the IL17A and other cytokines that are secreted from Th17 cells promote an increase in RORγt expression in different leukocytes. Subsequently this positive feedback leads ultimately to an increase in IL17A expression in these leukocytes. This proposed mechanism can be explained by the reduction of RORγt+ neutrophils that we have observed following the administration of RORγt inverse agonists daily treatment with three doses of TF-S14. The positive feedback of IL17A and other Th17/Tfh17 cytokines has been reported to work in both autocrine and paracrine fashion (Ogura et al., 2008). The second mechanism of graft rejection involving Th17 help, is the promotion of tertiary lymphoid tissue formation that requires IL21 cytokine secretion, which was reduced by RORγt inverse agonists (Deteix et al., 2010; Zhang & Reed, 2016). Our findings show that the inverse agonists of RORγt decrease IL21 expression in ROR+ T cells in vitro human PBMCs polarization, however we did not detect the difference in

the splenocytes isolated from transplanted mice. An explanation for this is that IL21 expression can be correlated to RORγt[hi] CD4+ rather than to RORγt+CD4+ cells, which indicates that IL21 expression in Th17 is a subsequent stage to IL17A production in peripheral RORγt+ cells and as well influenced by IL17A positive feedback loop. Previous reports have shown that IL21 works as an autocrine factor that promotes or sustains the Th17 phenotype (Wei et al., 2007). In our human in vitro Th17 polarization experiment, we found that IL21 secretion correlates with RORγt[hi] expression in Th17 which indicates a sustained Th17 phenotype.

The third mechanism by which Th17 cells mediate graft rejection is the through the promotion of antibody class switching which in addition to IL17A also requires IL21 and preferentially promotes IgG2a and IgG3 classes (Mitsdoerffer, M. et al., 2010; Zhang & Reed, 2016). Although we did not see a difference in IL21+/CD4+ fraction in splenocytes from the mice that were treated with TF-S14; however, we observed a reduction in IgG3 serum level and a reduction in IgM to IgG3 antibody class switching which can be both correlated to the reduction of IL21 expression in RORγt+CD4+ cells following RORγt inverse agonist treatment in mice. We can confirm this effect on IL21 production based on our observations in human PBMCs Th17 polarization and observations from other studies (Solt et al., 2015). Previous research identified that de novo alloantibodies produced during rejection are of IgG1 and IgG3 subtypes. These subtypes have strong complement binding capacity and are associated with acute AMR (Freitas et al., 2013). Both IgG1 and IgG3 subclasses were shown to be associated with acute and chronic AMR worse outcomes (Griffiths et al., 2004; Kaneku et al., 2012). In addition to those three mechanisms, as we previously mentioned, we found that sensitization in mouse

model promotes RORγt+ neutrophils and macrophages. Both cell types are considered among the professional antigen presenting cells. They are mainly known to be present antigens to T cells, but they also present antigens to B cells (Boswell et al., 1980; Puga et al., 2012). We observed an increase in neutrophil and macrophage B cell help in the spleen sections of sensitized mice and we found that they were both reduced in the mice that were treated daily with TF-S14. This can be a fourth mechanism by which RORγt inverse agonists decrease antibody class switching in B cells through the reduction of leukocytes recruitment at the inflammation site. This effect on leukocytes infiltration was observed in the skin allografts as a reduction or complete absence of neutrophils in the grafts of the mice treated with TF-S14. This effect can also explain the ability of the higher doses of TF-S14 to block the differentiation of pre-B cells to immature IgM^{hi} B cells.

Moreover, the daily treatment with the RORγt inverse agonist TF-S14 resulted in restoring ILC3 fraction in sensitized mice to near the normal levels found in non-sensitized mice which were, on the other hand, higher than normal in tacrolimus only treated mice. Previous research has shown that the percentage of ILC3 is reduced in patients undergoing acute cellular organ rejection compared to no rejection kidney transplantation patients (Pucci Molineris et al., 2020). Even though the reduction of ILC3 that we observed in sensitized mice compared to non-sensitized mice was not significant, this is still aligned with previously reported findings (Pucci Molineris et al., 2020). Other studies have shown that the increase in the ILC3 indicates a Th2 minimal persistent inflammation (Chen et al., 2022). This can explain the increase in the percentage of ILC3 in tacrolimus only treatment mice as it has previously demonstrated that tacrolimus decreases the Th1/Th2 ratio (Arias-Diaz et al., 2009). ILC3 are non-specific innate immune cells which

like other non-specific innate immune cells can be short lived first responders which explains both their exhaustion in active rejection and the increase in their percentage when the immune system is triggered in a minimal chronic fashion. The ability of the RORγt inverse agonist TF-S14 to restore the normal levels of ILC3 cells indicates an excellent control of the inflammation at the graft site. This effect can be mediated through the reduction of IL22 cytokine expression in RORγt+ cells. Like IL21, we found that IL22 production in Th17 cells is correlated with the percentage of RORγt[hi] rather than RORγt+ and can eventually be indirectly influenced by IL17A positive feedback loop trough RORγt. It has been shown that ILC3 express RORγt and they produce both IL17A and IL22 through which they mediate their innate immune function and eventually perform some functions of Th17 cells such as mucus protection against pathogens (Yang et al., 2020). We conclude that RORγt inverse agonist treatment prevents the exhaustion of ILC3 and reduces their recruitment at the inflammatory site as well and eventually does not result in an elevation of ILC3 overall percentage which can be a useful marker of successful RORγt inhibition. On the other hand, studies showed that ILC3 cells play a role in T-cell independent production of IgM, IgG2a and IgG3. In the current study both the restoration of normal levels of ILC3 and reduction of serum IgG3 levels was observed in the mice treated with TF-S14 compared to tacrolimus only treated mice.

Finally, we found that TF-S14 inverse agonist treatment prolonged, while tacrolimus treatment did not influence graft survival in sensitized mice as it is not as effective in blocking Th17 response which is a major player in hyperacute cellular, and AMR encountered in this model (Abadja et al., 2011; Arias-Diaz et al., 2009; Chung et al., 2012). This is because the Th17 response that develops in the accelerated rejection

mouse model starts as early as three days post transplantation, which has been shown to occur in mouse model of renal and skin transplantation (Hsieh et al., 2001; Vokaer et al., 2010). In fact, following a three BALB/C splenocyte IP injections sensitization protocol, memory Th17, memory B cells and preformed DSAs develop in the sensitized mice before the skin transplantation surgery as demonstrated in previous studies (Hsieh et al., 2001; Vokaer et al., 2010; Zhao et al., 2018). The subsequent events such as the neutrophilic infiltration that is the predominant end stage mechanism in the accelerated skin allograft rejection model can typically occur early at 24 h post transplantation and reach the peak within the first 6 days (Eichwald et al., 1966). On the other hand, the Th1 or IFNγ mediated cellular response typically peaks at 10-12 days post transplantation as seen in non-sensitized mouse model of skin transplantation and full rejection occurs at 18 days (Cheng et al., 2017). This onset of IFNγ response seems to be unchanged in sensitized mouse model of transplantation as the median survival that we observed in RORγt inverse agonist treated mice was at 18 days which matches with Th1 rejection timeline rather than 6 days that we concluded to be the Th17 hyperacute rejection timeline which is characterized with massive neutrophilic infiltration. Even though tacrolimus is effective in blocking Th1 responses, however its effect on Th17 is marginal and in fact it may potentiate Th17 response on long term use (Abadja et al., 2011; Arias-Diaz et al., 2009; Chung et al., 2012). Dysregulation of Th17 response can be mediated through its effect on Th1/Th2 or the reduction of Treg population (Arias-Diaz et al., 2009; Chung et al., 2012). The histological image of the skin grafts from the mice treated with TF-S14 in combination with tacrolimus that survived beyond 13 days showed resemblance to Th2 mediated scleroderma or eosinophilic fasciitis. This indicates that with successful

inhibition of Th1 and Th17 responses by tacrolimus and RORγt inverse agonist TF-S14, respectively, a third mechanism mediated through Th2 orchestrates the rejection. Previous research has shown that Th2 mediated chronic rejection develops in mice deficient in RORγt and T-bet (Sabet-Baktach et al., 2013). Further research is required to investigate Th2 mediated rejection mechanisms that develop under dual pharmacologic inhibition of both Th1 and Th17. In addition, further studies are required to evaluate the effects of TF-S14 on memory Th1 and CD8+ T cells and other immune cells activated during acute cellular rejection in a non-sensitized allogenic transplantation model. In such studies, the use of a non-sensitized mouse model is crucial to avoid the neutrophilic infiltration resulting from the early activation of memory Th17 response. This infiltration masks memory Th1 and CD8+ T-cell response.

In conclusion, we found that the RORγt inverse agonist TF-S14 is effective in improving graft survival by blocking four processes namely leukocyte recruitment, tertiary lymphoid tissue formation, B cell differentiation and de novo IgG3 DSAs production. These effects are mediated through the inhibition of RORγt in Th17 and other leukocytes such as neutrophils, macrophages and ILC3. These effects are immediate and long term, accordingly, TF-S14 can be used to prevent or treat solid graft rejection.

Methods

Human blood samples collection

Blood samples collection protocol (12-075-GEN) was approved by the Research Ethics Board of the Research Institute of the McGill University Health Centre. Written consents were received from the participants before inclusion in the study. Blood samples were

collected from healthy donors and kidney transplantation candidates on dialysis by a registered nurse. Samples were all coded and identified by number.

Human Th17 polarization

Peripheral blood mononuclear cells were isolated by density gradient centrifugation. Whole blood was diluted with 1x PBS and then layered gently over 14 ml of lymphocyte separation medium in a 50 ml centrifuge tube and centrifuged for 30–40 min at 400 × *g*. PBMCs layer and is a characteristically white and cloudy "blanket" was gently removed using a 10 ml pipette and added to warm medium or PBS (1:3) to wash off any remaining platelets and centrifuged at 400 × *g* for 10 min. The pelleted cells were counted, and the percentage viability estimated using trypan blue staining. PBMCs were resuspended to $5 × 10^6$ cells/ml in freezing medium containing 10% DMSO and 90% fetal bovine serum (FBS) and were placed inside a freezing container at −80 °C overnight to allow gradual and even cooling. The following day, samples were moved to a liquid nitrogen tank for long-term storage. In total, 500 ml bottle of RPMI at 4 °C was opened in a biological safety cabinet. Half of the media was transferred to a 500 ml 0.22 um bottle top filter (with the vacuum turned off). In total, 59 ml filtered heat inactivated FBS, 6 ml penicillin-streptomycin solution (100x), 6.0 ml of L-glutamine (100x), 6.0 ml MEM non-essential amino acids 100x, 6.0 ml of sodium pyruvate were added, and the volume was brought up to 500 ml by adding the RPMI. Culture media were stored at 4 °C and used for duration of 2 weeks. PBMCs were thawed carefully to avoid loss of cell viability and functionality. Samples were removed from liquid nitrogen and placed on ice, after which they were thawed in a 37 °C water bath. Once thawed, 500 µl warm complete RPMI medium supplemented with 10% FBS, 1% penicillin-streptomycin, and L-glutamine was added to

cryovials dropwise. The cells were then transferred to 15 ml polystyrene tubes containing 10 ml warm medium and centrifuged for 10 min at 400 × g to wash off the toxic DMSO. This wash step was repeated, and the cell pellet was then resuspended in medium to count as before. Once thawed, PBMCs were rested overnight to remove any apoptotic cells. After resting period, cells were washed to be used in culture. PBMCs were plated in 96 well plates using complete RPMI-1640 medium (10% FBS), and incubated at 37 °C in a humidified, 5% CO_2 atmosphere. Cells were treated with human T-cell activator CD3/CD28 magnetic beads (2 µl: 80,000 cells) for 12 days in presence of IL6 10 ng/ml, IL1β 10 ng/ml, TGFβ 10 ng/ml, and IL23 10 ng/ml. Culture medium was changed every other day for the whole duration. Compounds were added to the polarized cells on day 14 for 48 h. On the measurement day, CD3/CD28 beads were removed, and cells were treated with cell stimulation cocktail for 5 h at the end of 48 h incubation. Plates were centrifuged at 400 × g for 10 min. Supernatant was collected for further testing and cells were resuspended in 1x PBS and washed twice at 400 × g before staining for surface and intracellular markers. PBMCs cell suspension were stained cells with live/dead$_{455}$ $_{(UV)}$ viability dye in 1:1000 concentration in 1x PBS. Cells were incubated in dye solution for 30 min in 4 °C. Control wells were used where 50% of the cells in those wells were killed by heat (65 °C for 1 min) and then returned to their respective wells and stained similarly for 30 min. Cells were then centrifuged at 400 × g for 10 min and the dye solution was discarded. Cells were washed twice with 1x PBS before surface staining. After the last wash, supernatant was discarded, and plates were pulse vortexed to completely dissociate the pellets. Anti-human anti-CD3$_{BV510}$, anti-CD4$_{Alexa\ Fluor\ 488}$ and anti-CD8$_{PE-Cy7}$ were added to each well at 1:1000 concentration in 1% BSA in PBS. Cells were

incubated for 1 h at 4 °C. Cells were then centrifuged at 400 × g and washed with 1x PBS twice. After the last wash, supernatant was discarded, and plates were pulse vortexed to dissociate the pellets. Cells were treated with FOXP3 fixation/permeabilization buffer (100 µl/well) for 30 min at 4 °C. Plates were centrifuged at 400 × g and buffer was discarded followed by two washing steps with FOXP3 permeabilization buffer (200 µl) and centrifugation at 400 × g. Anti-human anti-IL17A$_{PE}$, anti-RORγt$_{BV650}$, anti-IL21$_{APC}$, anti-IL22$_{PerCP-eFluor\ 710}$ and anti-IFNγ$_{APC-eFluor\ 780}$ were added to each well used at 1:1000 concentration in permeabilization buffer. Cells were incubated for 1 h at 4 °C, centrifuged at 400 × g and washed with 1x PBS twice. Cell quantification, viability and intracellular cytokines expression were analyzed by flow cytometry using BD LSR-Fortessa flow cytometer.

Human Th1 polarization

PBMCs were plated in 96 well plates using complete RPMI-1640 medium (10% FBS), and incubated at 37 °C in a humidified, 5% CO_2 atmosphere. Cells were treated with human T-cell activator CD3/CD28 magnetic beads (2 µl: 80,000 cells) for 3 days in presence of IL2 (5 ng/ml). Culture medium was changed every other day for the whole duration and compounds were added to each well from day zero for 3 days. On the measurement day, CD3/CD28 beads were removed, and cells were treated with cell stimulation cocktail for 5 h. Plates were centrifuged at 400 × g for 10 min. Cells were resuspended in 1x PBS and washed twice at 400 × g before staining for surface and intracellular markers. PBMCs cell suspensions were stained cells with live/dead$_{455}$ $_{(UV)}$ viability dye, anti-human anti-CD3$_{BV510}$, anti-CD4$_{Alexa\ Fluor\ 488}$, anti-CD8$_{PE-Cy7}$, anti-

IL17A_{PE} and anti-IFNγ_{APC-eFluor 780}. Cell quantification, viability and intracellular cytokines expression were analyzed by flow cytometry using BD LSR-Fortessa flow cytometer.

Human Treg polarization

PBMCs were plated in 96 well plates using complete RPMI-1640 medium (10% FBS), and incubated at 37 °C in a humidified, 5% CO_2 atmosphere. Cells were treated with human T-cell activator CD3/CD28 magnetic beads (2 µl: 80,000 cells) for 6 days in presence of IL2 (5 ng/ml) and TGFβ (5 ng/ml). Culture medium was changed every other day for the whole duration and compounds were added to each well from day zero for 6 days. On the measurement day, CD3/CD28 beads were removed, and cells were treated with cell stimulation cocktail for 5 h. Plates were centrifuged at 400 × *g* for 10 min. Cells were resuspended in 1x PBS and washed twice at 400 × *g* before staining for surface and intracellular markers. PBMCs cell suspension were stained cells with live/dead_{455 (UV)} viability dye, anti-human antibodies for cell surface antigens namely anti-CD3_{BV510}, anti-CD4_{Alexa Fluor 488}, anti-CD8_{PE-Cy7}, anti-CD25_{BV786} and CD127_{PE-Cy5}, anti-IL17A_{PE}, anti-IFNγ_{APC-eFluor 780} and FOXP3_{PerCP-Cy5.5} Cell quantification, viability and intracellular cytokines expression were analyzed by flow cytometry using BD LSR-Fortessa flow cytometer.

RORγt TR-FRET binding assay

Five µl of compounds solutions in assay buffer were added to 15 µl of detection mix for 20 µl total assay volume (50 mM tris-HCl pH 7.0, 150 mM NaCl, 50 mM KCl, 5 mM MgCl2, 1 mM DTT, 0.1% BSA, 0.001% triton X); 1.5 nM GST-RORγt (LBD) (Creative BioMart, Shirley, NY, USA); 90 nM biotinylated RIP140 coactivator peptide (biotinyl-NH-Ahx-NSHQKVTLLQLLLGHKNEEN-CONH2) (CPC scientific inc., Sunnyvale, CA, USA);

50 nM SA-APC (PerkinElmer, Waltham, MA, USA); 1.5 nM Eu-anti GST IgG (PerkinElmer, Waltham, MA, USA); 1% DMSO). Compound dilutions (200x in pure DMSO) were prepared by making a 0.5 mM dilution from a 10 mM stock using 100% DMSO. Serial dilutions of the compounds were then prepared for 11 points beyond the 20 μM starting concentration in assay buffer. A 4x solutions containing europium-labeled antibody, and GST-RORγt (LBD) mixture were prepared, then 5 μl of each solution was added to each well on a 384-well plate, followed by the addition of 5 μl of each concentration of a compound previously diluted in assay buffer (described above). Assay controls (0% and 100% inhibition controls) were added into columns 1, 2, 23, and 24 of the 384 well assay plate. For 0% inhibition control, DMSO in assay buffer was used, while for 100% inhibition control, GSK2981278 (100 nM final concentration) was added. The plate was shaken for 1 min, centrifuged at 1000 rpm for 10 s, incubated at 4 °C overnight and followed by the addition of 5 μl of 4x biotinylated RIP140 peptide & streptavidin-APC, and read on a plate reader. For assay screening, Enspire plate reader was used. Settings were as follows: excitation: 320 nm, emission A: 615 nm; time delay: 220 μs; window: 600 μs, emission B: 699 nm (delay time 400 μs, window 800 μs); number of flashes: 100. RORγt TR-FRET assay is an end point assay with a readout (emission ratio) of acceptor/donor multiplied by 10,000. The assay dose response testing is performed in duplicate points per concentration, with ten dilution concentrations per compound curve. The conversion of raw data to % activity is performed using assay controls, where 100% activity is represented by the average DMSO controls. Zero percent activity is the average of two wells of 100 nM, GSK2981278 compound controls. Inhibitory concentration curve fitting is performed using the sigmoidal dose-response (variable slope) equation as

follows: $Y = 100/(1 + 10^{\wedge}((\log IC_{50}-X) * \text{hillslope})$ where X is the logarithm of concentration and Y is the normalized response. Y begins at the bottom (0%) and goes to top (100%) with a sigmoid shape.

Sensitized murine model of skin transplantation.

The animal protocol (MUHC-8128) was approved by the Animal Care Committee of the Research Institute of McGill University Health Centre. C57BL/6 mice were sensitized by IP injections of allogenic splenocytes (1×10^7 on day 0, 7, and 14) derived from spleens of donor BALB/C mice (Cravedi et al., 2013). his procedure was performed for 14 days following the initial sensitization step. BALB/C donor dorsal skin was transplanted to C57BL/6 recipient. The technique is described in detail by Cheng et al. (Cheng et al., 2017). BALB/C donor mice were anesthetized with isoflurane (induction vaporizer at 4%, maintenance at 1% through the mouse cone). Depth of anesthesia was monitored using toe pinch withdrawal reflex. The back of the donor mouse was shaved with electric razor and the skin was disinfected with 10% povidone iodine. Skin (from hip to neck) was harvested aseptically with blunt dissection at the level of the areolar connective tissue. Following skin harvest, animals were euthanized by cervical dislocation. Skin was separated from underlying panniculus carnosus layer, fat and connective tissues and cut out into squares (each square was used as a graft for an individual recipient mouse) of 12×12 mm size and stored on gauze with sterile PBS in petri dish. C57BL/6 mice were anesthetized with isoflurane (induction vaporizer at 4%, maintenance at 1% through the mouse cone). Depth of anesthesia was monitored using toe pinch withdrawal reflex. Buprenorphine (0.02 mg/kg) was administered for postoperative pain relief. The back of the donor mouse was shaved with electric razor and the skin was disinfected with 10%

povidone iodine. Graft beds were created by cutting out 11 × 11 mm to 13 × 13 mm square of skin, while preserving the underlying layers intact (i.e., panniculus carnosus). Grafts from BALB/C donor were placed on the graft beds and were sutured avoiding folding at the edges and across the panniculus carnosus. Following transplantation mice were left to recover partially from anesthesia and surgery. Drugs were administered either by intraperitoneal injection or applied topically to skin grafts. Topical administration, 0.1% compound ointment (hydrous lanolin) or sham were applied to the skin graft and covered with hydrogel dressing and wrapped in an adhesive bandage with folded gauze. Transplanted mice were placed in a clean cage over a microwavable heating pad until fully recovered from anesthesia and for at least 1 h before returning to the housing facility. Bandages were changed every other day and grafts were observed and clinical scores were given to each. Mice which show signs of scabbing, contraction, or hardness in the first 72 h were considered a technical failure and were excluded from the study. The severity of rejection was measured using a scoring function from 0 to 5. Lesions were photographed using a digital camera and were evaluated by a blinded investigator (Schwoebel et al., 2005). Score 5 was considered the end point for each animal (≥ 95% of the graft tissue becomes necrotic). At the end of rejection, animals were euthanized by cardiac puncture and blood was collected for further analysis. Skin grafts were harvested for histology. Spleens were collected for testing by flow cytometry. Animals were sacrificed on rejection day. ASEPESIS wound score for mice was used to evaluate surgical wound and rejection was scored according to graft area percent necrosis where complete rejection was >95% necrosis (Kick et al., 2019; Schwoebel et al., 2005).

Mouse T-cell to Th17 polarization

Splenocytes were isolated from mouse spleens using red blood cell lysis buffer and cell strainer (Fouda et al., 2017). Splenocytes were frozen in a medium containing 10% DMSO and 90% fetal bovine serum (FBS) and were placed inside a freezing container at -80°C overnight to allow gradual and even cooling. The following day, samples were moved to a liquid nitrogen tank for long-term storage. Samples were removed from liquid nitrogen and placed on ice, after which they were thawed in a 37°C water bath. Once thawed, 500 µl warm complete RPMI medium supplemented with 10% FBS, 1% penicillin-streptomycin, and L-glutamine was added to each cryovial dropwise. The cells were then transferred to 15 ml polystyrene tubes containing 10 ml warm medium and centrifuged for 10 min at 400 × g to wash off the toxic DMSO. This wash step was repeated, and the cell pellet was then resuspended in medium to count cells. T cells were isolated from −80 frozen mouse splenocytes using T cell isolation cocktail and magnetic streptavidin beads (Fouda et al., 2017). Following the isolation, cells were suspended in PBS and counted. Mouse T cells were plated in 96 well plates using complete RPMI-1640 medium (10% FBS), and incubated at 37 °C in a humidified, 5% CO2 atmosphere. Cells were treated with mouse T-cell activator CD3/CD28 magnetic beads (2 µl: 80,000 cells) for 4 days in presence of IL6 (20 ng/ml), IL1β (10 ng/ml), TGFβ (2 ng/ml), and IL23 (10 ng/ml). Compounds were added to the polarized cells on day zero for the whole duration of the polarization. On the measurement day, CD3/CD28 beads were removed, and cells were treated with cell stimulation cocktail for 5 h. Plates were centrifuged at 400 × g for 10 min. T cells were stained cells with live/dead$_{455\ (UV)}$ viability dye, anti-mouse anti-CD4$_{Alexa\ Fluor\ 488}$, anti-CD8$_{PE-Cy7}$, anti-IL17A$_{PE}$, anti-RORγt$_{BV650}$, anti-IL21$_{APC}$, anti-IL22$_{PerCP-eFluor\ 710}$ and

anti-IFNγ$_{APC-eFluor\ 780}$. Cell quantification, viability and intracellular cytokines expression were analyzed by flow cytometry using BD LSR-Fortessa flow cytometer.

Mouse splenocytes immunostaining

B cells: live/dead$_{eFluor\ 780}$, anti-CD3$_{BV510}$, anti-CD19$_{PE-Cy7}$, anti-CD138$_{PerCP-Cy5.5}$, anti-IgG3$_{Alexa\ Fluor\ 594}$, anti-IgM$_{Alexa\ Fluor\ 350}$; ILC3 cells: live/dead$_{eFluor\ 506}$, anti-CD4$_{Alexa\ Fluor\ 488}$, anti-CD8$_{PE-Cy7}$, anti-CD45 $_{APC-Cy7}$, anti-CD117$_{APC}$, anti-CD127$_{PerCP-eFluor\ 710}$, anti-Lin$_{eFluor\ 450}$; T cells: live/dead$_{455\ UV}$, anti-CD4$_{Alexa\ Fluor\ 488}$, anti-CD8$_{PE-Cy7}$, anti-IL17A$_{PE}$, anti-RORγt$_{BV650}$, anti-IL21$_{APC}$, anti-IL22$_{PerCP-eFluor\ 710}$, anti-IFNγ$_{APC-eFluor\ 780}$; Macrophages: live/dead$_{455\ UV}$, anti-CD169$_{Alexa\ Fluor\ 488}$, anti-IL17A$_{PE}$, anti-RORγt$_{BV650}$, anti-IL21$_{APC}$, anti-IL22$_{PerCP-eFluor\ 710}$, anti-IFNγ$_{APC-eFluor\ 780}$; Neutrophils: live/dead$_{455\ UV}$, anti-Ly6G$_{FITC}$, anti-IL17A$_{PE}$, anti-RORγt$_{BV650}$, anti-IL21$_{APC}$, anti-IL22$_{PerCP-eFluor\ 710}$, anti-IFNγ$_{APC-eFluor\ 780}$.

Statistics and reproducibility

Statistical analysis was performed using GraphPad Prism (version 10.1.2) (GraphPad Software, SanDiego, CA, USA) with the suitable statistical test as indicated in each analysis. *p* Values were classified as not significant (ns; $p > 0.05$), significant (*$0.01 < p < 0.05$), very significant (**$0.001 < p < 0.01$) or extremely significant (***$p < 0.001$ and ****$p < 0.0001$). Data are presented as mean ± standard deviation (SD). Scoring of skin grafts rejection or histology were done independently by the study authors. Independent evaluations of the grafts were done by veterinarians and veterinary technicians within their settings and events of graft rejections were reported to authors. Blinding was carried out to all authors and support scientists who participated in the study. Additional experiments were carried out to confirm results as necessary.

Data availability

All data supporting the findings of this study are available within the paper and its Supplementary Information. The supplier catalog numbers, and other relevant details of the antibodies, kits and other materials used in the study can be found in Supplementary Tables 1–8. Source data for the graphs are provided in Supplementary Data 1–5.

Acknowledgements

References

Abadja, F., Atemkeng, S., Alamartine, E., Berthoux, F., & Mariat, C. (2011). Impact of Mycophenolic Acid and Tacrolimus on Th17-Related Immune Response. *Transplantation*, *92*(4), 396-403.

Abikhair, M., Mitsui, H., Yanofsky, V., Roudiani, N., Ovits, C., Bryan, T., Oberyszyn, T. M., Tober, K. L., Gonzalez, J., Krueger, J. G., Felsen, D., & Carucci, J. A. (2016).

Cyclosporine A immunosuppression drives catastrophic squamous cell carcinoma through IL-22. *JCI Insight*, *1*(8), e86434.

Agorogiannis, E. I., Regateiro, F. S., Howie, D., Waldmann, H., & Cobbold, S. P. (2012). Th17 cells induce a distinct graft rejection response that does not require IL-17A. *Am J Transplant*, *12*(4), 835-845.

Arias-Diaz, J., Ildefonso, J. A., Muñoz, J. J., Zapata, A., & Jiménez, E. (2009). Both tacrolimus and sirolimus decrease Th1/Th2 ratio, and increase regulatory T lymphocytes in the liver after ischemia/reperfusion. *Laboratory Investigation*, *89*(4), 433-445.

Boswell, H. S., Sharrow, S. O., & Singer, A. (1980). Role of accessory cells in B cell activation. I. Macrophage presentation of TNP-Ficoll: evidence for macrophage-B cell interaction. *J Immunol*, *124*(2), 989-996.

Chen, X. J., Liu, C., Zhang, S., Zhang, L. F., Meng, W., Zhang, X., Sun, M., Zhang, Y., Wang, R. Z., & Yao, C. F. (2022). ILC3-like ILC2 subset increases in minimal persistent inflammation after acute type II inflammation of allergic rhinitis and inhibited by Biminkang: Plasticity of ILC2 in minimal persistent inflammation. *J Leukoc Biol*, *112*(6), 1445-1455.

Cheng, C. H., Lee, C. F., Fryer, M., Furtmuller, G. J., Oh, B., Powell, J. D., & Brandacher, G. (2017). Murine Full-thickness Skin Transplantation. *J Vis Exp*(119).

Chung, B. H., Kim, K. W., Kim, B.-M., Piao, S. G., Lim, S. W., Choi, B. S., Park, C. W., Kim, Y.-S., Cho, M.-L., & Yang, C. W. (2012). Dysregulation of Th17 Cells during the Early Post-Transplant Period in Patients under Calcineurin Inhibitor Based Immunosuppression. *PLoS One*, *7*(7), e42011.

Chung, B. H., Kim, K. W., Kim, B. M., Doh, K. C., Cho, M. L., & Yang, C. W. (2015). Increase of Th17 Cell Phenotype in Kidney Transplant Recipients with Chronic Allograft Dysfunction. *PLoS One*, *10*(12), e0145258.

Chung, B. H., Oh, H. J., Piao, S. G., Sun, I. O., Kang, S. H., Choi, S. R., Park, H. S., Choi, B. S., Choi, Y. J., Park, C. W., Kim, Y.-S., Cho, M.-L., & Yang, C. W. (2011). Higher infiltration by Th17 cells compared with regulatory T cells is associated with severe acute T-cell-mediated graft rejection. *Experimental & Molecular Medicine*, *43*(11), 630-637.

Cravedi, P., Lessman, D. A., & Heeger, P. S. (2013). Eosinophils are not required for the induction and maintenance of an alloantibody response. *Am J Transplant*, *13*(10), 2696-2702.

Deteix, C., Attuil-Audenis, V., Duthey, A., Patey, N., McGregor, B., Dubois, V., Caligiuri, G., Graff-Dubois, S., Morelon, E., & Thaunat, O. (2010). Intragraft Th17 infiltrate promotes lymphoid neogenesis and hastens clinical chronic rejection. *J Immunol*, *184*(9), 5344-5351.

Djamali, A., Kaufman, D. B., Ellis, T. M., Zhong, W., Matas, A., & Samaniego, M. (2014). Diagnosis and management of antibody-mediated rejection: current status and novel approaches. *Am J Transplant*, *14*(2), 255-271.

Eichwald, E. J., Wetzel, B., & Lustgraaf, E. C. (1966). GENETIC ASPECTS OF SECOND-SET SKIN GRAFTS IN MICE. *Transplantation*, *4*(3), 260-273.

Fouda, A., Negi, S., Zaremba, O., Gaidar, R. S., Moroz, Y. S., Rusanov, E., Paraskevas, S., & Tchervenkov, J. (2023). Discovery, Synthesis, and In Vitro Characterization of 2,3 Derivatives of 4,5,6,7-Tetrahydro-Benzothiophene as Potent Modulators of

Retinoic Acid Receptor-Related Orphan Receptor γt. *Journal of Medicinal Chemistry*, *66*(11), 7355-7373.

Fouda, A., Tahsini, M., Khodayarian, F., Al-Nafisah, F., & Rafei, M. (2017). A Fluorescence-based Lymphocyte Assay Suitable for High-throughput Screening of Small Molecules. *J Vis Exp*, (121), 55199.

Freitas, M. C. S., Rebellato, L. M., Ozawa, M., Nguyen, A., Sasaki, N., Everly, M., Briley, K. P., Haisch, C. E., Bolin, P., Parker, K., Kendrick, W. T., Kendrick, S. A., Harland, R. C., & Terasaki, P. I. (2013). The Role of Immunoglobulin-G Subclasses and C1q in De Novo HLA-DQ Donor-Specific Antibody Kidney Transplantation Outcomes. *Transplantation*, *95*(9), 1113-1119.

Garcia, G. G., Harden, P., & Chapman, J. (2012). The Global role of kidney transplantation. *J Nephropathol*, *1*(2), 69-76.

Gebel, H. M., Kasiske, B. L., Gustafson, S. K., Pyke, J., Shteyn, E., Israni, A. K., Bray, R. A., Snyder, J. J., Friedewald, J. J., & Segev, D. L. (2016). Allocating Deceased Donor Kidneys to Candidates with High Panel-Reactive Antibodies. *Clin J Am Soc Nephrol*, *11*(3), 505-511.

Ghali, J. R., O'Sullivan, K. M., Eggenhuizen, P. J., Holdsworth, S. R., & Kitching, A. R. (2017). Interleukin-17RA Promotes Humoral Responses and Glomerular Injury in Experimental Rapidly Progressive Glomerulonephritis. *Nephron*, *135*(3), 207-223.

Griffiths, E. J., Nelson, R. E., Dupont, P. J., & Warrens, A. N. (2004). Skewing of pretransplant anti-HLA class I antibodies of immunoglobulin G isotype solely toward immunoglobulin G1 subclass is associated with poorer renal allograft survival. *Transplantation*, *77*(11), 1771-1773.

Hasan, S. A., Eksteen, B., Reid, D., Paine, H. V., Alansary, A., Johannson, K., Gwozd, C., Goring, K. A., Vo, T., Proud, D., & Kelly, M. M. (2013). Role of IL-17A and neutrophils in fibrosis in experimental hypersensitivity pneumonitis. *J Allergy Clin Immunol*, *131*(6), 1663-1673.

Hsieh, H. G., Loong, C. C., Lui, W. Y., Chen, A., & Lin, C. Y. (2001). IL-17 expression as a possible predictive parameter for subclinical renal allograft rejection. *Transpl Int*, *14*(5), 287-298.

Hsu, H.-C., Yang, P., Wang, J., Wu, Q., Myers, R., Chen, J., Yi, J., Guentert, T., Tousson, A., Stanus, A. L., Le, T.-v. L., Lorenz, R. G., Xu, H., Kolls, J. K., Carter, R. H., Chaplin, D. D., Williams, R. W., & Mountz, J. D. (2008). Interleukin 17–producing T helper cells and interleukin 17 orchestrate autoreactive germinal center development in autoimmune BXD2 mice. *Nature Immunology*, *9*(2), 166-175.

Ivanov, II, McKenzie, B. S., Zhou, L., Tadokoro, C. E., Lepelley, A., Lafaille, J. J., Cua, D. J., & Littman, D. R. (2006). The orphan nuclear receptor RORgammat directs the differentiation program of proinflammatory IL-17+ T helper cells. *Cell*, *126*(6), 1121-1133.

Kandeva, T., Liu, S., & Tchervenkov, J. (2010). THE PRESENCE OF INCREASED PERIPHERAL TH17 LYMPHOCYTES IN HIGHLY SENSITIZED RENAL TRANSPLANT PATIENTS: IMPLICATIONS FOR IMMUNE MODULATION: 3135. *Transplantation*, *90*, 191.

Kaneku, H., O'Leary, J. G., Taniguchi, M., Susskind, B. M., Terasaki, P. I., & Klintmalm, G. B. (2012). Donor-specific human leukocyte antigen antibodies of the

immunoglobulin G3 subclass are associated with chronic rejection and graft loss after liver transplantation. *Liver Transpl*, *18*(8), 984-992.

Kick, B. L., Gumber, S., Wang, H., Moore, R. H., & Taylor, D. K. (2019). Evaluation of 4 Presurgical Skin Preparation Methods in Mice. *J Am Assoc Lab Anim Sci*, *58*(1), 71-77.

Kim, H. P., Korn, L. L., Gamero, A. M., & Leonard, W. J. (2005). Calcium-dependent activation of interleukin-21 gene expression in T cells. *J Biol Chem*, *280*(26), 25291-25297.

Lachmann, N., Duerr, M., Schönemann, C., Pruß, A., Budde, K., & Waiser, J. (2017). Treatment of Antibody-Mediated Renal Allograft Rejection: Improving Step by Step. *J Immunol Res*, *2017*, 6872046.

Loupy, A., Hill, G. S., & Jordan, S. C. (2012). The impact of donor-specific anti-HLA antibodies on late kidney allograft failure. *Nature Reviews Nephrology*, *8*(6), 348-357.

Magri, G., Miyajima, M., Bascones, S., Mortha, A., Puga, I., Cassis, L., Barra, C. M., Comerma, L., Chudnovskiy, A., Gentile, M., Llige, D., Cols, M., Serrano, S., Aróstegui, J. I., Juan, M., Yagüe, J., Merad, M., Fagarasan, S., & Cerutti, A. (2014). Innate lymphoid cells integrate stromal and immunological signals to enhance antibody production by splenic marginal zone B cells. *Nat Immunol*, *15*(4), 354-364.

McDonald-Hyman, C., Turka, L. A., & Blazar, B. R. (2015). Advances and challenges in immunotherapy for solid organ and hematopoietic stem cell transplantation. *Sci Transl Med*, *7*(280), 280rv2.

Mitsdoerffer, M., Lee, Y., Jäger, A., Kim, H. J., Korn, T., Kolls, J. K., Cantor, H., Bettelli, E., & Kuchroo, V. K. (2010). Proinflammatory T helper type 17 cells are effective B-cell helpers. *Proc Natl Acad Sci U S A*, *107*(32), 14292-14297.

Ogura, H., Murakami, M., Okuyama, Y., Tsuruoka, M., Kitabayashi, C., Kanamoto, M., Nishihara, M., Iwakura, Y., & Hirano, T. (2008). Interleukin-17 Promotes Autoimmunity by Triggering a Positive-Feedback Loop via Interleukin-6 Induction. *Immunity*, *29*(4), 628-636.

Pucci Molineris, M., González Polo, V., Rumbo, C., Fuxman, C., Lowestein, C., Nachman, F., Rumbo, M., Gondolesi, G., & Meier, D. (2020). Acute cellular rejection in small-bowel transplantation impairs NCR+ innate lymphoid cell subpopulation 3/interleukin 22 axis. *Transplant Immunology*, *60*, 101288.

Puga, I., Cols, M., Barra, C. M., He, B., Cassis, L., Gentile, M., Comerma, L., Chorny, A., Shan, M., Xu, W., Magri, G., Knowles, D. M., Tam, W., Chiu, A., Bussel, J. B., Serrano, S., Lorente, J. A., Bellosillo, B., Lloreta, J., . . . Cerutti, A. (2012). B cell–helper neutrophils stimulate the diversification and production of immunoglobulin in the marginal zone of the spleen. *Nature Immunology*, *13*(2), 170-180.

Sabet-Baktach, M., Eggenhofer, E., Rovira, J., Renner, P., Lantow, M., Farkas, S. A., Malaisé, M., Edtinger, K., Shaotang, Z., Koehl, G. E., Dahlke, M. H., Schlitt, H. J., Geissler, E. K., & Kroemer, A. (2013). Double deficiency for RORγt and T-bet drives Th2-mediated allograft rejection in mice. *J Immunol*, *191*(8), 4440-4446.

Schwoebel, F., Barsig, J., Wendel, A., & Hamacher, J. (2005). Quantitative assessment of mouse skin transplant rejection using digital photography. *Lab Anim*, *39*(2), 209-214.

Shen, C., Xue, X., Zhang, X., Wu, L., Duan, X., & Su, C. (2021). Dexamethasone reduces autoantibody levels in MRL/lpr mice by inhibiting Tfh cell responses. *Journal of Cellular and Molecular Medicine*, *25*(17), 8329-8337.

Sicard, A., Phares, T. W., Yu, H., Fan, R., Baldwin, W. M., 3rd, Fairchild, R. L., & Valujskikh, A. (2012). The spleen is the major source of antidonor antibody-secreting cells in murine heart allograft recipients. *Am J Transplant*, *12*(7), 1708-1719.

Solt, L. A., Banerjee, S., Campbell, S., Kamenecka, T. M., & Burris, T. P. (2015). ROR inverse agonist suppresses insulitis and prevents hyperglycemia in a mouse model of type 1 diabetes. *Endocrinology*, *156*(3), 869-881.

Song, C., Luo, L., Lei, Z., Li, B., Liang, Z., Liu, G., Li, D., Zhang, G., Huang, B., & Feng, Z.-H. (2008). IL-17-Producing Alveolar Macrophages Mediate Allergic Lung Inflammation Related to Asthma1. *The Journal of Immunology*, *181*(9), 6117-6124.

Tonelli, M., Wiebe, N., Knoll, G., Bello, A., Browne, S., Jadhav, D., Klarenbach, S., & Gill, J. (2011). Systematic Review: Kidney Transplantation Compared With Dialysis in Clinically Relevant Outcomes. *American Journal of Transplantation*, *11*(10), 2093-2109.

Tuzlak, S., Dejean, A. S., Iannacone, M., Quintana, F. J., Waisman, A., Ginhoux, F., Korn, T., & Becher, B. (2021). Repositioning TH cell polarization from single cytokines to complex help. *Nature Immunology*, *22*(10), 1210-1217.

Vokaer, B., Van Rompaey, N., Lemaître, P. H., Lhommé, F., Kubjak, C., Benghiat, F. S., Iwakura, Y., Petein, M., Field, K. A., Goldman, M., Le Moine, A., & Charbonnier, L.

M. (2010). Critical role of regulatory T cells in Th17-mediated minor antigen-disparate rejection. *J Immunol*, *185*(6), 3417-3425.

Wei, L., Laurence, A., Elias, K. M., & O'Shea, J. J. (2007). IL-21 Is Produced by Th17 Cells and Drives IL-17 Production in a STAT3-dependent Manner. *Journal of Biological Chemistry*, *282*(48), 34605-34610.

Yang, W., Yu, T., Huang, X., Bilotta, A. J., Xu, L., Lu, Y., Sun, J., Pan, F., Zhou, J., Zhang, W., Yao, S., Maynard, C. L., Singh, N., Dann, S. M., Liu, Z., & Cong, Y. (2020). Intestinal microbiota-derived short-chain fatty acids regulation of immune cell IL-22 production and gut immunity. *Nature Communications*, *11*(1), 4457.

Yuan, X., Paez-Cortez, J., Schmitt-Knosalla, I., D'Addio, F., Mfarrej, B., Donnarumma, M., Habicht, A., Clarkson, M. R., Iacomini, J., Glimcher, L. H., Sayegh, M. H., & Ansari, M. J. (2008). A novel role of CD4 Th17 cells in mediating cardiac allograft rejection and vasculopathy. *J Exp Med*, *205*(13), 3133-3144.

Zachary, A. A., & Leffell, M. S. (2014). Desensitization for solid organ and hematopoietic stem cell transplantation. *Immunol Rev*, *258*(1), 183-207.

Zhang, Q., & Reed, E. F. (2016). The importance of non-HLA antibodies in transplantation. *Nat Rev Nephrol*, *12*(8), 484-495.

Zhao, D., Liao, T., Li, S., Zhang, Y., Zheng, H., Zhou, J., Han, F., Dong, Y., & Sun, Q. (2018). Mouse Model Established by Early Renal Transplantation After Skin Allograft Sensitization Mimics Clinical Antibody-Mediated Rejection. *Front Immunol*, *9*, 1356.

Discussion

Th17 cells play a critical role in acute cellular as well as in acute and chronic antibody mediated allograft rejection. In the current study we employed an accelerated rejection transplantation animal model to evaluate home designed and developed novel RORγt inverse agonist. (Fouda et al., 2023) TF-S14 (compound **13**) was selected based on its potency in a Th17 polarization cellular assay. Tacrolimus was used as control for its ability to suppress Th1 response. The main finding of this study was the ability of TF-S14 to reverse the effect of sensitization resulting from the administration of the three IP injections of BALB/C suspension. The administration of TF-S14 daily resulted in the restoration of the non-sensitized mice allograft survival levels. Our research group previously found an increase in Th17 phenotype in highly sensitized patients. (Kandeva et al., 2010) In addition, they found that sensitized mice have higher serum DSAs concentration compared to non-sensitized mice in allogenic tail skin transplantation mouse model. (Jean & Sahakian, 2015) Moreover, they found an increase in mRNA expression of Th17 specific cytokines IL17, IL21 upon stimulation of PBMCs from highly sensitized patients with a **R848** and IL2 compared to non-sensitized patients. **R848** and IL2 combination is known to induce B-cell proliferation and immunoglobulin secretion. Furthermore, our team found that the percentages of IL17 and IL21 positive CD4 cells are higher in highly sensitized compared to non-sensitized transplantation candidates following 6-days of mixed lymphocyte reaction allogenic stimulation of CD4+ cells when the were mixed with non-sensitized candidates negative crossmatch donor APCs. (Negi et al., 2024) In our mouse model we could achieve sensitization through the IP injections of BALB/C splenocytes cell suspension. This was confirmed by comparing the total serum IgG in sensitized mice to non-sensitized mice and additionally we performed a

crossmatching and we saw the same results in flowcytometry, see appendix supporting information. There was no difference in the total IgG between RORγt inverse agonist treated or non-treated mice which indicates the successful sensitization of recipient mice. On the other hand, there was a difference in IgG3+ B cells and IgG3 serum content between non-treated and RORγt inverse agonist treated mice. This difference can be attributed to inhibition of Th17 cytokine production IL17A and IL21 that promote the class switching to IgG3 subtype. Even though all the IgG subtypes are found during AMR, both IgG1 and IgG3 are the complement binding classes and they are involved in the acute and hyperacute AMR. (Valenzuela & Schaub, 2018) While both IgG1 and IgG3 subclasses are promoted by IL21, the class switching to IgG3 rearrangements requires IL17A cytokine. (Mitsdoerffer et al., 2010; Pène et al., 2004) In our results, the reduction in IgG3+ B cells in mice treated with TF-S14 who were administered the drug daily from 2-3 weeks can be attributed to the inhibition of de novo production of IgG3 antibodies against the allograft over that time span and following the inhibition of RORγt and subsequent reduction of IL17A production. This time frame is sufficient to observe such an effect, as the de novo synthesized IgG DSAs can be detected in serum within 4 days of the onset of antigen presence in serum and this peaks at 14 days. (Hsueh et al., 2004) The increase in graft survival in TF-S14 treated mice can be attributed partially to the reduction of IgG3+ B cells and eventually the decrease in the number of the acute and hyperacute rejection injuries to the allograft resulting from complement binding. The elevated levels of IgG3 and the activation of Th17 are present in various autoimmune diseases and inflammatory conditions. Some of the diseases and conditions linked to these elevations include rheumatoid arthritis, systemic lupus erythematosus,

inflammatory bowel disease, multiple sclerosis, psoriasis, and ankylosing spondylitis. The patients suffering from these conditions can be candidates for RORγt inverse agonist treatment.   Preclinical animal studies and clinical studies have been conducted to evaluate the effect of RORγt inverse agonists in autoimmune conditions especially psoriasis, rheumatoid arthritis, multiple sclerosis, and inflammatory bowel disease. Several studies have shown that Th17 cells induce proliferation of B cells and antibody production directly through the action of IL17. (Ghali et al., 2017; Mitsdoerffer et al., 2010; Suárez-Fueyo et al., 2017) This activation of humoral immunity can trigger autoimmune diseases or acute inflammatory conditions such as glomerunephritis. (Ghali et al., 2017; Suárez-Fueyo et al., 2017) A remarkable animal study has shown that the antibody production was impaired in IL17 null mice. (Nakae et al., 2002) Other studies have shown that IL17 activates the production of IL1, IL6, IL8 cytokines from monocytes, macrophages which all promote the proliferation of activated B cells. In addition to the IL17 cytokines family which are the Th17 signature cytokines, Th17 cells produce IL21 which induce B cells expansion, isotype class switching and the maturation to plasma cells. (Mitsdoerffer et al., 2010) Moreover, Th17 regulates the glycosylation profile during maturation of plasma blasts in the germinal centers. It was found that Th17 promotes the production of autoantibodies with a lower sialic acid content in arthritis mouse models. Follicular Th17 cells were identified in clusters in spleens of arthritis mouse while were absent in IL23 null mouse. Detailed analysis showed that Th17 inhibit "beta-galactoside alpha-2,6-sialyltransferase 1" mRNA and protein expression in IL21, IL22 (two cytokines secreted by Th17), and IL-23 dependent manner. These findings may explain the role of

Th17 cells in promoting subclass of IgG antibodies that contribute to autoantibody driven disease. (Pfeifle et al., 2017)

At the graft level, the hallmark of Th17 mediated rejection was the massive neutrophilic infiltration that was decreased or completely absent in TF-S14 treated mice. In addition to the effect on cytokine production as seen in mouse splenocytes, TF-S14 decreased the RORγt protein levels in neutrophils. This reduction can be explained in the light of RORγt inhibition which leads eventually to the blockade of RORγt enhanced survival pathways such as Bcl-xL expression leading to an increase in the apoptosis of neutrophils. (Sun et al., 2000) Bcl-xL is a transmembrane antiapoptotic protein that prevent the release of cytochrome c to cytoplasm which initiates the caspase activation and cell death. These effects of RORγt inverse agonists are beneficial in controlling the inflammation in a similar fashion to disease modifying anti rheumatic drugs. RORγt inverse agonists through their unique mechanism of action can be used as immunosuppressants in alloimmune inflammation, disease modifying anti rheumatic drug in autoimmune diseases or anticancer agents for their effect on apoptosis and antiapoptotic protein expression. Azathioprine, leflunomide, methotrexate are close examples of the drugs that have shown to be effective in organ transplantation, autoimmune diseases, and cancer. The broad activity is of such drugs is attributed to their central mode of action in the nucleus which have a broader effect on cell functions leading to apoptosis. (Bacal et al., 2000; Bedoui et al., 2019; Chocair et al., 2022; Genestier et al., 2000; Leca, 2009; Ozturk et al., 2020) The advantage of RORγt inverse agonists over DMARDs is that they will likely have a better toxicity index due to their specificity. RORγt is a transcription factor that binds to RORE sites which are promoter regions located near

super enhancer sequences that determine the cell fate and function. The inhibition of RORγt binding to RORE results in the reduction of specific gene products that were otherwise increased by the activation of RORE without causing a direct damage to DNA compared to the three DMARDs which target DNA synthesis and repair. (Lytle et al., 2019; Solt et al., 2011) On the other hand, RORγt inverse agonists share some similarities with corticosteroids in terms of pharmacological target class. The main difference in this context is the mechanism of action where the corticosteroids act as agonists in their effect upon binding to glucocorticoid receptors leading to immunosuppression and anti-inflammatory effects rather than being inverse agonists. (Dashti-Khavidaki et al., 2021; Reichardt et al., 2021) Apo RORγt or RORγ are intrinsically active, and their activities are increased through the binding of endogenous cholesterol derivatives leading to immune activation and improved survival which is the contrary to the immunosuppressive effects of the agonist activated glucocorticoid receptors. This fundamental difference between the two mechanisms delineates the different determinants of the specificity and the side effects of RORγt inverse agonists compared to glucocorticoids. In basic comparison, the RORγt/RORγ inverse agonists can only exert their effects in the cells and tissues where the RORγt receptors are already active making them more specific and less toxic compared to glucocorticoids which activate rather inactive glucocorticoid receptors leading to immune suppressive and metabolic effects. (Pufall, 2015) For example, while the activation of glucocorticoid receptor implies beneficial therapeutic effects in autoimmune diseases and graft rejection, this is not essentially the case in cancer, where glucocorticoid can have both pro-tumor and anti-tumor effects depending on the cancer

type, histological subtype, and microenvironment. (Dashti-Khavidaki et al., 2021; Kalfeist et al., 2022; Reichardt et al., 2021; Zhidkova et al., 2020)

In our skin allograft mouse model, we observed a non-significant decrease in ILC3 cells in non-treated sensitized mice compared to the normal levels in non-sensitized mice. At the same time, we observed an increase in ILC3 fraction in tacrolimus only treated control group. A recent study has shown that ILC3 cells are decreased in patients undergoing intestinal transplant rejection while those that maintain high levels of ILC3 had healthy intestinal grafts and those levels are not correlated with tacrolimus treatment. (Kang et al., 2021) Another study showed that tolerant lung transplants infiltrating ILC3 are important in maintaining healthy lung lymphoid tissue. (Tanaka et al., 2020) Previous research have shown that tacrolimus/mycophenolate mofetil/corticosteroids triple therapy does not affect the helper innate lymphoid cells populations helper ILC cells namely ILC1 (Lin-CD127+CRTH2-CD117-), ILC2 (Lin-CD127+CRTH2+CD117-), ILC2 (Lin-CD127+CRTH2+CD117+) and pre ILC (Lin-CD127+CRTH-CD117+) cells in kidney and liver transplanted patients; however the same research group published contradicting results showing that ILC2 (Lin-CD45+CD117-CRTH2+) and ILC3 (Lin-CD45+CD117+ CRTH2-) cells are both increased in patients treated with triple therapy . (Gómez-Massa et al., 2020; Massa et al., 2018) They explained this increase in ILC2 and ILC3 percentages to the decrease in absolute number of ILC1, while the ILC2 and ILC3 absolute numbers remained the same. (Massa et al., 2018) In the current study we observed an increase in ILC3 cells which are defined as Lin-CD45+CD127+CD117+ in the mice treated with tacrolimus only compared to non-treated sensitized controls, this effect was reversed when tacrolimus was combined with TF-S14. In addition, in groups

treated with TF-S14 only, the ILC3 cell fraction was like that of the non-sensitized mice. The cell counts were variable between mice but not between groups and eventually the effect that we observed is not due to the changes in the absolute number of ILC1 cells. One explanation of this can be derived from a recent study which concluded that ILC3 like ILC2 cells are increased in minimal persistent inflammation. (Chen et al., 2022) A similar grade of inflammation is observed in transplantation patients treated with tacrolimus because it changes the Th1/Th2 ratio in favor of Th2. The effect of Th2 on Th17 and other IL17 producing cells have been investigated and it have been shown that IL4 is suppressive to IL17 program in early stages after differentiation, however prolonged stimulations render Th17 cells imperviable to IL4 regulation. (Cooney et al., 2011) As a result, the percentage of Th17 to CD4 will be on rise following prolonged use of tacrolimus. The same principle may apply to ILC3 and other IL17A producing cells. In the current study we could only observe this in ILC3 cells and not Th17 due to their role as first responders. In addition, Th17 cells play a role in regulating ILC3 cells as it has been shown in a recent study that Th17 cells suppress ILC3 response in the gut indirectly through the suppression of SFB which according to author occurs through the action of both IL17A and IL17F. The authors also concluded that in the absence of a dominant adaptive Th17 response, ILC3 cells become persistently activated because of increased bacterial burden in the gut. (Mao et al., 2018) In summary, an increase in Th2 response will result in decrease of Th17 activity and eventually increases ILC3 activity which can be seen in tacrolimus only treated mice. In sensitized non-treated mice, Th1/Th2 ratio is unchanged and the ILC3 cells are suppressed due to the increase in Th17 activity. In the mice treated with TF-S14, the activity of both Th17 and ILC3 are suppressed through

RORγt modulation. This pharmacologic suppression physiologically antagonizes tacrolimus activation of ILC3 cells. These results highlight the importance of ILC2 and ILC3 (Lin-CD127+CD117+) cells as biomarkers of Th17 program activation or suppression as well as Th2 program activity. The RORγt inverse agonists can have beneficial therapeutic effects in conditions where either RORγt or RORγ expression is increased. In addition to its role as a master regulator of Th17, the RORγt isoform is highly expressed in premature thymocytes such as CD4+CD8+ double positive T cells, ILC3 cells and peripheral neutrophils. (Eberl, 2017; Tan et al., 2013) On the other hand, the nuclear receptor RORγ isoform is highly expressed in variety of cancer cell types and its expression is specifically linked with the existence of distinct cancer stem cell phenotypes as well as the pathologic progression in non-cancer inflammatory conditions. RORγ expression is high in cancer types characterized by high metastatic potential such as pancreatic cancer and more specifically in cancer stem cells. (Lytle et al., 2019) It was found to be highly expressed in castration resistant prostate cancer, metastatic breast cancer, invasive melanoma, NSC lung cancer and fibrosarcoma. (Brożyna et al., 2016; Huang et al., 2016; Oh et al., 2016; Wang et al., 2016) RORγt is also highly expressed in PBMCs, and lymphocytes and lymphoid cells found in microenvironments of NSC lung cancer, hepatoma, multiple myeloma, breast cancer, melanoma, colorectal cancer and cervical cancer. (Benevides et al., 2013; Feng et al., 2015; Kathania et al., 2016; Li et al., 2014; Lin et al., 2015; Slominski et al., 2014; Zhang et al., 2015) RORγt is also highly expressed in myeloid cells in fibrosarcoma. (Strauss et al., 2015) Tumors that have high RORγ expression have metastatic potential and invasiveness. On the contrary, the RORγ deficiency leads to lymphoma and metastasis in RORγ knockout mice. (Ueda et al., 2002)

In such conditions, the modulation of RORγ receptor can confer a therapeutic effect either solely or as an adjuvant by promoting apoptosis of the cells that highly express RORγ. This has been proven experimentally in "in vivo" cancer animal models such as in the case of castration resistant prostate cancer and pancreatic cancer. (Lytle et al., 2019; Wang et al., 2016) In addition to promoting apoptosis in pancreatic cancer adenocarcinoma cancer model it is believed that RORγ/RORγt inverse agonist can change the cancer stem cell phenotype to non-stem cancer cell. (Lytle et al., 2019) Other suggested mechanisms are the modulation of proteins regulated by RORγ such as IL17, PRMT2, and AR or through the competition with RORγ agonists (cholesterol derivatives), such as in the case of vitamin D3 derivatives. (Fan et al., 2018) In non-cancer inflammatory conditions, it has been shown that RORγ expression is high in hepatitis, cirrhotic liver and found to mediate epithelial to mesenchymal transition in fibrosis. (Kim et al., 2017) In a recent review, it was suggested that RORγ/RORγt inverse agonists can improve the prognosis of nonalcoholic fatty liver disease and nonalcoholic steatohepatitis based on their ability to suppress NLRP3 inflammasome. (Billon et al., 2019; Welch et al., 2022) It was also suggested that RORγ/RORγt inverse agonists can reduce Th17 driven hepatitis through their direct inhibitory effect on Th17 differentiation. (Welch et al., 2022)

As previously mentioned, TF-S14 was selected to be tested in-vivo based on its high potency in a Th17 polarization cellular assay. In the RORγ (LBD) TR-FRET assay the potency determined by IC50 was less than 1nM. The high potency of TF-S14 explains the similarity in the therapeutic outcome between 1, 10, or 100 mg/kg doses of the compound, when they were used in the mouse model of skin allograft. In this context there was only a slight difference between 1-10 and 10-100 dose ranges and no

difference between 10 and 100 mg/kg. We didn't observe any adverse effects of TF-S14 at the doses of 1 and 10 mg/kg. On the other hand, apart from a transient weight loss we didn't observe considerable side effects at 100 mg/kg. In addition to IP route, we also tested SC injections and there was no site of injection adverse effects. Despite of their lipophilicity, a good toxicity profile of the 4,5,6,7 tetrahydro-benzothiophene derivatives have been sought in the initial design by avoiding some functional groups that further increase lipophilicity and accumulation in liver such as the trifluoromethyl group. (Yale, 1959) In addition, the linkers between the cyclic components of the compounds were based on amide bondage which is readily cleaved by the cytosol of hepatocytes that requires less energy. (Gao et al., 2006) On the other hand, we extensively tested different analogues to improve the potency that we predetermined in silico. As a result, the lipophilic efficiency of 4,5,6,7 tetrahydro-benzothiophene derivatives RORγt inverse agonists were superior to many of the newly discovered RORγt inverse agonists. Such favorable physicochemical properties are crucial for further development as they provide good candidates for pharmaceutical formulation with superior bioavailability, specificity, and reduced toxicity. In our initial in vitro screens, we evaluated the effects of two other compounds TF-S1 (compound **1**) and TF-S2 (compound **2**) for their effects on other cytokines and transcription factors such as Treg transcription factor FOXP3 and Th1 specific cytokine IFNγ. The proper comparisons have been done against control drugs such as sirolimus that reduces Treg phenotype or tacrolimus, dexamethasone and cyclosporine that reduce the Th1 specific cytokine IFNγ. In those in vitro assays we observed high specificity towards RORγt regulated Th17 cytokines IL17, IL21 and IL22. On the other hand, even though some compounds had high clearance as observed in

microsomal stability assays, the efficacy of TF-S14 in the mouse model was established with one daily dosing at as low as 1 mg/kg. The explanation for this is that the selected 4,5,6,7 tetra-hydrobenzothiophene derivatives have shown high binding affinity to the RORγt as predicted in silico which allows for RORγt receptor modulation at low blood level threshold that lies below the levels required to engage liver enzymes and follow non-linear pharmacokinetics which can be concluded as having a wide therapeutic index. (Esteves et al., 2021) Further studies are required to determine toxic levels such as the maximum tolerated dose and no-observed-adverse-effect level; however considering the moderate to high clearance of the compounds, the metabolic pathways involved and the structure of the possible metabolites, the maximum tolerated dose in human can be more than the current regulatory established FDA and European limits of 1000 mg/kg/day which makes the compounds safe for human and animal administration. (Sewell et al., 2022; Chiba et al., 2009) In addition, further studies are required to evaluate the effectiveness of the drugs in non-sensitized animal models of transplantation and to study their effects in sensitized mice following induction immunosuppression with anti-CD20 or anti-CD52.

The first aim of the current study was to discover efficient RORγt small molecule modulators that can be developed for clinical use in transplantation and other potential applications. The second aim was to evaluate the pharmacological effects on these RORγt modulators in transplantation and more specifically on highly sensitized transplantation candidates and sensitized murine model of transplantation. The first aim was achieved through drug design discovery approaches which led us to discover 4,5,6,7 tetrahydro-benzothiophene derivatives as potent modulators of RORγt/RORγ receptors. (Fouda et al., 2020; Fouda et al., 2023) This group has shown diversity in

physicochemical properties with slight differences in their RORγt binding orientation and the subsequent effects on the protein dynamics and conformation. Such subtle differences broaden the range of usefulness of the compounds as each compound can produce a slightly different effects at the molecular level where for example one compound can cause complete inhibition of RORγt binding to DNA leaving the DNA RORE region unoccupied, while another can weaken the binding affinity causing intermittent binding of the RORγt receptor to the RORE binding site. These differences at the molecular level are collectively translated to relative potency of each compound in relation to a specific biomarker. Putting in mind that RORγt is an upstream regulator of many genes, this eventually means that compounds can have diverse effects on many gene products under the regulation of RORγt. For example, in the context of Th17 RORγt regulated genes, one compound can be a potent inhibitor of IL17A while having a slight or no effect on IL21 or IL22 production, while another compound would inhibit IL22 and IL21 with the same potency that it inhibits IL17A. Such diversity can allow for the use of this class of compounds in a variety of conditions that can have important differences in their molecular predispositions. For the second aim of the study, we have demonstrated that TF-S14 is effective in increasing graft survival in sensitized murine model of skin allograft. The TF-S14 was selected based on its suppressive effect on all Th17 cytokines IL17A, IL21 and IL22 which all have negative impact on graft survival by promoting inflammatory responses leading to cellular or antibody mediated rejection. We concluded that the novel 2,3 derivatives of 4,5,6,7 tetrahydro-benzothiophene RORγt inverse agonists offer a new therapeutic mechanism to treat rejection in highly sensitized patients regardless of degree of donor mismatch.

Summary & conclusions

Sensitization constitutes an insurmountable challenge in the field of solid organ transplantation. The current strategies to overcome the problem are through performing HLA compatible transplantations, plasmapheresis, administration of IVIG, rituximab, bortezomib or a combination of more than one of these interventions. Anti-IL6 and Anti-IL6R antibodies have shown great potential in small clinical trials in reducing DSAs and improving clinical outcomes in patients undergoing chronic AMR. An animal study showed beneficial effects of neutralizing IL17 in reversal of corneal rejection in full mismatch transplantation. Another animal study showed that IL17 neutralization prolonged graft survival in Tbet-/- recipient mouse that received MHC II mismatched heart graft and improved the signs of vasculopathy. In the current study we demonstrated that RORγt inverse agonists can prolong the graft survival in sensitized recipient mice who were transplanted with a complete mismatch skin graft. The RORγt inverse agonist that was used in the study was designed and developed to be used in the study. The hypothesis we developed early in the study was that RORγt inhibitors can prevent or treat AMR through the inhibition of IL17A, IL21 and IL22 cytokine production and subsequent inhibition of tertiary lymphoid tissue formation, B-cell differentiation and antibody class switching. Our objectives were to design and develop a novel RORγt inverse agonist with favorable pharmacological and toxicological properties. To address this objective, we designed a novel class of RORγt inverse agonists based on 4,5,6,7 tetrahydro-benzothiophene scaffold using silico methods. The novel class was evaluated in cell free and showed high potency in disrupting the RORγt conformation. The second objective of the study was to evaluate their effect on Th17 signature cytokines. The compounds showed high potency in decreasing the IL17A, IL21 and IL22 in cell-based assay by 20-

40%. The third objective of the study was to evaluate the effects of RORγt in vivo on a sensitized mouse model of transplantation. To address this objective, we elected compound 13 which was later named TF-S14 based on its superior potency in vitro. We have demonstrated that RORγt inverse agonist TF-S14 administered daily to sensitized mice who were transplanted with complete mismatch skin graft, was able to prolong graft survival at small dose 1 mg/kg/day. In addition, we tested higher doses 10 and 100 mg/kg/day of the drug in the same model, and we observed a marginal improvement in graft survival at 10 mg/kg/day and no further improvement was seen at 100 mg/kg/day dose. At the same time, we did not observe toxic adverse effects resulting from the drug administration until the experimental endpoint was reached. In conclusion, we have discovered developed a high potency RORγt inverse agonists with favorable adverse effects profile that was proven in vitro and in vivo. The novel class have few advantages over previously identified RORγt inverse agonists as they have high potency and moderate to high clearance which reduce their accumulation in the liver and lymphatic tissue and eventually will have fewer toxic effects on these two compartments. In vitro RORγt inhibitory effects of 4,5,6,7 tetrhydro-benzothiophene were proven in cellular assays where they inhibited the downstream products of RORγt such as IL17A, IL21, IL22. In vivo immune modulatory effects of 4,5,6,7 tetrhydro-benzothiophene were proven in a sensitized mouse model of skin transplantation, where TF-S14 a potent member of this class of RORγt inverse agonists efficiently prolonged graft survival, reduced neutrophilic infiltration into skin grafts, inhibited B -cell differentiation and antibody class switching to IgG3 class. The novel class has high specificity in vitro with regards to targets of immune system as they did not affect percentage of IFNγ+ T cells or Tregs.

References

for introduction, literature review & discussion

Ajlan, A., Aleid, H., Ali, T. Z., Joharji, H., Almeshari, K., Nazmi, A. M., Shah, Y., Devol, E., Alkortas, D., Alabdulkarim, Z., Broering, D., Alahmadi, I., Ullah, A., Alotaibi, A., & Aljedai, A. (2021). Standard induction with basiliximab versus no induction in low immunological risk kidney transplant recipients: study protocol for a randomized controlled trial. *Trials*, *22*(1), 414.

Alloway, R. R., Woodle, E. S., Abramowicz, D., Segev, D. L., Castan, R., Ilsley, J. N., Jeschke, K., Somerville, K. T., & Brennan, D. C. (2019). Rabbit anti-thymocyte globulin for the prevention of acute rejection in kidney transplantation. *Am J Transplant*, *19*(8), 2252-2261.

Anstey, A. V., Wakelin, S., & Reynolds, N. J. (2004). Guidelines for prescribing azathioprine in dermatology. *Br J Dermatol*, *151*(6), 1123-1132.

Arth, G. E., Johnston, D. B. R., Fried, J., Spooncer, W. W., Hoff, D. R., & Sarett, L. H. (1958). 16-METHYLATED STEROIDS. I. 16α-METHYLATED ANALOGS OF CORTISONE, A NEW GROUP OF ANTI-INFLAMMATORY STEROIDS. *Journal of the American Chemical Society*, *80*(12), 3160-3161.

Azzi, J. R., Sayegh, M. H., & Mallat, S. G. (2013). Calcineurin Inhibitors: 40 Years Later, Can't Live Without …. *The Journal of Immunology*, *191*(12), 5785-5791.

Bacal, F., Veiga, V. C., Fiorelli, A. I., Bellotti, G., Bocchi, E. A., Stolf, N. A., & Ramires, J. A. (2000). Treatment of persistent rejection with methotrexate in stable patients submitted to heart transplantation. *Arquivos brasileiros de cardiologia*, *74*(2), 141-148.

Bedoui, Y., Guillot, X., Sélambarom, J., Guiraud, P., Giry, C., Jaffar-Bandjee, M. C., Ralandison, S., & Gasque, P. (2019). Methotrexate an Old Drug with New Tricks. *Int J Mol Sci*, *20*(20), 5023.

Benevides, L., Cardoso, C. R., Tiezzi, D. G., Marana, H. R., Andrade, J. M., & Silva, J. S. (2013). Enrichment of regulatory T cells in invasive breast tumor correlates with the upregulation of IL-17A expression and invasiveness of the tumor. *Eur J Immunol*, *43*(6), 1518-1528.

Benoit, G., Malewicz, M., & Perlmann, T. (2004). Digging deep into the pockets of orphan nuclear receptors: insights from structural studies. *Trends Cell Biol*, *14*(7), 369-376.

Bentata, Y. (2020). Tacrolimus: 20 years of use in adult kidney transplantation. What we should know about its nephrotoxicity. *Artif Organs*, *44*(2), 140-152.

Billon, C., Murray, M. H., Avdagic, A., & Burris, T. P. (2019). RORγ regulates the NLRP3 inflammasome. *J Biol Chem*, *294*(1), 10-19.

Bisson, W. H., Koch, D. C., O'Donnell, E. F., Khalil, S. M., Kerkvliet, N. I., Tanguay, R. L., Abagyan, R., & Kolluri, S. K. (2009). Modeling of the aryl hydrocarbon receptor (AhR) ligand binding domain and its utility in virtual ligand screening to predict new AhR ligands. *J Med Chem*, *52*(18), 5635-5641.

Borngraeber, S., Budny, M. J., Chiellini, G., Cunha-Lima, S. T., Togashi, M., Webb, P., Baxter, J. D., Scanlan, T. S., & Fletterick, R. J. (2003). Ligand selectivity by seeking hydrophobicity in thyroid hormone receptor. *Proc Natl Acad Sci U S A*, *100*(26), 15358-15363.

Brennan, D. C., Flavin, K., Lowell, J. A., Howard, T. K., Shenoy, S., Burgess, S., Dolan, S., Kano, J. M., Mahon, M., Schnitzler, M. A., Woodward, R., Irish, W., & Singer, G. G. (1999). A randomized, double-blinded comparison of Thymoglobulin versus Atgam for induction immunosuppressive therapy in adult renal transplant recipients. *Transplantation*, *67*(7), 1011-1018.

Bronner, S. M., Zbieg, J. R., & Crawford, J. J. (2017). RORγ antagonists and inverse agonists: a patent review. *Expert Opin Ther Pat*, *27*(1), 101-112.

Brożyna, A. A., Jóźwicki, W., Skobowiat, C., Jetten, A., & Slominski, A. T. (2016). RORα and RORγ expression inversely correlates with human melanoma progression. *Oncotarget*, *7*(39), 63261-63282.

Cardinal, H., Dieudé, M., & Hébert, M. J. (2017). The Emerging Importance of Non-HLA Autoantibodies in Kidney Transplant Complications. *J Am Soc Nephrol*, *28*(2), 400-406.

Chen, J., Liu, C., Liu, B., Kong, D., Wen, L., & Gong, W. (2018). Donor IL-6 deficiency evidently reduces memory T cell responses in sensitized transplant recipients. *Transpl Immunol*, *51*, 66-72.

Chen, X.-J., Liu, C., Zhang, S., Zhang, L.-F., Meng, W., Zhang, X., Sun, M., Zhang, Y., Wang, R.-Z., & Yao, C.-F. (2022). ILC3-like ILC2 subset increases in minimal persistent inflammation after acute type II inflammation of allergic rhinitis and inhibited by Biminkang: Plasticity of ILC2 in minimal persistent inflammation. *Journal of Leukocyte Biology*, *112*(6), 1445-1455.

Chiba, M., Ishii, Y., & Sugiyama, Y. (2009). Prediction of hepatic clearance in human from in vitro data for successful drug development. *Aaps j*, *11*(2), 262-276.

Chinnadurai, R., Ibrahim, S. T., Tay, T., Bhutani, S., & Kalra, P. A. (2021). Body weight-based initial dosing of tacrolimus in renal transplantation: Is this an ideal approach? *J Ren Care*, *47*(1), 51-57.

Chocair, P. R., Neves, P., Mohrbacher, S., Neto, M. P., Sato, V. A. H., Oliveira É, S., Barbosa, L. V., Bales, A. M., da Silva, F. P., Cuvello-Neto, A. L., & Duley, J. A. (2022). Case Report: Azathioprine: An Old and Wronged Immunosuppressant. *Front Immunol*, *13*, 903012.

Choi, J., Aubert, O., Vo, A., Loupy, A., Haas, M., Puliyanda, D., Kim, I., Louie, S., Kang, A., Peng, A., Kahwaji, J., Reinsmoen, N., Toyoda, M., & Jordan, S. C. (2017). Assessment of Tocilizumab (Anti-Interleukin-6 Receptor Monoclonal) as a Potential Treatment for Chronic Antibody-Mediated Rejection and Transplant Glomerulopathy in HLA-Sensitized Renal Allograft Recipients. *Am J Transplant*, *17*(9), 2381-2389.

Chua, J. C. M., Mount, P. F., & Lee, D. (2022). Lower versus higher starting tacrolimus dosing in kidney transplant recipients. *Clin Transplant*, *36*(6), e14606.

Chukwu, C. A., Spiers, H. V. M., Middleton, R., Kalra, P. A., Asderakis, A., Rao, A., & Augustine, T. (2022). Alemtuzumab in renal transplantation. Reviews of literature and usage in the United Kingdom. *Transplant Rev (Orlando)*, *36*(2), 100686.

Chung, B. H., Kim, K. W., Kim, B.-M., Doh, K. C., Cho, M.-L., & Yang, C. W. (2016). Increase of Th17 Cell Phenotype in Kidney Transplant Recipients with Chronic Allograft Dysfunction. *PLoS One*, *10*(12), e0145258.

Clatworthy, M. R. (2011). Targeting B cells and antibody in transplantation. *Am J Transplant*, *11*(7), 1359-1367.

Clayton, P. A., McDonald, S. P., Chapman, J. R., & Chadban, S. J. (2012). Mycophenolate Versus Azathioprine for Kidney Transplantation: A 15-Year Follow-Up of a Randomized Trial. *Transplantation*, *94*(2), 152-158.

Cooney, L. A., Towery, K., Endres, J., & Fox, D. A. (2011). Sensitivity and resistance to regulation by IL-4 during Th17 maturation. *J Immunol*, *187*(9), 4440-4450.

Cornell, L. D., Schinstock, C. A., Gandhi, M. J., Kremers, W. K., & Stegall, M. D. (2015). Positive crossmatch kidney transplant recipients treated with eculizumab: outcomes beyond 1 year. *Am J Transplant*, *15*(5), 1293-1302.

Cyr, P., Bronner, S. M., & Crawford, J. J. (2016). Recent progress on nuclear receptor RORγ modulators. *Bioorg Med Chem Lett*, *26*(18), 4387-4393.

Dalal, P., Grafals, M., Chhabra, D., & Gallon, L. (2009). Mycophenolate mofetil: safety and efficacy in the prophylaxis of acute kidney transplantation rejection. *Ther Clin Risk Manag*, *5*(1), 139-149.

Dashti-Khavidaki, S., Saidi, R., & Lu, H. (2021). Current status of glucocorticoid usage in solid organ transplantation. *World J Transplant*, *11*(11), 443-465.

Dave, V., Polkinghorne, K. R., Leong, K. G., Kanellis, J., & Mulley, W. R. (2020). Initial mycophenolate dose in tacrolimus treated renal transplant recipients, a cohort study comparing leukopaenia, rejection and long-term graft function. *Sci Rep*, *10*(1), 19379.

De Sainte Marie, B., Urban, M. L., Vély, F., Seguier, J., Grados, A., Daniel, L., Ebbo, M., & Schleinitz, N. (2020). Pathophysiology of IgG4-related disease: A T follicular helper cells disease? *Presse Med*, *49*(1), 104013.

de Wit, J., Al-Mossawi, M. H., Hühn, M. H., Arancibia-Cárcamo, C. V., Doig, K., Kendrick, B., Gundle, R., Taylor, P., McClanahan, T., Murphy, E., Zhang, H., Barr, K., Miller, J. R., Hu, X., Aicher, T. D., Morgan, R. W., Glick, G. D., Zaller, D., Correll, C., . . . Bowness, P. (2016). RORγt inhibitors suppress T(H)17 responses in inflammatory arthritis and inflammatory bowel disease. *J Allergy Clin Immunol*, *137*(3), 960-963.

Deteix, C., Attuil-Audenis, V., Duthey, A., Patey, N., McGregor, B., Dubois, V., Caligiuri, G., Graff-Dubois, S., Morelon, E., & Thaunat, O. (2010). Intragraft Th17 infiltrate promotes lymphoid neogenesis and hastens clinical chronic rejection. *J Immunol*, *184*(9), 5344-5351.

Diao, Y., Jiang, J., Zhang, S., Li, S., Shan, L., Huang, J., Zhang, W., & Li, H. (2018). Discovery of Natural Products as Novel and Potent FXR Antagonists by Virtual Screening. *Front Chem*, *6*, 140.

Ding, Q., Zhao, M., Yu, B., Bai, C., & Huang, Z. (2015). Identification of Tetraazacyclic Compounds as Novel Potent Inhibitors Antagonizing RORγt Activity and Suppressing Th17 Cell Differentiation. *PLoS One*, *10*(9), e0137711.

Djamali, A., Kaufman, D. B., Ellis, T. M., Zhong, W., Matas, A., & Samaniego, M. (2014). Diagnosis and management of antibody-mediated rejection: current status and novel approaches. *Am J Transplant*, *14*(2), 255-271.

Doberer, K., Duerr, M., Halloran, P. F., Eskandary, F., Budde, K., Regele, H., Reeve, J., Borski, A., Kozakowski, N., Reindl-Schwaighofer, R., Waiser, J., Lachmann, N., Schranz, S., Firbas, C., Mühlbacher, J., Gelbenegger, G., Perkmann, T., Wahrmann, M., Kainz, A., . . . Böhmig, G. A. (2021). A Randomized Clinical Trial

of Anti-IL-6 Antibody Clazakizumab in Late Antibody-Mediated Kidney Transplant Rejection. *J Am Soc Nephrol*, *32*(3), 708-722.

Dussault, I., Fawcett, D., Matthyssen, A., Bader, J. A., & Giguère, V. (1998). Orphan nuclear receptor ROR alpha-deficient mice display the cerebellar defects of staggerer. *Mech Dev*, *70*(1-2), 147-153.

Eberl, G. (2017). RORγt, a multitask nuclear receptor at mucosal surfaces. *Mucosal Immunology*, *10*(1), 27-34.

Engelen, W., Verpooten, G. A., Van der Planken, M., Helbert, M. F., Bosmans, J. L., & De Broe, M. E. (2003). Four cases of red blood cell aplasia in association with the use of mycophenolate mofetil in renal transplant patients. *Clin Nephrol*, *60*(2), 119-124.

Eskandary, F., Dürr, M., Budde, K., Doberer, K., Reindl-Schwaighofer, R., Waiser, J., Wahrmann, M., Regele, H., Spittler, A., Lachmann, N., Firbas, C., Mühlbacher, J., Bond, G., Halloran, P. F., Chong, E., Jilma, B., & Böhmig, G. A. (2019). Clazakizumab in late antibody-mediated rejection: study protocol of a randomized controlled pilot trial. *Trials*, *20*(1), 37.

Esteves, F., Rueff, J., & Kranendonk, M. (2021). The Central Role of Cytochrome P450 in Xenobiotic Metabolism-A Brief Review on a Fascinating Enzyme Family. *J Xenobiot*, *11*(3), 94-114.

Fabio, Huang, P., Serge, Eugene, David, Brad, Keber, R., Lorbek, G., Konijn, T., Brittany, Rozman, D., Horvat, S., Rahier, A., Reina, Rastinejad, F., W, & Dan. (2015). Identification of Natural RORγ Ligands that Regulate the Development of Lymphoid Cells. *Cell Metabolism*, *21*(2), 286-298.

Fan, J., Lv, Z., Yang, G., Liao, T. T., Xu, J., Wu, F., Huang, Q., Guo, M., Hu, G., Zhou, M., Duan, L., Liu, S., & Jin, Y. (2018). Retinoic Acid Receptor-Related Orphan Receptors: Critical Roles in Tumorigenesis. *Front Immunol*, *9*, 1187.

Fang, C., Zhang, X., Miwa, T., & Song, W. C. (2009). Complement promotes the development of inflammatory T-helper 17 cells through synergistic interaction with Toll-like receptor signaling and interleukin-6 production. *Blood*, *114*(5), 1005-1015.

Feng, P., Yan, R., Dai, X., Xie, X., Wen, H., & Yang, S. (2015). The alteration and clinical significance of Th1/Th2/Th17/Treg cells in patients with multiple myeloma. *Inflammation*, *38*(2), 705-709.

Firacative, C., Gressler, A. E., Schubert, K., Schulze, B., Müller, U., Brombacher, F., von Bergen, M., & Alber, G. (2018). Identification of T helper (Th)1- and Th2-associated antigens of Cryptococcus neoformans in a murine model of pulmonary infection. *Sci Rep*, *8*(1), 2681.

Fouda, A., Negi, S., Paraskevas, S., & Tchervenkov, J. I. (2020). *Preparation of 4,5,6,7-tetrahydro-1-benzothiophene as modulators of retinoic acid receptor related (RAR) orphan nuclear receptors (RORs)* WO2020102889A1).

Fouda, A., Negi, S., Zaremba, O., Gaidar, R. S., Moroz, Y. S., Rusanov, E., Paraskevas, S., & Tchervenkov, J. (2023). Discovery, Synthesis, and In Vitro Characterization of 2,3 Derivatives of 4,5,6,7-Tetrahydro-Benzothiophene as Potent Modulators of Retinoic Acid Receptor-Related Orphan Receptor γt. *Journal of Medicinal Chemistry*, *66*(11), 7355-7373.

Gaber, A. O., First, M. R., Tesi, R. J., Gaston, R. S., Mendez, R., Mulloy, L. L., Light, J. A., Gaber, L. W., Squiers, E., Taylor, R. J., Neylan, J. F., Steiner, R. W., Knechtle,

S., Norman, D. J., Shihab, F., Basadonna, G., Brennan, D. C., Hodge, E. E., Kahan, B. D., . . . et al. (1998). Results of the double-blind, randomized, multicenter, phase III clinical trial of Thymoglobulin versus Atgam in the treatment of acute graft rejection episodes after renal transplantation. *Transplantation*, *66*(1), 29-37.

Gaber, A. O., Monaco, A. P., Russell, J. A., Lebranchu, Y., & Mohty, M. (2010). Rabbit Antithymocyte Globulin (Thymoglobulin®). *Drugs*, *70*(6), 691-732.

Gao, W., Wu, Z., Bohl, C. E., Yang, J., Miller, D. D., & Dalton, J. T. (2006). Characterization of the in vitro metabolism of selective androgen receptor modulator using human, rat, and dog liver enzyme preparations. *Drug Metab Dispos*, *34*(2), 243-253.

Garcia, G. G., Harden, P., & Chapman, J. (2012). The Global role of kidney transplantation. *J Nephropathol*, *1*(2), 69-76.

Gebel, H. M., Kasiske, B. L., Gustafson, S. K., Pyke, J., Shteyn, E., Israni, A. K., Bray, R. A., Snyder, J. J., Friedewald, J. J., & Segev, D. L. (2016). Allocating Deceased Donor Kidneys to Candidates with High Panel-Reactive Antibodies. *Clin J Am Soc Nephrol*, *11*(3), 505-511.

Gege, C. (2015). Retinoid-related orphan receptor γ t modulators: comparison of Glenmark's me-too patent application (WO2015008234) with the originator application from Merck Sharp and Dohme (WO2012106995). *Expert Opin Ther Pat*, *25*(10), 1215-1221.

Gege, C. (2017). RORγt inhibitors as potential back-ups for the phase II candidate VTP-43742 from Vitae Pharmaceuticals: patent evaluation of WO2016061160 and US20160122345. *Expert Opin Ther Pat*, *27*(1), 1-8.

Genestier, L., Paillot, R., Quemeneur, L., Izeradjene, K., & Revillard, J. P. (2000). Mechanisms of action of methotrexate. *Immunopharmacology*, *47*(2-3), 247-257.

Ghali, J. R., O'Sullivan, K. M., Eggenhuizen, P. J., Holdsworth, S. R., & Kitching, A. R. (2017). Interleukin-17RA Promotes Humoral Responses and Glomerular Injury in Experimental Rapidly Progressive Glomerulonephritis. *Nephron*, *135*(3), 207-223.

Ghasemi, G., Shahidi, S., Farajzadegan, Z., Shahidi, S., & Mohammadi, M. (2020). Sirolimus Dose Requirement in Kidney Transplant Recipients in Iran. Iran J Kidney Dis, 14(6), 510-516.

Gill, J. S., & Tonelli, M. (2012). Penny wise, pound foolish? Coverage limits on immunosuppression after kidney transplantation. *N Engl J Med*, *366*(7), 586-589.

Gómez-Massa, E., Talayero, P., Utrero-Rico, A., Laguna-Goya, R., Andrés, A., Mancebo, E., Leivas, A., Polanco-Fernández, N., Justo, I., Jimenez-Romero, C., Pleguezuelo, D., & Paz-Artal, E. (2020). Number and function of circulatory helper innate lymphoid cells are unaffected by immunosuppressive drugs used in solid organ recipients – a single centre cohort study. *Transplant International*, *33*(4), 402-413.

Grafals, M., Smith, B., Murakami, N., Trabucco, A., Hamill, K., Marangos, E., Gilligan, H., Pomfret, E. A., Pomposelli, J. J., Simpson, M. A., Azzi, J., Najafian, N., & Riella, L. V. (2014). Immunophenotyping and efficacy of low dose ATG in non-sensitized

kidney recipients undergoing early steroid withdrawal: a randomized pilot study. *PLoS One*, *9*(8), e104408.

Guarnera, C., Bramanti, P., & Mazzon, E. (2017). Alemtuzumab: a review of efficacy and risks in the treatment of relapsing remitting multiple sclerosis. *Ther Clin Risk Manag*, *13*, 871-879.

Guendisch, U., Weiss, J., Ecoeur, F., Riker, J. C., Kaupmann, K., Kallen, J., Hintermann, S., Orain, D., Dawson, J., Billich, A., & Guntermann, C. (2017). Pharmacological inhibition of RORgammat suppresses the Th17 pathway and alleviates arthritis in vivo. *PLoS One*, *12*(11), e0188391.

Guntermann, C., Piaia, A., Hamel, M.-L., Theil, D., Rubic-Schneider, T., del Rio-Espinola, A., Dong, L., Billich, A., Kaupmann, K., Dawson, J., Hoegenauer, K., Orain, D., Hintermann, S., Stringer, R., Patel, D. D., Doelemeyer, A., Deurinck, M., & Schümann, J. (2017). Retinoic-acid-orphan-receptor-C inhibition suppresses Th17 cells and induces thymic aberrations. *JCI Insight*, *2*(5), e91127.

Guthoff, M., Berger, K., Althaus, K., Mühlbacher, T., Bakchoul, T., Steurer, W., Nadalin, S., Königsrainer, A., & Heyne, N. (2020). Low-dose alemtuzumab induction in a tailored immunosuppression protocol for sensitized kidney transplant recipients. *BMC Nephrology*, *21*(1), 178.

Haas, M. (2013). Pathology of C4d-negative antibody-mediated rejection in renal allografts. *Curr Opin Organ Transplant*, *18*(3), 319-326.

Hanaway, M. J., Woodle, E. S., Mulgaonkar, S., Peddi, V. R., Kaufman, D. B., First, M. R., Croy, R., & Holman, J. (2011). Alemtuzumab Induction in Renal Transplantation. *New England Journal of Medicine*, *364*(20), 1909-1919.

Hardinger, K. L., Rhee, S., Buchanan, P., Koch, M., Miller, B., Enkvetchakul, D., Schuessler, R., Schnitzler, M. A., & Brennan, D. C. (2008). A Prospective, Randomized, Double-Blinded Comparison of Thymoglobulin Versus Atgam for Induction Immunosuppressive Therapy: 10-Year Results. *Transplantation*, *86*(7), 947-952.

Hardinger, K. L., Schnitzler, M. A., Miller, B., Lowell, J. A., Shenoy, S., Koch, M. J., Enkvetchakul, D., Ceriotti, C., & Brennan, D. C. (2004). Five-year follow up of thymoglobulin versus ATGAM induction in adult renal transplantation. *Transplantation*, *78*(1), 136-141.

Heifets, M., Saeed, M. I., Parikh, M. H., Sierka, D., & Kumar, M. S. A. (2004). Induction Immunosuppression in Kidney Transplant Recipients Older than 60 Years of Age. *Drugs & Aging*, *21*(11), 747-756.

Hintermann, S., Guntermann, C., Mattes, H., Carcache, D. A., Wagner, J., Vulpetti, A., Billich, A., Dawson, J., Kaupmann, K., Kallen, J., Stringer, R., & Orain, D. (2016). Synthesis and Biological Evaluation of New Triazolo- and Imidazolopyridine RORγt Inverse Agonists. *ChemMedChem*, *11*(24), 2640-2648.

Holmøy, T., Fevang, B., Olsen, D. B., Spigset, O., & Bø, L. (2019). Adverse events with fatal outcome associated with alemtuzumab treatment in multiple sclerosis. *BMC Research Notes*, *12*(1), 497.

Hsueh, P. R., Huang, L. M., Chen, P. J., Kao, C. L., & Yang, P. C. (2004). Chronological evolution of IgM, IgA, IgG and neutralisation antibodies after infection with SARS-associated coronavirus. *Clin Microbiol Infect*, *10*(12), 1062-1066.

Huang, Q., Fan, J., Qian, X., Lv, Z., Zhang, X., Han, J., Wu, F., Chen, C., Du, J., Guo, M., Hu, G., & Jin, Y. (2016). Retinoic acid-related orphan receptor C isoform 2 expression and its prognostic significance for non-small cell lung cancer. *J Cancer Res Clin Oncol*, *142*(1), 263-272.

Huh, J. R., Englund, E. E., Wang, H., Huang, R., Huang, P., Rastinejad, F., Inglese, J., Austin, C. P., Johnson, R. L., Huang, W., & Littman, D. R. (2013). Identification of Potent and Selective Diphenylpropanamide RORγ Inhibitors. *ACS Med. Chem. Lett.*, *4*(1), 79-84.

Huh, J. R., Leung, M. W., Huang, P., Ryan, D. A., Krout, M. R., Malapaka, R. R., Chow, J., Manel, N., Ciofani, M., Kim, S. V., Cuesta, A., Santori, F. R., Lafaille, J. J., Xu, H. E., Gin, D. Y., Rastinejad, F., & Littman, D. R. (2011). Digoxin and its derivatives suppress TH17 cell differentiation by antagonizing RORγt activity. *Nature*, *472*(7344), 486-490.

Huh, J. R., & Littman, D. R. (2012). Small molecule inhibitors of RORγt: targeting Th17 cells and other applications. *Eur J Immunol*, *42*(9), 2232-2237.

Hünemörder, S., Treder, J., Ahrens, S., Schumacher, V., Paust, H. J., Menter, T., Matthys, P., Kamradt, T., Meyer-Schwesinger, C., Panzer, U., Hopfer, H., & Mittrücker, H. W. (2015). TH1 and TH17 cells promote crescent formation in experimental autoimmune glomerulonephritis. *J Pathol*, *237*(1), 62-71.

Hwang, Y. H., Kim, H., Min, K., & Yang, J. (2021). Tacrolimus trough levels in kidney transplant recipients. *BMC Nephrology*, *22*(1), 405.

Hychko, G., Mirhosseini, A., Parhizgar, A., & Ghahramani, N. (2011). A Systematic Review and Meta-Analysis of Rituximab in Antibody-mediated Renal Allograft Rejection. *Int J Organ Transplant Med*, *2*(2), 51-56.

Ide, K., Tanaka, Y., Sasaki, Y., Tahara, H., Ohira, M., Ishiyama, K., Tashiro, H., & Ohdan, H. (2015). A Phased Desensitization Protocol With Rituximab and Bortezomib for Highly Sensitized Kidney Transplant Candidates. *Transplant Direct*, *1*(5), e17.

Ingraham, H. A., & Redinbo, M. R. (2005). Orphan nuclear receptors adopted by crystallography. *Curr Opin Struct Biol*, *15*(6), 708-715.

Ivanov, II, Zhou, L., & Littman, D. R. (2007). Transcriptional regulation of Th17 cell differentiation. *Semin Immunol*, *19*(6), 409-417.

Jean, I. T., & Sahakian, S. (2015). *The alloimmune response of T-cells in a single MHC-mismatch murine model of allosensitization* McGill University]. https://escholarship.mcgill.ca/concern/theses/ms35tc26r

Jeong, J. C., Jambaldorj, E., Kwon, H. Y., Kim, M. G., Im, H. J., Jeon, H. J., In, J. W., Han, M., Koo, T. Y., Chung, J., Song, E. Y., Ahn, C., & Yang, J. (2016). Desensitization Using Bortezomib and High-dose Immunoglobulin Increases Rate of Deceased Donor Kidney Transplantation. *Medicine (Baltimore)*, *95*(5), e2635.

Jha, P. K., Rana, A., Kher, A., Bansal, S. B., Sethi, S., Nandwani, A., Jain, M., Bansal, D., Yadav, D. K., Gadde, A., Mahapatra, A. K., Sodhi, P., & Kher, V. (2021). Grafalon® vs. Thymoglobulin® as an Induction Agent in Renal Transplantation - A Retrospective Study. *Indian J Nephrol*, *31*(4), 336-340.

Jia, L., Oh, E. C., Ng, L., Srinivas, M., Brooks, M., Swaroop, A., & Forrest, D. (2009). Retinoid-related orphan nuclear receptor RORbeta is an early-acting factor in rod photoreceptor development. *Proc Natl Acad Sci U S A*, *106*(41), 17534-17539.

Jin, L., & Li, Y. (2010). Structural and functional insights into nuclear receptor signaling. *Adv Drug Deliv Rev*, *62*(13), 1218-1226.

Jordan, S. C., Ammerman, N., Choi, J., Huang, E., Najjar, R., Peng, A., Sethi, S., Sandhu, R., Atienza, J., Toyoda, M., Ge, S., Lim, K., Gillespie, M., Zhang, X., Haas, M., & Vo, A. (2022). Evaluation of Clazakizumab (Anti-Interleukin-6) in Patients With Treatment-Resistant Chronic Active Antibody-Mediated Rejection of Kidney Allografts. *Kidney Int Rep*, *7*(4), 720-731.

Jordan, S. C., Choi, J., Kim, I., Wu, G., Toyoda, M., Shin, B., & Vo, A. (2017). Interleukin-6, A Cytokine Critical to Mediation of Inflammation, Autoimmunity and Allograft Rejection: Therapeutic Implications of IL-6 Receptor Blockade. *Transplantation*, *101*(1), 32-44.

Jordan, S. C., Choi, J., & Vo, A. (2015). Kidney transplantation in highly sensitized patients. *Br Med Bull*, *114*(1), 113-125.

Kahan, B. D., Rajagopalan, P. R., & Hall, M. (1999). Reduction of the occurrence of acute cellular rejection among renal allograft recipients treated with basiliximab, a chimeric anti-interleukin-2-receptor monoclonal antibody. United States Simulect Renal Study Group. *Transplantation*, *67*(2), 276-284.

Kalfeist, L., Galland, L., Ledys, F., Ghiringhelli, F., Limagne, E., & Ladoire, S. (2022). Impact of Glucocorticoid Use in Oncology in the Immunotherapy Era. *Cells*, *11*(5), 770.

Kandeva, T., Liu, S., & Tchervenkov, J. (2010). THE PRESENCE OF INCREASED PERIPHERAL TH17 LYMPHOCYTES IN HIGHLY SENSITIZED RENAL TRANSPLANT PATIENTS: IMPLICATIONS FOR IMMUNE MODULATION: 3135. *Transplantation*, *90*, 191.

Kang, J., Loh, K., Belyayev, L., Cha, P., Sadat, M., Khan, K., Gusev, Y., Bhuvaneshwar, K., Ressom, H., Moturi, S., Kaiser, J., Hawksworth, J., Robson, S. C., Matsumoto, C. S., Zasloff, M., Fishbein, T. M., & Kroemer, A. (2021). Type 3 innate lymphoid cells are associated with a successful intestinal transplant. *Am J Transplant*, *21*(2), 787-797.

Kashiwagi, N., Brantigan, C. O., Brettschneider, L., Groth, C. G., & Starzl, T. E. (1968). Clinical reactions and serologic changes after the administration of heterologous antilymphocyte globulin to human recipients of renal homografts. *Ann Intern Med*, *68*(2), 275-286.

Kathania, M., Khare, P., Zeng, M., Cantarel, B., Zhang, H., Ueno, H., & Venuprasad, K. (2016). Itch inhibits IL-17-mediated colon inflammation and tumorigenesis by ROR-γt ubiquitination. *Nat Immunol*, *17*(8), 997-1004.

Kim, E. J., Kim, S. J., Huh, K. H., Kim, B. S., Kim, M. S., Kim, S. I., Kim, Y. S., & Lee, J. (2021). Clinical significance of tacrolimus intra-patient variability on kidney transplant outcomes according to pre-transplant immunological risk. *Sci Rep*, *11*(1), 12114.

Kim, J. M., Jang, H. R., Ko, J. S., Kwon, C. H., Kwak, M. S., Hur, W. S., Kim, S. J., Kim, G. S., Joh, J. W., Lee, S. K., & Oh, H. Y. (2012). Comparison between

thymoglobulin and ATGAM as an induction agent in adult kidney transplantation: a single-center experience. *Transplant Proc*, *44*(1), 171-174.

Kim, S. M., Choi, J. E., Hur, W., Kim, J. H., Hong, S. W., Lee, E. B., Lee, J. H., Li, T. Z., Sung, P. S., & Yoon, S. K. (2017). RAR-Related Orphan Receptor Gamma (ROR-γ) Mediates Epithelial-Mesenchymal Transition Of Hepatocytes During Hepatic Fibrosis. *J Cell Biochem*, *118*(8), 2026-2036.

Kolonko, A., Słabiak-Błaż, N., Karkoszka, H., Więcek, A., & Piecha, G. (2020). The Preliminary Results of Bortezomib Used as A Primary Treatment for An Early Acute Antibody-Mediated Rejection after Kidney Transplantation-A Single-Center Case Series. *J Clin Med*, *9*(2).

Konvalinka, A., & Tinckam, K. (2015). Utility of HLA Antibody Testing in Kidney Transplantation. *J Am Soc Nephrol*, *26*(7), 1489-1502.

Lachmann, N., Duerr, M., Schönemann, C., Pruß, A., Budde, K., & Waiser, J. (2017). Treatment of Antibody-Mediated Renal Allograft Rejection: Improving Step by Step. *J Immunol Res*, *2017*, 6872046.

Lamb, K. E., Lodhi, S., & Meier-Kriesche, H. U. (2011). Long-term renal allograft survival in the United States: a critical reappraisal. *Am J Transplant*, *11*(3), 450-462.

Leca, N. (2009). Leflunomide use in renal transplantation. *Curr Opin Organ Transplant*, *14*(4), 370-374.

Li, S., Li, Y., Qu, X., Liu, X., & Liang, J. (2014). Detection and significance of TregFoxP3(+) and Th17 cells in peripheral blood of non-small cell lung cancer patients. *Arch Med Sci*, *10*(2), 232-239.

Li, X., Anderson, M., Collin, D., Muegge, I., Wan, J., Brennan, D., Kugler, S., Terenzio, D., Kennedy, C., Lin, S., Labadia, M. E., Cook, B., Hughes, R., & Farrow, N. A. (2017). Structural studies unravel the active conformation of apo RORγt nuclear receptor and a common inverse agonism of two diverse classes of RORγt inhibitors. *J Biol Chem*, *292*(28), 11618-11630.

Liljevald, M., Rehnberg, M., Söderberg, M., Ramnegård, M., Börjesson, J., Luciani, D., Krutrök, N., Brändén, L., Johansson, C., Xu, X., Bjursell, M., Sjögren, A. K., Hornberg, J., Andersson, U., Keeling, D., & Jirholt, J. (2016). Retinoid-related orphan receptor γ (RORγ) adult induced knockout mice develop lymphoblastic lymphoma. *Autoimmun Rev*, *15*(11), 1062-1070.

Lin, Z. W., Wu, L. X., Xie, Y., Ou, X., Tian, P. K., Liu, X. P., Min, J., Wang, J., Chen, R. F., Chen, Y. J., Liu, C., Ye, H., & Ou, Q. J. (2015). The expression levels of transcription factors T-bet, GATA-3, RORγt and FOXP3 in peripheral blood lymphocyte (PBL) of patients with liver cancer and their significance. *Int J Med Sci*, *12*(1), 7-16.

Lytle, N. K., Ferguson, L. P., Rajbhandari, N., Gilroy, K., Fox, R. G., Deshpande, A., Schurch, C. M., Hamilton, M., Robertson, N., Lin, W., Noel, P., Wartenberg, M., Zlobec, I., Eichmann, M., Galvan, J. A., Karamitopoulou, E., Gilderman, T., Esparza, L. A., Shima, Y., . . . Reya, T. (2019). A Multiscale Map of the Stem Cell State in Pancreatic Adenocarcinoma. *Cell*, *177*(3), 572-586 e522.

Ma, J., Patel, A., & Tinckam, K. (2016). Donor-Specific Antibody Monitoring: Where Is the Beef? *Adv Chronic Kidney Dis*, *23*(5), 317-325.

Mabasa, V. H., & Ensom, M. H. (2005). The role of therapeutic monitoring of everolimus in solid organ transplantation. Ther Drug Monit, 27(5), 666-676.

Madauss, K. P., Deng, S. J., Austin, R. J., Lambert, M. H., McLay, I., Pritchard, J., Short, S. A., Stewart, E. L., Uings, I. J., & Williams, S. P. (2004). Progesterone receptor ligand binding pocket flexibility: crystal structures of the norethindrone and mometasone furoate complexes. *J Med Chem*, *47*(13), 3381-3387.

Mahalati, K., Belitsky, P., West, K., Kiberd, B., Fraser, A., Sketris, I., Macdonald, A. S., McAlister, V., & Lawen, J. (2001). Approaching the therapeutic window for cyclosporine in kidney transplantation: a prospective study. *JOURNAL-AMERICAN SOCIETY OF NEPHROLOGY*, *12*(4), 828-833.

Mao, K., Baptista, A. P., Tamoutounour, S., Zhuang, L., Bouladoux, N., Martins, A. J., Huang, Y., Gerner, M. Y., Belkaid, Y., & Germain, R. N. (2018). Innate and adaptive lymphocytes sequentially shape the gut microbiota and lipid metabolism. *Nature*, *554*(7691), 255-259.

Massa, E. G., Talayero, P., Utrero, A., Laguna, R., Andrés, A., Auñón, P., Sevillano, Á., Mancebo, E., Castro, M. J., & Estela, P. (2018). Helper Innate Lymphoid Cells (hILC) resist Immunosuppressive Therapy: an Observation from Kidney and Liver Transplantation. *Transplantation*, *102*, S283-S284.

McDonald-Hyman, C., Turka, L. A., & Blazar, B. R. (2015). Advances and challenges in immunotherapy for solid organ and hematopoietic stem cell transplantation. *Sci Transl Med*, *7*(280), 280rv282.

Meyer, D., Coles, A., Oyuela, P., Purvis, A., & Margolin, D. H. (2013). Case report of anti-glomerular basement membrane disease following alemtuzumab treatment of relapsing-remitting multiple sclerosis. *Mult Scler Relat Disord*, *2*(1), 60-63.

Mitsdoerffer, M., Lee, Y., Jäger, A., Kim, H. J., Korn, T., Kolls, J. K., Cantor, H., Bettelli, E., & Kuchroo, V. K. (2010). Proinflammatory T helper type 17 cells are effective B-cell helpers. *Proc Natl Acad Sci U S A*, *107*(32), 14292-14297.

Mohty, M. (2007). Mechanisms of action of antithymocyte globulin: T-cell depletion and beyond. *Leukemia*, *21*(7), 1387-1394.

Mourad, G., Rostaing, L., Legendre, C., Garrigue, V. e., Thervet, E., & Durand, D. (2004). Sequential Protocols using Basiliximab versus Anti-Thymocyte Globulins in Renal-Transplant Patients Receiving Mycophenolate Mofetil and Steroids. *Transplantation*, *78*(4), 584-590.

Murata, K., & Baldwin, W. M., 3rd. (2009). Mechanisms of complement activation, C4d deposition, and their contribution to the pathogenesis of antibody-mediated rejection. *Transplant Rev (Orlando)*, *23*(3), 139-150.

Nakae, S., Komiyama, Y., Nambu, A., Sudo, K., Iwase, M., Homma, I., Sekikawa, K., Asano, M., & Iwakura, Y. (2002). Antigen-specific T cell sensitization is impaired in IL-17-deficient mice, causing suppression of allergic cellular and humoral responses. *Immunity*, *17*(3), 375-387.

Nakamura, H. (1993). [Immunosuppressive therapy in renal transplantation]. *Nihon Hinyokika Gakkai Zasshi*, *84*(8), 1359-1384.

Nashan, B., Moore, R., Amlot, P., Schmidt, A. G., Abeywickrama, K., & Soulillou, J. P. (1997). Randomised trial of basiliximab versus placebo for control of acute cellular

rejection in renal allograft recipients. CHIB 201 International Study Group. *Lancet*, *350*(9086), 1193-1198.

Negi, S., Rutman, A., Saw, C. L., Paraskevas, S., & Tchervenkov, J. (2024). Pretransplant Th17 dominant alloreactivity in highly sensitized kidney transplant candidates. *Frontiers in Transplantation*, 3, https://doi.org/10.3389/frtra.2024.1336563

Nelson, J., Alvey, N., Bowman, L., Schulte, J., Segovia, M. C., McDermott, J., Te, H. S., Kapila, N., Levine, D. J., Gottlieb, R. L., Oberholzer, J., & Campara, M. (2022). Consensus recommendations for use of maintenance immunosuppression in solid organ transplantation: Endorsed by the American College of Clinical Pharmacy, American Society of Transplantation, and the International Society for Heart and Lung Transplantation. *Pharmacotherapy*, *42*(8), 599-633.

Nickerson, P. W., Böhmig, G. A., Chadban, S., Kumar, D., Mannon, R. B., van Gelder, T., Lee, J. C., Adler, S., Chong, E., & Djamali, A. (2022). Clazakizumab for the treatment of chronic active antibody-mediated rejection (AMR) in kidney transplant recipients: Phase 3 IMAGINE study rationale and design. *Trials*, *23*(1), 1042.

Nobile, A. (1994). The discovery of the Δ1,4-steroids, prednisone, and prednisolone at the Schering Corporation (USA). *Steroids*, *59*(3), 227-228.

Oh, T. G., Wang, S. M., Acharya, B. R., Goode, J. M., Graham, J. D., Clarke, C. L., Yap, A. S., & Muscat, G. E. O. (2016). The Nuclear Receptor, RORgamma, Regulates Pathways Necessary for Breast Cancer Metastasis. *EBioMedicine*, *6*, 59-72.

Okada, S., Markle, J. G., Deenick, E. K., Mele, F., Averbuch, D., Lagos, M., Alzahrani, M., Al-Muhsen, S., Halwani, R., Ma, C. S., Wong, N., Soudais, C., Henderson, L. A., Marzouqa, H., Shamma, J., Gonzalez, M., Martinez-Barricarte, R., Okada, C.,

Avery, D. T., . . . Casanova, J. L. (2015). IMMUNODEFICIENCIES. Impairment of immunity to Candida and Mycobacterium in humans with bi-allelic RORC mutations. *Science*, *349*(6248), 606-613.

Olaso, D., Manook, M., Moris, D., Knechtle, S., & Kwun, J. (2021). Optimal Immunosuppression Strategy in the Sensitized Kidney Transplant Recipient. *J Clin Med*, *10*(16), 3656.

Olatunde, A. C., Hale, J. S., & Lamb, T. J. (2021). Cytokine-skewed Tfh cells: functional consequences for B cell help. *Trends Immunol*, *42*(6), 536-550.

Olyaei, A. J., Thi, K., deMattos, A. M., & Bennett, W. M. (2001). Use of basiliximab and daclizumab in kidney transplantation. *Prog Transplant*, *11*(1), 33-37; quiz 38-39.

Opelz, G., & Döhler, B. (2000). Critical threshold of azathioprine dosage for maintenance immunosuppression in kidney graft recipients. Collaborative Transplant Study. *Transplantation*, *69*(5), 818-821.

Opelz, G., Naujokat, C., Daniel, V., Terness, P., & Döhler, B. (2006). Disassociation between risk of graft loss and risk of non-Hodgkin lymphoma with induction agents in renal transplant recipients. *Transplantation*, *81*(9), 1227-1233.

Ozturk, S., Mathur, D., Zhou, R. W., Mulholland, D., & Parsons, R. (2020). Leflunomide triggers synthetic lethality in PTEN-deficient prostate cancer. *Prostate Cancer Prostatic Dis*, *23*(4), 718-723.

Park, Y., Ko, E. J., Chung, B. H., & Yang, C. W. (2021). Kidney transplantation in highly sensitized recipients. *Kidney Res Clin Pract*, *40*(3), 355-370.

Parsons, R. F., Locke, J. E., Redfield, R. R., 3rd, Roll, G. R., & Levine, M. H. (2017). Kidney transplantation of highly sensitized recipients under the new kidney

allocation system: A reflection from five different transplant centers across the United States. *Hum Immunol*, *78*(1), 30-36.

Pascual, J. (2009). The use of everolimus in renal-transplant patients. Int J Nephrol Renovasc Dis, 2, 9-21.

Patakas, A., Benson, R. A., Withers, D. R., Conigliaro, P., McInnes, I. B., Brewer, J. M., & Garside, P. (2012). Th17 effector cells support B cell responses outside of germinal centres. *PLoS One*, *7*(11), e49715.

Pawlak, M., Lefebvre, P., & Staels, B. (2015). Molecular mechanism of PPARα action and its impact on lipid metabolism, inflammation and fibrosis in non-alcoholic fatty liver disease. *J Hepatol*, *62*(3), 720-733.

Pearl, M., Weng, P. L., Chen, L., Dokras, A., Pizzo, H., Garrison, J., Butler, C., Zhang, J., Reed, E. F., Kim, I. K., Choi, J., Haas, M., Zhang, X., Vo, A., Chambers, E. T., Ettenger, R., Jordan, S., & Puliyanda, D. (2022). Long term tolerability and clinical outcomes associated with tocilizumab in the treatment of refractory antibody mediated rejection (AMR) in pediatric renal transplant recipients. *Clin Transplant*, *36*(8), e14734.

Pène, J., Gauchat, J. F., Lécart, S., Drouet, E., Guglielmi, P., Boulay, V., Delwail, A., Foster, D., Lecron, J. C., & Yssel, H. (2004). Cutting edge: IL-21 is a switch factor for the production of IgG1 and IgG3 by human B cells. *J Immunol*, *172*(9), 5154-5157.

Perosa, M., Ferreira, G. F., Modelli, L. G., Medeiros, M. P., Neto, S. R., Moreira, F., Zampieri, F. G., de Marco, R., Bortoluzzo, A. B., & Venezuela, M. K. (2021).

Disparity in the access to kidney transplantation for sensitized patients in the state of Sao Paulo-Brazil. *Transpl Immunol*, *68*, 101441.

Pfeifle, R., Rothe, T., Ipseiz, N., Scherer, H. U., Culemann, S., Harre, U., Ackermann, J. A., Seefried, M., Kleyer, A., Uderhardt, S., Haugg, B., Hueber, A. J., Daum, P., Heidkamp, G. F., Ge, C., Böhm, S., Lux, A., Schuh, W., Magorivska, I., . . . Krönke, G. (2017). Regulation of autoantibody activity by the IL-23-T(H)17 axis determines the onset of autoimmune disease. *Nat Immunol*, *18*(1), 104-113.

Pufall, M. A. (2015). Glucocorticoids and Cancer. *Adv Exp Med Biol*, *872*, 315-333.

Reichardt, S. D., Amouret, A., Muzzi, C., Vettorazzi, S., Tuckermann, J. P., Lühder, F., & Reichardt, H. M. (2021). The Role of Glucocorticoids in Inflammatory Diseases. *Cells*, *10*(11).

Resch, T., Fabritius, C., Ebner, S., Ritschl, P., & Kotsch, K. (2015). The Role of Natural Killer Cells in Humoral Rejection. *Transplantation*, *99*(7), 1335-1340.

Ricklin, D., Hajishengallis, G., Yang, K., & Lambris, J. D. (2010). Complement: a key system for immune surveillance and homeostasis. *Nat Immunol*, *11*(9), 785-797.

Rodriguez-Ramirez, S., Al Jurdi, A., Konvalinka, A., & Riella, L. V. (2022). Antibody-mediated rejection: prevention, monitoring and treatment dilemmas. *Curr Opin Organ Transplant*, *27*(5), 405-414.

Ruggenenti, P., Cravedi, P., Gotti, E., Plati, A., Marasà, M., Sandrini, S., Bossini, N., Citterio, F., Minetti, E., Montanaro, D., Sabadini, E., Tardanico, R., Martinetti, D., Gaspari, F., Villa, A., Perna, A., Peraro, F., & Remuzzi, G. (2021). Mycophenolate mofetil versus azathioprine in kidney transplant recipients on steroid-free, low-

dose cyclosporine immunosuppression (ATHENA): A pragmatic randomized trial. *PLoS Med*, *18*(6), e1003668.

Sablik, K. A., Clahsen-van Groningen, M. C., Hesselink, D. A., van Gelder, T., & Betjes, M. G. H. (2018). Tacrolimus intra-patient variability is not associated with chronic active antibody mediated rejection. *PLoS One*, *13*(5), e0196552.

Santori, F. R., Huang, P., van de Pavert, S. A., Douglass, E. F., Jr., Leaver, D. J., Haubrich, B. A., Keber, R., Lorbek, G., Konijn, T., Rosales, B. N., Rozman, D., Horvat, S., Rahier, A., Mebius, R. E., Rastinejad, F., Nes, W. D., & Littman, D. R. (2015). Identification of natural RORgamma ligands that regulate the development of lymphoid cells. *Cell Metab*, *21*(2), 286-298.

Scheepstra, M., Leysen, S., Van Almen, G. C., Miller, J. R., Piesvaux, J., Kutilek, V., Van Eenennaam, H., Zhang, H., Barr, K., Nagpal, S., Soisson, S. M., Kornienko, M., Wiley, K., Elsen, N., Sharma, S., Correll, C. C., Trotter, B. W., Van Der Stelt, M., Oubrie, A., . . . Brunsveld, L. (2015). Identification of an allosteric binding site for RORγt inhibition. *Nature Communications*, *6*(1), 8833.

Schuler, W., Sedrani, R., Cottens, S., Häberlin, B., Schulz, M., Schuurman, H.-J., Zenke, G., Zerwes, H.-G., & Schreier, M. H. (1997). SDZ RAD, A NEW RAPAMYCIN DERIVATIVE: Pharmacological Properties In Vitro and In Vivo. Transplantation, 64(1), 36-42.

Sewell, F., Corvaro, M., Andrus, A., Burke, J., Daston, G., Delaney, B., Domoradzki, J., Forlini, C., Green, M. L., Hofmann, T., Jäckel, S., Lee, M. S., Temerowski, M., Whalley, P., & Lewis, R. (2022). Recommendations on dose level selection for repeat dose toxicity studies. *Arch Toxicol*, *96*(7), 1921-1934.

Sheiko, M. A., Sundaram, S. S., Capocelli, K. E., Pan, Z., McCoy, A. M., & Mack, C. L. (2017). Outcomes in Pediatric Autoimmune Hepatitis and Significance of Azathioprine Metabolites. *J Pediatr Gastroenterol Nutr*, *65*(1), 80-85.

Shim, Y. E., Ko, Y., Lee, J. P., Jeon, J. S., Jun, H., Yang, J., Kim, M. S., Lim, S. J., Kwon, H. E., Jung, J. H., Kwon, H., Kim, Y. H., Lee, J., Shin, S., Kong, J. M., Kwon, O. J., Kim, D. G., Jung, C. W., Kim, Y. H., . . . the Korean Organ Transplantation Registry study, g. (2023). Evaluating anti-thymocyte globulin induction doses for better allograft and patient survival in Asian kidney transplant recipients. *Scientific Reports*, *13*(1), 12560.

Slominski, A. T., Kim, T. K., Takeda, Y., Janjetovic, Z., Brozyna, A. A., Skobowiat, C., Wang, J., Postlethwaite, A., Li, W., Tuckey, R. C., & Jetten, A. M. (2014). RORα and ROR γ are expressed in human skin and serve as receptors for endogenously produced noncalcemic 20-hydroxy- and 20,23-dihydroxyvitamin D. *FASEB J*, *28*(7), 2775-2789.

Solt, L. A., Kojetin, D. J., & Burris, T. P. (2011). The REV-ERBs and RORs: molecular links between circadian rhythms and lipid homeostasis. *Future Med Chem*, *3*(5), 623-638.

Song, X., Dai, D., He, X., Zhu, S., Yao, Y., Gao, H., Wang, J., Qu, F., Qiu, J., Wang, H., Li, X., Shen, N., & Qian, Y. (2015). Growth Factor FGF2 Cooperates with Interleukin-17 to Repair Intestinal Epithelial Damage. *Immunity*, *43*(3), 488-501.

Sood, P., & Hariharan, S. (2018). Anti-CD20 Blocker Rituximab in Kidney Transplantation. *Transplantation*, *102*(1), 44-58.

Soroosh, P., Wu, J., Xue, X., Song, J., Sutton, S. W., Sablad, M., Yu, J., Nelen, M. I., Liu, X., Castro, G., Luna, R., Crawford, S., Banie, H., Dandridge, R. A., Deng, X., Bittner, A., Kuei, C., Tootoonchi, M., Rozenkrants, N., . . . Sun, S. (2014). Oxysterols are agonist ligands of RORγt and drive Th17 cell differentiation. *Proc. Natl. Acad. Sci. U. S. A.*, *111*(33), 12163-12168.

Steiner, R. W., & Awdishu, L. (2011). Steroids in kidney transplant patients. *Semin Immunopathol*, *33*(2), 157-167.

Strauss, L., Sangaletti, S., Consonni, F. M., Szebeni, G., Morlacchi, S., Totaro, M. G., Porta, C., Anselmo, A., Tartari, S., Doni, A., Zitelli, F., Tripodo, C., Colombo, M. P., & Sica, A. (2015). RORC1 Regulates Tumor-Promoting "Emergency" Granulo-Monocytopoiesis. *Cancer Cell*, *28*(2), 253-269.

Suárez-Fueyo, A., Bradley, S. J., Klatzmann, D., & Tsokos, G. C. (2017). T cells and autoimmune kidney disease. *Nat Rev Nephrol*, *13*(6), 329-343.

Sun, N., Yuan, C., Ma, X., Wang, Y., Gu, X., & Fu, W. (2018). Molecular mechanism of action of RORγt agonists and inverse agonists: insights from molecular dynamics simulation. Molecules, 23(12), 3181/3181-3181/3114.

Sun, Z., Unutmaz, D., Zou, Y. R., Sunshine, M. J., Pierani, A., Brenner-Morton, S., Mebius, R. E., & Littman, D. R. (2000). Requirement for RORgamma in thymocyte survival and lymphoid organ development. *Science*, *288*(5475), 2369-2373.

Tan, Z., Jiang, R., Wang, X., Wang, Y., Lu, L., Liu, Q., Zheng, S. G., Sun, B., & Ryffel, B. (2013). RORγt+IL-17+ neutrophils play a critical role in hepatic ischemia-reperfusion injury. *J Mol Cell Biol*, *5*(2), 143-146.

Tanaka, S., Gauthier, J. M., Fuchs, A., Li, W., Tong, A. Y., Harrison, M. S., Higashikubo, R., Terada, Y., Hachem, R. R., Ruiz-Perez, D., Ritter, J. H., Cella, M., Colonna, M., Turnbull, I. R., Krupnick, A. S., Gelman, A. E., & Kreisel, D. (2020). IL-22 is required for the induction of bronchus-associated lymphoid tissue in tolerant lung allografts. *Am J Transplant*, *20*(5), 1251-1261.

Tedesco, D., & Haragsim, L. (2012). Cyclosporine: a review. *J Transplant*, *2012*, 230386.

Tonelli, M., Wiebe, N., Knoll, G., Bello, A., Browne, S., Jadhav, D., Klarenbach, S., & Gill, J. (2011). Systematic Review: Kidney Transplantation Compared With Dialysis in Clinically Relevant Outcomes. *American Journal of Transplantation*, *11*(10), 2093-2109.

Tuzlak, S., Dejean, A. S., Iannacone, M., Quintana, F. J., Waisman, A., Ginhoux, F., Korn, T., & Becher, B. (2021). Repositioning TH cell polarization from single cytokines to complex help. *Nature Immunology*, *22*(10), 1210-1217.

Ueda, E., Kurebayashi, S., Sakaue, M., Backlund, M., Koller, B., & Jetten, A. M. (2002). High incidence of T-cell lymphomas in mice deficient in the retinoid-related orphan receptor RORgamma. *Cancer Res*, *62*(3), 901-909.

Valenzuela, N. M., & Schaub, S. (2018). The Biology of IgG Subclasses and Their Clinical Relevance to Transplantation. *Transplantation*, *102*(1S Suppl 1), S7-s13.

Varma, P. P., Prasher, P. K., Madan, H., & Yashpal, B. (1996). AZATHIOPRINE INDUCED BONE MARROW SUPPRESSION IN LIVE RELATED RENAL ALLOGRAFT RECIPIENTS. *Med J Armed Forces India*, *52*(1), 45-47.

Vidarsson, G., Dekkers, G., & Rispens, T. (2014). IgG subclasses and allotypes: from structure to effector functions. *Front Immunol*, *5*, 520.

Vo, A. A., Choi, J., Cisneros, K., Reinsmoen, N., Haas, M., Ge, S., Toyoda, M., Kahwaji, J., Peng, A., Villicana, R., & Jordan, S. C. (2014). Benefits of rituximab combined with intravenous immunoglobulin for desensitization in kidney transplant recipients. *Transplantation*, *98*(3), 312-319.

Vo, A. A., Huang, E., Ammerman, N., Toyoda, M., Ge, S., Haas, M., Zhang, X., Peng, A., Najjar, R., Williamson, S., Myers, C., Sethi, S., Lim, K., Choi, J., Gillespie, M., Tang, J., & Jordan, S. C. (2022). Clazakizumab for desensitization in highly sensitized patients awaiting transplantation. *Am J Transplant*, *22*(4), 1133-1144.

Vo, A. A., Lukovsky, M., Toyoda, M., Wang, J., Reinsmoen, N. L., Lai, C. H., Peng, A., Villicana, R., & Jordan, S. C. (2008). Rituximab and intravenous immune globulin for desensitization during renal transplantation. *N Engl J Med*, *359*(3), 242-251.

Waiser, J., Budde, K., Schütz, M., Liefeldt, L., Rudolph, B., Schönemann, C., Neumayer, H. H., & Lachmann, N. (2012). Comparison between bortezomib and rituximab in the treatment of antibody-mediated renal allograft rejection. *Nephrol Dial Transplant*, *27*(3), 1246-1251.

Wang, J., Zou, J. X., Xue, X., Cai, D., Zhang, Y., Duan, Z., Xiang, Q., Yang, J. C., Louie, M. C., Borowsky, A. D., Gao, A. C., Evans, C. P., Lam, K. S., Xu, J., Kung, H. J., Evans, R. M., Xu, Y., & Chen, H. W. (2016). ROR-gamma drives androgen receptor expression and represents a therapeutic target in castration-resistant prostate cancer. *Nat Med*, *22*(5), 488-496.

Wang, K., Xu, X., & Fan, M. (2018). Induction therapy of basiliximab versus antithymocyte globulin in renal allograft: a systematic review and meta-analysis. *Clinical and Experimental Nephrology*, *22*(3), 684-693.

Wang, Y., Cai, W., Cheng, Y., Yang, T., Liu, Q., Zhang, G., Meng, Q., Han, F., Huang, Y., Zhou, L., Xiang, Z., Zhao, Y.-G., Xu, Y., Cheng, Z., Lu, S., Wu, Q., Xiang, J.-N., Elliott, J. D., Leung, S., . . . Lin, X. (2015). Discovery of Biaryl Amides as Potent, Orally Bioavailable, and CNS Penetrant RORγt Inhibitors. *ACS Med. Chem. Lett.*, *6*(7), 787-792.

Wang, Y., Kumar, N., Solt, L. A., Richardson, T. I., Helvering, L. M., Crumbley, C., Garcia-Ordonez, R. D., Stayrook, K. R., Zhang, X., Novick, S., Chalmers, M. J., Griffin, P. R., & Burris, T. P. (2010). Modulation of retinoic acid receptor-related orphan receptor alpha and gamma activity by 7-oxygenated sterol ligands. J Biol Chem, 285(7), 5013-5025.

Wasilewska, A., Winiarska, M., Olszewska, M., & Rudnicka, L. (2016). Interleukin-17 inhibitors. A new era in treatment of psoriasis and other skin diseases. *Postepy Dermatol Alergol*, *33*(4), 247-252.

Webster, A. C., Playford, E. G., Higgins, G., Chapman, J. R., & Craig, J. C. (2004). Interleukin 2 receptor antagonists for renal transplant recipients: a meta-analysis of randomized trials1. *Transplantation*, *77*(2), 166-176.

Welch, R. D., Billon, C., Losby, M., Bedia-Diaz, G., Fang, Y., Avdagic, A., Elgendy, B., Burris, T. P., & Griffett, K. (2022). Emerging Role of Nuclear Receptors for the Treatment of NAFLD and NASH. *Metabolites*, *12*(3).

Willoughby, L. M., Schnitzler, M. A., Brennan, D. C., Pinsky, B. W., Dzebisashvili, N., Buchanan, P. M., Neri, L., Rocca-Rey, L. A., Abbott, K. C., & Lentine, K. L. (2009). Early outcomes of thymoglobulin and basiliximab induction in kidney

transplantation: application of statistical approaches to reduce bias in observational comparisons. *Transplantation*, *87*(10), 1520-1529.

Withers, D. R., Hepworth, M. R., Wang, X., Mackley, E. C., Halford, E. E., Dutton, E. E., Marriott, C. L., Brucklacher-Waldert, V., Veldhoen, M., Kelsen, J., Baldassano, R. N., & Sonnenberg, G. F. (2016). Transient inhibition of ROR-γt therapeutically limits intestinal inflammation by reducing TH17 cells and preserving group 3 innate lymphoid cells. *Nat Med*, *22*(3), 319-323.

Woodle, E. S., Gill, J. S., Clark, S., Stewart, D., Alloway, R., & First, R. (2021). Early Corticosteroid Cessation vs Long-term Corticosteroid Therapy in Kidney Transplant Recipients: Long-term Outcomes of a Randomized Clinical Trial. *JAMA Surgery*, *156*(4), 307-314.

Yale, H. L. (1959). The Trifluoromethyl Group in Medical Chemistry. *Journal of Medicinal and Pharmaceutical Chemistry*, *1*(2), 121-133.

Yang, X. O., Pappu, B. P., Nurieva, R., Akimzhanov, A., Kang, H. S., Chung, Y., Ma, L., Shah, B., Panopoulos, A. D., Schluns, K. S., Watowich, S. S., Tian, Q., Jetten, A. M., & Dong, C. (2008). T helper 17 lineage differentiation is programmed by orphan nuclear receptors ROR alpha and ROR gamma. *Immunity*, *28*(1), 29-39.

Yin, X. T., Zobell, S., Jarosz, J. G., & Stuart, P. M. (2015). Anti-IL-17 therapy restricts and reverses late-term corneal allorejection. *J Immunol*, *194*(8), 4029-4038.

Yuan, X., Paez-Cortez, J., Schmitt-Knosalla, I., D'Addio, F., Mfarrej, B., Donnarumma, M., Habicht, A., Clarkson, M. R., Iacomini, J., Glimcher, L. H., Sayegh, M. H., & Ansari, M. J. (2008). A novel role of CD4 Th17 cells in mediating cardiac allograft rejection and vasculopathy. *J Exp Med*, *205*(13), 3133-3144.

Zachary, A. A., & Leffell, M. S. (2014). Desensitization for solid organ and hematopoietic stem cell transplantation. *Immunol Rev*, *258*(1), 183-207.

Zhang, Q., & Reed, E. F. (2016). The importance of non-HLA antibodies in transplantation. *Nat Rev Nephrol*, *12*(8), 484-495. https://doi.org/10.1038/nrneph.2016.88

Zhang, R. (2018). Donor-Specific Antibodies in Kidney Transplant Recipients. *Clin J Am Soc Nephrol*, *13*(1), 182-192.

Zhang, W., Tian, X., Mumtahana, F., Jiao, J., Zhang, T., Croce, K. D., Ma, D., Kong, B., & Cui, B. (2015). The existence of Th22, pure Th17 and Th1 cells in CIN and Cervical Cancer along with their frequency variation in different stages of cervical cancer. *BMC Cancer*, *15*, 717.

Zhidkova, E. M., Lylova, E. S., Savinkova, A. V., Mertsalov, S. A., Kirsanov, K. I., Belitsky, G. A., Yakubovskaya, M. G., & Lesovaya, E. A. (2020). A Brief Overview of the Paradoxical Role of Glucocorticoids in Breast Cancer. *Breast Cancer (Auckl)*, *14*, 1178223420974667.

Zhou, X. S., Lu, Y. Y., Gao, Y. F., Shao, W., & Yao, J. (2021). Bone marrow inhibition induced by azathioprine in a patient without mutation in the thiopurine S-methyltransferase pathogenic site: A case report. *World J Clin Cases*, *9*(17), 4230-4237.
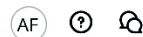
CCC
RightsLink

(AF) ⑦ ⚲

ACS Publications
Most Trusted. Most Cited. Most Read.

Discovery, Synthesis, and In Vitro Characterization of 2,3 Derivatives of 4,5,6,7-Tetrahydro-Benzothiophene as Potent Modulators of Retinoic Acid Receptor-Related Orphan Receptor yt

Author: Ahmed Fouda, Sarita Negi, Oleg Zaremba, et al

Publication: Journal of Medicinal Chemistry

Publisher: American Chemical Society

Date: Jun 1, 2023

Copyright © 2023, American Chemical Society

CCC
RightsLink

⑦ ⌾

RORγt inverse agonist TF-S14 inhibits Th17 cytokines and prolongs skin allograft survival in sensitized mice

SPRINGER NATURE

Author: Ahmed Fouda et al

Publication: Communications Biology

Publisher: Springer Nature

Date: Apr 12, 2024

Copyright © 2024, The Author(s)